Summary of the Bulletin of the International Seismological Centre

2008

September – December

Inside Cover

Guest:

- Image relating to a notable event (see later section).

IB:

- Map of GT events.

BD:

- Map of new stations (not in the previous 12 months).

Contents

1

The International Seismological Centre

1.1 Brief history of the ISC

Earthquake effects have been noted and documented from the earliest times, but it is only since the development of earthquake detecting instruments within the last hundred years that a proper study of their occurrence has been possible. The need for international exchange of readings was soon recognised by Professor John Milne, whose work resulted in the International Seismological Summary being set up immediately after the First World War.

After Milne's death, the International Seismological Summary operated with funding principally from colleges of U.K. universities under the directorship of several professors of seismology at Oxford University, and Sir Harold Jeffreys (Cambridge).

The present International Seismological centre was formed in Edinburgh in 1964, with Dr. P.L. Willmore as its first director, to continue the work of the International Seismological Summary (ISS), which was the first gathering of all observations of earthquakes world-wide.

In 1970, with the help of UNESCO and other international scientific bodies, the Centre was reconstituted as an international non-governmental body, funded by interested institutions from various countries. Initially there were supporting members from seven countries, now there are more than 50, and member institutions include national academies, government departments and universities. Each member contributing a minimum unit of subscription or more, appoints a representative to the Centre's Governing Council, which meets every two years to decide the Centre's policy and operational programme. Representatives from UNESCO and the International Association of Seismology and Physics of the Earth's Interior also attend these meetings. The Governing Council appoints the Director and a small Executive Committee to oversee the Centre's operations.

Most of the ISC budget is financed by Members' subscriptions but since 1978 a new category of Associate Membership has been available to organisations in the commercial sector, such as insurance offices, engineering enterprises and exploration companies, which have a professional need for the Centre's results, and wish to contribute to its continuing operations. Both members and associate members are afforded certain privileges.

In 1975, the Centre moved to Newbury in southern England to make use of better computing facilities there. The Centre subsequently acquired its own computer and in 1986 moved to its own building at Pipers Lane, Thatcham, near Newbury. The internal layout of the new premises was designed for the Centre and includes not only office space but provision for the storage of extensive stocks of ISS and ISC publications and a library of seismological bulletins, journals and books.

Scientific Operation

The main scientific goal of the Centre is the definitive compilation of earthquake information and the readings on which they are based. Collection of reports of earthquake effects is also an important part of its operation and the Centre recomputes the location and occurrence time of earthquakes world-wide, making use of all available information.

Since 1957 the manipulation of the large volume of data has been mainly carried out by computer. Up until then ISS locations were determined manually with the help of a large globe. The ISC now uses a network of Linux/Unix workstations accessing a relational database of nearly 50 Gbytes of on-line data.

The analysis of the earthquake data is undertaken in monthly batches and begins after at least 18 months to allow the information used to be as complete as possible. Although much of the work would be impossible without the Centre's large suite of computer programs, the final editing of events large enough to be detected by several independently operated networks is always carried out by seismologists who scrutinise the output for unlikely events and chance misassociation of readings.

During analysis the computer program first groups origin estimates from different agencies and then associates the individual station readings with the most likely event. In a typical month more than 200,000 station readings are analysed leading to an average of 10,000 events per month being identified, of which some 4,000 require manual review. Misassociations and other discrepancies are rectified and the remaining unassociated readings are searched for new events and previously unreported earthquakes are added to the database. The total number of events listed each month is several times greater than those obtained by any other world-wide location service and results from ISC's goal to provide a fully comprehensive list.

DS:

- ISC mandate

DS:

- Evolution of the products

2

Member Institutions of the ISC

DS:

- Working statutes - concept of membership

Argentina:	Instituto Nacional de Prevencion Sismica (INPRES)	www.inpres.gov.ar
Australia:	Geoscience Australia	www.ga.gov.au
	Seismology Research Centre	www.seis.com.au
Austria:	Bundesministerium für Wissenschaft und Forschung	www.bmbwk.gv.at
Belgium:	Observatoire Royal de Belgique	www.astro.oma.be
Canada:	The Geological Survey of Canada, Department of Natural Resources	gsc.nrcan.gc.ca
Cyprus:	Geological Survey Department	www.moa.gov.cy
China:	China Earthquake Administration	www.gov.cn

Institute of Earth Sciences, Academia Sinica, Chinese Taipei	www.earth.sinica.edu.tw

Czech Republic:

Academy of Sciences of the Czech Republic	www.cas.cz

Denmark:

Geological Survey of Denmark and Greenland - GEUS	www.geus.dk

Egypt:

National Research Institute for Astronomy and Geophysics (NRIAG)	www.nriag.sci.eg

Finland:

The University of Helsinki	www.helsinki.fi

France:

Institute National des Sciences de l'Univers	www.insu.cnrs.fr
Laboratoire de Detection et de Geophysique	www-dase.cea.fr

Greece:

The Seismological Institute, National Observatory of Athens	www.noa.gr

Germany:

Bundesanstalt für Geowissenschaften und Rohstoffe	www.bgr.bund.de
GeoForschungsZentrum Potsdam	www.gfz-potsdam.de

Hungary:

The Hungarian Academy of Sciences	www.mta.hu

Iceland:

The Icelandic Meteorological Office	www.vedur.is

India:

India Meteorological Department	www.imd.ernet.in

Iraq:

Iraqi Seismic Network	www.imos-tm.com

Ireland:

Dublin Institute for Advanced Studies	www.dias.ie

Israel:

The Geophysical Institute of Israel	www.gii.co.il
Soreq Nuclear Research Centre (SNRC)	www.soreq.gov.il

Italy:

Instituto Nazionale di Geofisica e Vulcanologia	www.ingv.it
Instituto Nationale de Oceanografia e di Giofisica Sperimentale	www.ogs.trieste.it

Jamaica:

University of the West Indies	www.mona.uwi.edu

Japan:

The Japan Meteorological Agency (JMA)	www.jma.go.jp
Earthquake Research Institute, University of Tokyo	www.eri.u-tokyo.ac.jp

	Japan Agency for Marine-Earth Science and Technology (JAMSTEC)	www.jamstec.go.jp
Jordan:	Natural Resources Authority, Amman	www.nra.gov.jo
Korea:	Korean Meterological Administration	www.kma.go.kr
Mexico:	Institute of Geophysics, National University of Mexico	www.igeofcu.unam.mx
The Netherlands:	The Royal Netherlands Meteorological Institute	www.knmi.nl
New Zealand:	Institute of Geological and Nuclear Sciences Ltd.	www.gns.cri.nz
Norway:	The University of Bergen	www.uib.no
	Norwegian Seismic Array (NTNF/NORSAR)	www.norsar.no
Poland:	Institute of Geophysics, Polish Academy of Sciences	www.igf.edu.pl
Portugal:	The Institute for Meteorology	www.meteo.pt

Romania:

	National Institute for Earth Physics	www.infp.ro

Russia:

	Russian Academy of Sciences	www.ras.ru

Slovenia:

AGENCIJA RS ZA OKOLJE	Environmental Agency of Slovenia	www.arso.gov.si

South Africa:

Council for Geoscience	Council for Geoscience	www.geoscience.org.za

Spain:

	Instituto Geográfico Nacional	www.ign.es

Sudan:

	Geological Research Authority of Sudan	www.gras.gov.sd

Sweden:

UPPSALA UNIVERSITET	Uppsala Universitet	www.uu.se
FOI	National Defence Research Establishment	www.foi.se

Switzerland:

sc | nat	The Swiss Academy of Sciences	www.scnat.ch

Trinidad and Tobago:

	University of the West Indies	sta.uwi.edu

Turkey:

AFAD	Disaster and Emergency Management Presidency	www.deprem.gov.tr

Kandilli Observatory and Earthquake Research Institute	www.koeri.boun.edu.tr

United Kingdom:

AWE Blacknest	www.blacknest.gov.uk
British Geological Survey	www.bgs.ac.uk
The Royal Society of London	www.royalsociety.org

United Stated of America:

The National Science Foundation	www.nsf.gov
Incorporated Research Institutions for Seismology	www.iris.edu
National Earthquake Information Center, U.S. Geological Survey	www.neic.usgs.gov
University of Texas at Austin	www.utexas.edu
Red Sismica de Puerto Rico	redsismica.uprm.edu

3

Sponsoring organisations

www.kinemetrics.com

Kinemetrics is a leader in earthquake instrumentation. For forty years, Kinemetrics has been creating products for monitoring earthquakes, volcanoes, tsunamis, and nuclear proliferation while helping society to understand these events on a global, regional and local scale. In addition the company has been creating products for monitoring civil structures, bridges, dams, and nuclear power plants as this monitoring provides important information about the structures' responses to natural or man-induced seismicity.

4

ISC staff

The listing below shows the staff (and their country of origin) who were employed at the ISC at the time of the Bulletin review.

ISC director:		
Dmitry Storchak	Director	Russia

Administration:		
Maureen Aspinwall	Administration officer	United Kingdom

Data collection:		
John Eve	Data collection officer	United Kingdom

IT/Developers:		
James Harris	System and database administrator	United Kingdom
Ben Dando	Seismologist/Developer	United Kingdom
Juan Benjumea	Seismologist/Developer	Columbia

Senior seismologists:		
István Bondár	Senior seismologist	Hungary
Wayne Richardson	Senior seismologist	New Zealand

Analysts:		
Beatriz Vera	Seismologist/senior analyst	Columbia
Elizabeth Robertson	Seismologist/analyst	New Zealand
Emily Delahaye	Seismologist/analyst	Canada
Blessing Shumba	Seismologist/analyst	Zimbabwe

GEM project team:		
Domenico Di Giacomo	Seismologist	Italy
Rosemary Wylie	Historical data entry officer	United Kingdom
Agne Baranauskaite	Historical data entry officer	Lithuania
Rebecca Verney	Historical data entry officer	United Kingdom
Hepsi Simpson	Historical data entry officer	Mexico
Jessica Wilson	Historical data entry officer	United Kingdom

5

ISC procedures

- Data collection

BD, JE:

  - Explain parsing of data.

5.1 Data collection

Data collection at the ISC involves.

In table 5.1, all 181 agencies that have reported directly to the ISC are shown. With some agencies reporting data from additional agencies, a total of 480 agencies have contributed to data within all ISC Bulletins.

5.1: Table of all 181 agencies that have directly reported to the ISC. The 114 agencies highlighted in bold have reported data to the ISC Bulletin for this issue (September 2008 – December 2008).

Agency Code	Agency Name
AAE	**University of Addis Ababa, Ethiopia**
AAM	University of Michigan, USA
ADH	Observatorio Afonso Chaves, Portugal
AFAR	Afar Depression:interpretation of the 1960-2000 earthquakes, Israel
ASIES	**Academia Sinica, Chinese Taipei**
ASL	Albuquerque Seismological Laboratory, USA
ASM	University of Asmara, Eritrea
ASRS	**Geophysical Survey SB RAS, Russia**
ATH	**National Observatory of Athens, Greece**
AUST	**Geoscience Australia, Australia**
AWI	**Alfred Wegener Institute for Polar and Marine Research, Germany**
AZER	Republic Center of Seismic Survey, Republic of Azerbaijan
BELR	**Centre of Geophysical Monitoring, Republic of Belarus**
BEO	**Seismological Survey of Serbia, Serbia**
BER	**Seismologcal Observatory in Bergen, Norway**
BGR	**Bundesanstalt fuer Geowissenschaften und Rohstoffe, Germany**
BGS	**British Geological Survey, United Kingdom**
BHUJ2	Study of Aftershocks of the Bhuj Earthquake by Japanese Research Team, Japan
BIAK	Biak earthquake aftershocks (17-Feb-1996), USA
BJI	**China Earthquake Administration, China**
BKK	**Thai Meteorological Department, Thailand**
BOG	Universidad Javeriana, Colombia
BRA	**Slovak Academy of Sciences, Republic of Slovakia**
BRG	**Institutes für Geophysik der TU Bergakademie Freiberg, Germany**
BUC	**National Institute for Earth Physics of Bucharest, Romania**
BUD	**Hungarian Seismological Institute, Hungary**
BUL	Goetz Observatory, Zimbabwe
BYKL	**GS Siberian Branch RAS, Russia**
CAR	Instituto Sismologico de Caracas, Venezuela
CASC	**Central American Seismic Center, Costa Rica**
CERI	Center for Earthquake Research and Information, USA
CLL	**Geophysikalisches Observatorium Collm, Germany**
COSMOS	Consortium of Organizations for Strong Motion Observations, USA
CRAAG	**Centre de Recherche en Astronomie, Astrophysique et Geophysique, Algeria**
CSEM	**Centre Sismologique Euro-Mediterraneen, France**
DBN	**Koninklijk Nederlands Meteorologisch Instituut, Netherlands**
DDA	**Disaster and Emergency Management Presidency, Turkey**

5.1: Continued.

Agency Code	Agency Name
DHMR	**Yemen National Seismological Center, Yemen**
DIAS	**Dublin Institute for Advanced Studies, Ireland**
DJA	**Badan Meteorologi dan Geofisika, Indonesia**
DMN	**Department of Mines and Geology, Ministry of Industry of Nepal, Nepal**
DNK	**Geological Survey of Denmark and Greenland, Denmark**
DUSS	Damascus Univeristy, Syria
EAF	East African Network, Ethiopia, Kenya, Malawi, Uganda, Zambia, Zimbabwe
EBR	Observatori de l,Ebre, Spain
ECX	**Red Sismica del Noroeste de Mexico (RESOM), Mexico**
EFATE	OBS Experiment near Efate, Vanuatu, USA
EHB	Engdahl, van der Hilst and Buland, USA
EIDC	Experimental (GSETT3) International Data Center, USA
EKA	Eskdalemuir Array Station, United Kingdom
EPSI	Reference events computed by the ISC for EPSI project, United Kingdom
FUNV	**Fundacion Venezolana De Investigaciones Sismologicas, Venezuela**
FUR	Geophysikalisches Observatorium der Universitat Munchen, Germany
GBZT	Marmara Research Center, Turkey
GCMT	The Global CMT Project, USA
GEN	Dipartimento per lo Studio del Territorio e delle sue Risorse (RSNI), Italy
GFZ	GeoForschungsZentrum (GFZ) Potsdam, Germany
GII	**The Geophysical Institute of Israel, Israel**
GRAL	**National Council for Scientific Research, Lebanon**
GTFE	German Task Force for Earthquakes, Germany
GUC	**Departamento de Geofisica, Universidad de Chile, Chile**
HEL	**Institute of Seismology, University of Helsinki, Finland**
HKC	**Hong Kong Observatory, Hong Kong**
HLW	**National Research Institute of Astronomy and Geophysics, Egypt**
HNR	Honiara, Solomon Islands
HRVD	Harvard University, USA
HRVD_LR	Department of Geological Sciences, Harvard University, USA
HYB	**National Geophysical Research Institute, India**
IAG	Instituto Andaluz de Geofisica, Spain
IASPEI	Working Group on Reference Events, USA
IDC	**The International Data Centre, Austria**
IGIL	**Instituto Geofisico do Infante D.Luiz, Portugal**
IGQ	**Instituto Geofisico Quito, Ecuador**
INMG	**Instituto de Meteorologia IP, Portugal**
IRIS	**IRIS Data Management Center, USA**
ISK	**Istanbul, Turkey**
ISN	**Iraqi Meteorological and Seismology Organisation, Iraq**
ISS	International Seismological Summary, United Kingdom
IST	Institute of Physics of the Earth, Turkey
JEN	**Geodynamisches Observatorium Moxa, Germany**
JMA	**Japan Meteorological Agency, Japan**
JSN	**Jamaica Seismic Network, Jamaica**
JSO	**Jordan Seismological Observatory, Jordan**
KISR	**Kuwait Institute for Scientific Research, Kuwait**
KLM	**Malaysian Meteorological Service, Malaysia**
KMA	**Korea Meteorological Administraion, Republic of Korea**
KNET	**IVTRAN Scientific Station, Kyrgyzstan**
KRSC	**Kamchatkan Experimental and Methodical Seismological Department, Russia**
LDG	**Laboratoire de detection et de geophysique, France**
LEDBW	**Landeserdbebendienst Baden-Wuerttemberg, Germany**
LIB	Tripoli, Libya
LIC	**Lamto Station, Ivory Coast**
LIS	Lisbon, Portugal
LIT	**Geological Survey of Lithuania, Lithuania**
LJU	**Environmental Agency of the Republic of Slovenia, Republic of Slovenia**
LPA	**Universidad Nacional de La Plata, Argentina**
LSZ	Geological Survey Department of Zambia, Zambia
MAN	**Philippine Institute of Volcanology and Seismology, Philippines**
MAT	**The Matsushiro Seismological Observatory, Japan**
MDD	**Instituto Geografico Nacional, Spain**
MED_RCMT	MedNet Regional Centroid - Moment Tensors, Italy
MEX	**Instituto de Geofisica de la UNAM, Mexico**
MOLD	**Institute of Geophysics and Geology, Republic of Moldova**
MOS	**Geophysical Survey of Russian Academy of Sciences, Russia**
MOZ	Direccao Nacional de Geologia, Mozambique
MSSP	**Micro Seismic Studies Programme, PINSTECH, Pakistan**
NAO	**NORSAR, Norway**
NDI	**India Meteorological Department, India**
NEIC	**National Earthquake Information Center, USA**
NEIS	National Earthquake Information Service, USA
NERS	**North Eastern Regional Seismological Centre, Russia**
NIC	**Cyprus Geological Survey Department, Cyprus**
NIED	**National Research Institute for Earth Science and Disaster Prevention, Japan**
NNC	**Kazakhstan National Data Center, Kazakhstan**
NOU	**IRD Centre de Noumea, New Caledonia**
NSSC	**National Syrian Seismological Center, Syria**
NSSP	**National Survey of Seismic Protection, Armenia**
OMAN	**Sultan Qaboos University, Oman**
ORF	Orfeus Data Center, Netherlands
OTT	**National Earthquake Hazards Program, Canada**
PDG	**Seismological Institute of Montenegro, Montenegro**
PGC	Pacific Geoscience Centre, Canada
PIST	P. Stahl, France

5.1: Continued.

Agency Code	Agency Name
PLV	**National Center for Scientific Research, Vietnam**
PMEL	Pacific seismicity from hydrophones, USA
PNSN	**Pacific Northwest Seismic Network, USA**
PPT	**Laboratoire de Geophysique/CEA, French Polynesia**
PRE	**Council for Geoscience, South Africa**
PRU	**Geophysical Institute, Academy of Sciences of the Czech Republic, Czech Republic**
QCP	**Manila Observatory, Philippines**
RBA	Universite Mohammed V, Morocco
REY	Vedurstofa Islands Bulletin, Iceland
ROM	**Istituto Nazionale di Geofisica e Vulcanologia, Italy**
ROTZ	Geophysikalisches Observatorium - Rotzenmuhle, Germany
RSPR	**Red Sismica de Puerto Rico, USA**
RYD	King Saud University, Saudi Arabia
SAPSE	Southern Alps Passive Seismic Experiment, New Zealand
SEA	Geophysics Program AK-50, USA
SEPA	Seismic Experiment in Patagonia and Antarctica, USA
SGS	**Saudi Geological Survey, Saudi Arabia**
SIK	Seismic Institute of Kosovo, Kosovo
SIO	**Scripps Institution of Oceanography, USA**
SKHL	**Sakhalin Experimental and Methodological Seismological Expedition, Russia**
SKO	**Republic of Macedonia Seismological Observatory, Republic of Macedonia**
SLC	Salt Lake City, USA
SNSN	Saudi National Seismic Network, Saudi Arabia
SOF	**Bulgarian Academy of Sciences, Bulgaria**
SPA	USGS - South Pole, Antarctica
SSN	Sudan Seismic Network, Sudan
SSNC	**Servicio Sismologico Nacional de Cuba, Cuba**
STR	**Institut de Physique du Globe, France**
SVSA	**Sistema de Vigilancia Sismologica dos Acores, Portugal**
SYO	**National Institute of Polar Research, Japan**
SZGRF	Seismologisches Zentralobservatorium Grafenburg, Germany
TAB	Tabriz Seismological Observatory, Iran
TAN	Antananarivo, Madagascar
TANZANIA	Tanzania Broadband Seismic Experiment, USA
TAP	**CWB, Chinese Taipei**
TEH	**Tehran University, Iran**
THE	**Aristotle University, Greece**
THR	**Int. Institute of Earthquake Engineering & Seismology, Iran**
TIF	**Seismic Monitoring Centre of Georgia, Georgia**
TIR	**Academy of Sciences of Albania, Albania**
TRI	**Osserv. Geofisico Sperimentale, Italy**
TRN	**University of the West Indies, Trinidad and Tobago**
TUL	Oklahoma Geological Survey, USA
TUN	Institut National de la Meteorologie, Tunisia
UAV	Red Sismologica de Los Andes Venezolanos, Venezuela
UCC	**Royal Observatory of Belgium, Belgium**
ULE	University of Leeds, United Kingdom
UNK	Unknown source, Unknown
UPP	University of Uppsala, Sweden
USGS	**US Geological Survey, USA**
VAO	**Instituto Astronomico e Geofisico, Brazil**
VIE	**Vsterreichischer Geophysikalischer Dienst, Austria**
WAR	**Polish Academy of Sciences, Poland**
WBNET	**West Bohemia Seismic Network, Czech Republic**
WEL	**Institute of Geological and Nuclear Sciences, New Zealand**
ZAG	**Seismological Survey of the Republic of Croatia, Croatia**
ZUR	**ETH Zurich, Switzerland**

5.2 ISC location algorithm

The new ISC location algorithm is described in detail in *Bondár and Storchak* (in press); here we give a short summary of the major features. Ever since the ISC came into existence in 1964, it has been committed to providing a homogeneous bulletin that benefits scientific research. Hence the location algorithm used by the ISC, except for some minor modifications, remained largely unchanged for the past 40 years (*Adams et al.*, 1982; *Bolt*, 1960). While the ISC location procedures have served the scientific community well in the past, they can certainly be improved.

Linearised location algorithms are very sensitive to the initial starting point for the location. The old procedures made the assumption that a good initial hypocentre is available among the reported hypocentres. However, there is no guarantee that any of the reported hypocentres are close to the global minimum in the search space. Furthermore, attempting to find a free depth solution was futile when the data had no resolving power for depth (e.g. when the first arrival is not within the inflection point of the P travel-time curve). When there was no depth resolution, the algorithm would simply pick a point on the origin time – depth trade-off curve. The old ISC locator assumed that the observational errors are independent. The recent years have seen a phenomenal growth both in the number of reported events and phases, owing to the ever-increasing number of stations worldwide. Similar ray paths will produce correlated travel-time prediction errors due to unmodeled heterogeneities in the Earth, resulting in underestimated location uncertainties, and for unfavourable network geometries, location bias. Hence, accounting for correlated travel-time prediction errors becomes imperative if we wanted to improve (or simply maintain) location accuracy as station networks become progressively denser. Finally, publishing network magnitudes that may have been derived from a single station measurement was rather prone to producing erroneous event magnitude estimates.

To meet the challenge imposed by the ever-increasing data volume from heavily unbalanced networks we introduced a new ISC location algorithm to ensure the efficient handling of data and to further improve the location accuracy of events reviewed by the ISC. The new ISC location algorithm

- Uses all ak135 (*Kennett et al.*, 1995) predicted phases (including depth phases) in the location;
- Obtains the initial hypocentre guess via the Neighbourhood Algorithm (NA) (*Sambridge*, 1999; *Sambridge and Kennett*, 2001);
- Performs iterative linearised inversion using an *a priori* estimate of the full data covariance matrix to account for correlated model errors (*Bondár and McLaughlin*, 2009a);
- Attempts a free-depth solution if and only if there is depth resolution, otherwise it fixes the depth to a region-dependent default depth;
- Scales uncertainties to 90% confidence level and calculates location quality metrics for various distance ranges;
- Obtains a depth-phase depth estimate based on reported surface reflections via depth-phase stacking (*Murphy and Barker*, 2006);
- Provides robust network magnitude estimates with uncertainties.

Seismic Phases

One of the major advantages of using the ak135 travel-time predictions (*Kennett et al.*, 1995) is that they do not suffer from the baseline difference between P, S and PKP phases compared to the Jeffreys-Bullen tables (*Jeffreys and Bullen*, 1940). Furthermore, ak135 offers an abundance of phases from the IASPEI Standard Seismic List that can be used in the location, most notably the PKP branches and depth-sensitive phases. Elevation and ellipticity corrections (*Dziewonski and Gilbert*, 1976; *Engdahl et al.*, 1998; *Kennett et al.*, 1996), using the WG84 ellipsoid parameters, are added to the ak135 predictions. For depth phases, bounce point (elevation correction at the surface reflection point) and water depth (for pwP) corrections are calculated by the algorithm of *Engdahl et al.* (1998). We use the ETOPO1 global relief model (*Amante and Eakins*, 2009) to obtain the elevation or the water depth at the bounce point.

Phase picking errors are described by *a priori* measurement error estimates derived from the inspection of the distribution of ground truth residuals (residuals calculated with respect to the ground truth location) from the IASPEI Reference Event List (*Bondár and McLaughlin*, 2009b). For phases that do not have sufficient number of observations in the ground truth database we established *a priori* measurement errors so that the consistency of the relative weighting schema is maintained. First-arriving P-type phases (P, Pn, Pb, Pg) are picked more accurately than later phases, so their measurement error estimates are the smallest, 0.8s. The measurement error for first-arriving S-phases (S, Sn, Sb, Sg) is set to 1.5s. Phases traversing through or reflecting from the inner/outer core of the Earth have somewhat larger (1.3s for PKP, PKS, PKKP, PKKS and P'P' branches as well as PKiKP, PcP and PcS, and 1.8s for SKP, SKS, SKKP, SKKS and S'S' branches as well as SKiKP, ScP and ScS) measurement error estimates to account for possible identification errors among the various branches. Free-surface reflections and conversions (PnPn, PbPb, PgPg, PS, PnS, PgS and SnSn, SbSb, SgSg, SP, SPn, SPg) are observed less frequently and with larger uncertainty, and therefore suffer from large, 2.5s, measurement errors. Similarly, a measurement error of 2.8s is assigned to the longer period and typically emergent diffracted phases (Pdif, Sdif, PKPdif). The *a priori* measurement error for the commonly observed depth phases (pP, sP, pS, sS and pwP) is set to 1.3s, while for the rest of depth phases (pPKP, sPKP, pSKS, sSKS branches and pPb, sPb, sSb, pPn, sPn, sSn) the measurement error estimate is set to 1.8s. We set the measurement error estimate to 2.5s for the less reliable depth phases (pPg, sPg, sSg, pPdif, pSdif, sPdif and sSdif). Note that we also allow for distance-dependent measurement errors. For instance, to account for possible phase identification errors at far-regional distances the *a priori* measurement error for Pn and P is increased from 0.8s to 1.2s and for Sn and S from 1.5s to 1.8s between 15 and 28°. The measurement errors between 40 and 180° are set to 1.3s and 1.8s for the prominent PP and SS arrivals respectively, but they are increased to 1.8s and 2.5s between 25 and 40°.

The relative weighting scheme (Figure 5.1) described above ensures that arrivals picked less reliably or prone to phase identification errors are down-weighted in the location algorithm. Since the ISC works with reported parametric data with wildly varying quality, we opted for a rather conservative set of *a priori* measurement error estimates.

Correlated travel-time prediction error structure

Most location algorithms, either linearised or non-linear, assume that all observational errors

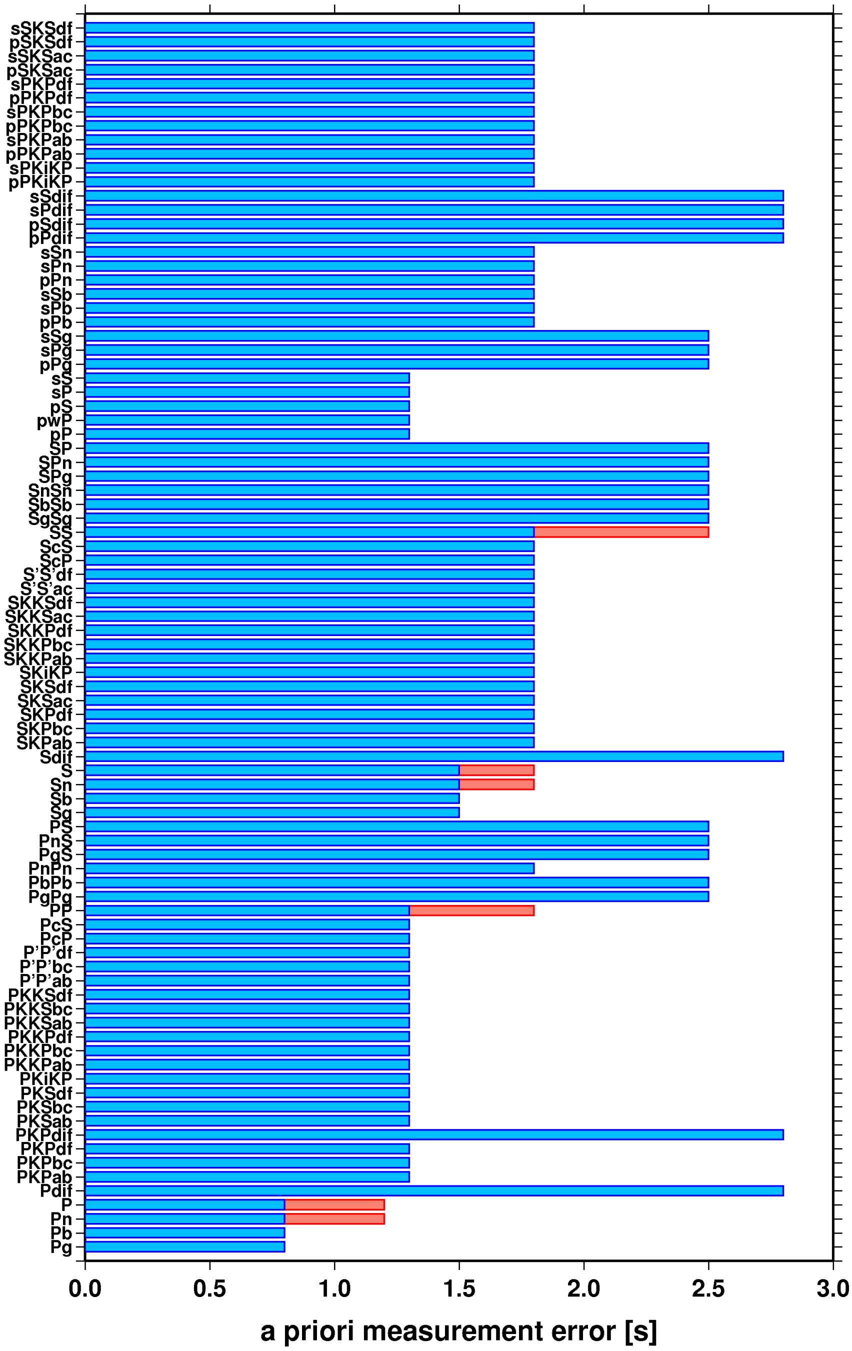

Figure 5.1: *A priori* measurement error estimates for phases used in the location algorithm.

are independent. This assumption is violated when the separation between stations is less than the scale length of local velocity heterogeneities. When correlated travel-time prediction errors are present, the data covariance matrix is no longer diagonal, and the redundancy in the observations reduces the effective number of degrees of freedom. Thus, ignoring the correlated error structure inevitably results in underestimated location uncertainty estimates. For events located by an unbalanced seismic network this may also lead to a biased location estimate. *Chang et al.* (1983) demonstrated that accounting for correlated error structure in a linearised location algorithm is relatively straightforward once an estimate of the non-diagonal data covariance matrix is available. To determine the data covariance matrix we follow the approach described by *Bondár and McLaughlin* (2009a). They assume that the similarity between ray paths is well approximated by the station separation. This simplifying assumption allows for the estimation of covariances between station pairs from a generic P variogram model derived from ground truth residuals. Because the overwhelming number of phases in the ISC bulletin is teleseismic P, we expect that the generic variogram model will perform reasonably well anywhere on the globe.

Since in this representation the covariances depend only on station separations, the covariance matrix (and its inverse) needs to be calculated only once. We assume that different phases owing to the different ray paths they travel along, as well as station pairs with a separation larger than 1000 km are uncorrelated. Hence, the data covariance matrix is a sparse, block-diagonal matrix. Furthermore, if the stations in each phase block are ordered by their nearest neighbour distance, the phase blocks themselves become block-diagonal. To reduce the computational time of inverting large matrices we exploit the inherent block-diagonal structure by inverting the covariance matrix block-by-block. The *a priori* measurement error variances are added to the diagonal of the data covariance matrix.

Depth resolution

In principle, depth can be resolved if there is a mixture of upgoing and downgoing waves emanated from the source, that is, if there are stations covering the distance range where the vertical partial derivative of the travel-time of the first-arriving phase changes sign (local networks), or if there are phases with vertical slowness of opposite sign (depth phases). Core reflections, such as PcP, and to a lesser extent, secondary phases (S in particular) could also help in resolving the depth.

We developed a number of criteria to test whether the reported data for an event have sufficient depth resolution:

- local network: one or more stations within 0.2° with time-defining phases
- depth phases: five or more time-defining depth phases reported by at least two agencies (to reduce a chance of misinterpretation by a single inexperienced analyst)
- core reflections: five or more time-defining core reflections (PcP, ScS) reported by at least two agencies

- local/near regional S: five or more time-defining S and P pairs within 5°

We attempt a free-depth solution if any of the above criteria are satisfied; otherwise we fix the depth to a default depth dependent on the epicentre location. The default depth grid was derived from the EHB (*Engdahl et al.*, 1998) free-depth solutions, including the fixed-depth EHB earthquakes that were flagged as having reliable depth estimate (personal communication with Bob Engdahl), as well as from free-depth solutions obtained by the new locator when relocating the entire ISC bulletin. As Figure 5.2 indicates, the default depth grid provides a reasonable depth estimate where seismicity is well established. Note that the depths of known anthropogenic events and landslides are fixed to the surface.

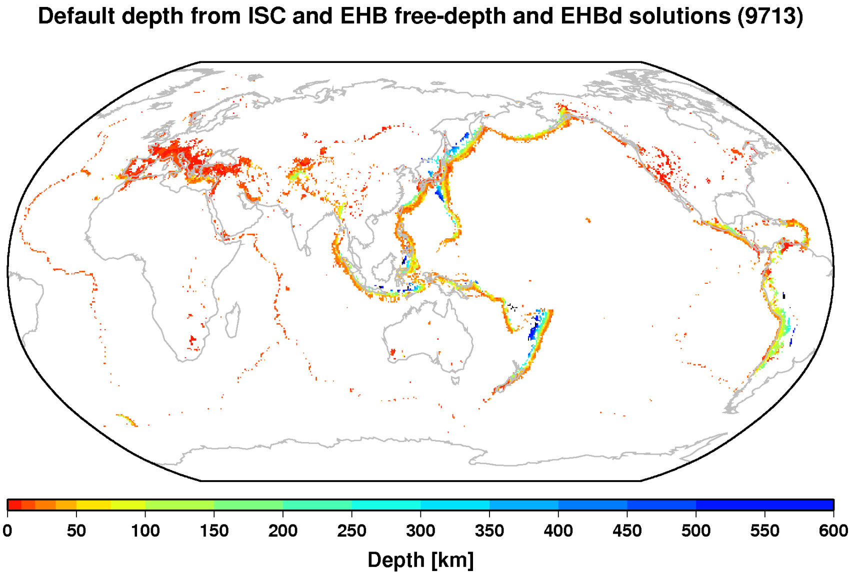

Figure 5.2: Default depths on a 0.5×0.5 degree grid derived from EHB free-depth solutions and EHB events flagged as reliable depth, as well as free-depth solutions from the entire ISC bulletin relocated with the new locator.

Depth-phase stack

While we use depth phases directly in the location, the depth-phase stacking method (*Murphy and Barker*, 2006) provides an independent means to obtain robust depth estimates. Because the depth obtained from the depth-phase stacking method implicitly depends on the epicentre itself, we perform the depth-phase stack only twice: first, with respect to the initial location in order to obtain a reasonable starting point for the depth in the grid search described in the following section; second, with respect to the final location to obtain the final estimate for the depth-phase constrained depth.

Initial hypocentre

For poorly recorded events the reported hypocentres may exhibit a large scatter and they could suffer from large location errors, especially if they are only recorded teleseismically. In order to obtain a good initial hypocentre guess for the linearised location algorithm we employ the Neighbourhood Algorithm (NA) (*Sambridge*, 1999; *Sambridge and Kennett*, 2001). NA is a nonlinear grid search method capable of exploring a large search space and rapidly closing on the global optimum. *Kennett* (2006) discusses in detail the NA algorithm and its use for locating earthquakes.

We perform a search around the median of reported hypocentre parameters with a generously defined search region – within a 2-degree radius circle around the median epicentre, 10 seconds around the median origin time and 150 km around the median reported depth. These default search parameters were obtained by trial-and-error runs to achieve a compromise between execution time and allowance for gross errors in the median reported hypocentre parameters. Note that if our test for depth resolution fails, we fix the depth to the region-dependent default depth. The initial hypocentre estimate will be the one with the smallest L1-norm misfit among the NA trial hypocentres. Once close to the global optimum, we proceed with the linearised location algorithm to obtain the final solution and corresponding formal uncertainties.

Iterative linearised location algorithm

We adopt the location algorithm described in detail in *Bondár and McLaughlin* (2009a). Recall that in the presence of correlated travel-time prediction errors the data covariance matrix is no longer diagonal. Using the singular value decomposition of the data covariance matrix we construct a projection matrix that orthogonalises the data set and projects redundant observations into the null space. In other words, we solve the inversion problem in the eigen coordinate system in which the transformed observations are independent.

The model covariance matrix yields the four-dimensional error ellipsoid whose projections provide the two-dimensional error ellipse and one-dimensional errors for depth and origin time. These uncertainties are scaled to the 90% confidence level. Note that since we projected the system of equations into the eigen coordinate system, the number of independent observations is less than the total number of observations. Hence, the estimated location error ellipses necessarily become larger, providing a more realistic representation of the location uncertainties. The major advantage of this approach is that the projection matrix is calculated only once for each event location.

Validation tests

To demonstrate improvements due to the new location procedures, we relocated some 7,200 GT0-5 events in the IASPEI Reference Event List (*Bondár and McLaughlin*, 2009b) both with the old ISC locator (which constitutes the baseline) and with the new location algorithm. We also relocated the entire (1960-2010) ISC Bulletin, including four years of the International Seismological Summary (ISS, the predecessor of the ISC) catalogue (*Villaseñor and Engdahl*, 2005; 2007).

The relocation of GT events demonstrated that the new ISC location algorithm provides small, but consistent location improvements, considerable improvements in depth determination and significantly more accurate formal uncertainty estimates. Even using a 1D model and a variogram model that fits teleseismic observations we could achieve realistic uncertainty estimates, as the 90% confidence error ellipses cover the true locations 80-85% of the time. The default depth grid provides reasonable depth estimates where there is seismicity. We have shown that the location and depth accuracy obtained by the new algorithm matches or surpasses the EHB accuracy. We noted above that the location improvements for the ground truth events are consistent, but minor. This is not surprising as most of the events in the IASPEI Reference Event List are very well-recorded with a small azimuthal gap and dominated by P-type phases. In these circumstances we could expect significant location improvements only for heavily unbalanced networks where large numbers of correlated ray paths conspire to introduce location bias. On the other hand, the ISC Bulletin represents a plethora of stations configurations ranging from reasonable to the most unfavourable network geometries. Hence, we could expect more dramatic location improvements when relocating the entire ISC Bulletin. Although in this case we cannot measure the improvement in location accuracy due to the lack of ground truth information, we show that with the new locator we obtain significantly better clustering of event locations (Figure 5.3), thus providing an improved view of the seismicity of the Earth.

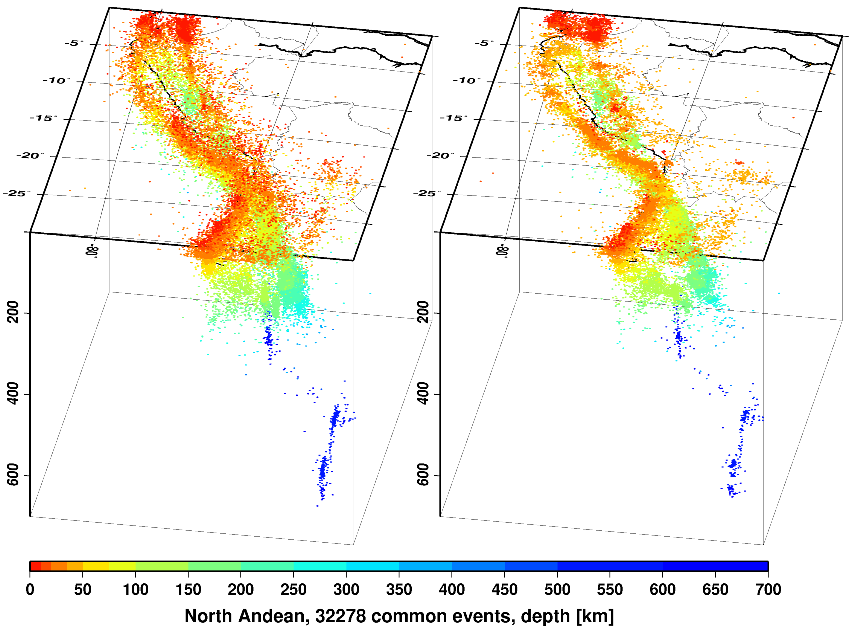

(a)

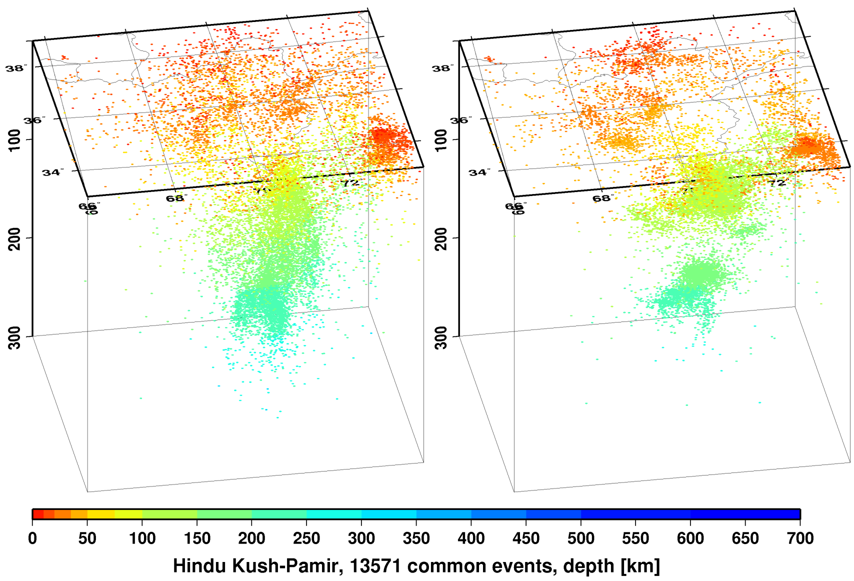

(b)

Figure 5.3: Comparison of seismicity maps for common events in the reviewed ISC Bulletin (old locator, left) and the relocated ISC bulletin (new locator, right) for the North Andean and Hindu Kush - Pamir region. The events are better clustered when located with the new locator.

5.3 Review Process

The ISC Bulletin editors review all events with reported magnitudes greater than 3.5, all events reported by the International Data Centre in Vienna (IDC), and all events that follow the criteria described by the automatic thresholding process. This typically accounts for approximately 20% of all events reported to the ISC and usually consists of 3500–5000 events per month.

The automatic thresholding process creates a monthly listing of the events for the editors to review. The analysis takes place for one month at a time and is processed in batches (therefore, an event is not finished one at a time, and only whole months are published at once). The first batch of editing consists of the editors reviewing all events for the month. The entire month is relocated after the necessary changes have been executed as decided by an editor. The editor then reviews the same events and compares the first solution and the revised solution with the changes that were made. Once an editor is satisfied with an event, it is no longer revised for the subsequent pass. But the analysis will continue in 'passes' until all events are satisfactory.

The editors print the entire monthly listing, which is split up into sections separated by number of events (typically 150 events in a section). Each event (one unique ID per event) on the monthly printout shows all reported hypocentres (there can be multiple reported hypocentres for each event), reported magnitudes (when available), the geographic region and phase arrival times and phase arrival time residuals.

The editors have the capability to execute a variety of commmands which can be used to move phase arrivals or hypocentres from one event to another or modify phase arrivals. There are several commands to change the depth of an event or change the starting location of the location algorithm.

The basic philosophy of reviewing the ISC Bulletin is to:

1. Check that the depth of the event is suitable for the seismic region and for the reported phase arrivals.
2. Check that an event is not missing any data that is expected for the region/magnitude and also that all of the data in the event belongs to it.
3. Examine phase time residuals.
4. Look for outliers and or misassociated phases

When editors remove misassociated phases from an event, the phases are introduced to the data flow. These phases are made available to be associated to a different event if the time and location are suitable.

Along with examining each individual event closely, it is also important to look at all events (and hypocentres) reported closely in time and space to ensure that the grouping of the events was done correctly. In some cases, two separately grouped events will be merged into one event.

In other cases, one event with more than one hypocentre can be split into two events, when the grouping has created one event from two closely occurring yet different events.

Final checks

For quality control, there is a set of programs that are run once a data month has been processed. These programs check for inconsistencies and errors. Also, at the end of the monthly analysis, 'Search' events can be created. These are events with no reported hypocentres and are created with unassociated phase arrivals (from one or more agencies).

6

Availability of the ISC Bulletin

BD:

- This volume.
- Web searches - include explanation.
- CD-ROMs.
- Mirror services.

7

IASPEI standards

7.1 Standard nomenclature of seismic phases

The following list of seismic phases was approved by the IASPEI Commission on Seismological Observation and Interpretation (CoSOI) and adopted by IASPEI on 9th July 2003. More details can be found in *Storchak et al.* (2003). Ray paths for some of these phases are shown in figures 7.1–7.6.

Crustal Phases	
Pg	At short distances, either an upgoing P wave from a source in the upper crust or a P wave bottoming in the upper crust. At larger distances also arrivals caused by multiple P-wave reverberations inside the whole crust with a group velocity around 5.8 km/s.
Pb	Either an upgoing P wave from a source in the lower crust or a P wave bottoming in the lower crust (alt: P*)
Pn	Any P wave bottoming in the uppermost mantle or an upgoing P wave from a source in the uppermost mantle
PnPn	Pn free-surface reflection
PgPg	Pg free-surface reflection
PmP	P reflection from the outer side of the Moho
PmPN	PmP multiple free surface reflection; N is a positive integer. For example, PmP2 is PmPPmP.
PmS	P to S reflection from the outer side of the Moho
Sg	At short distances, either an upgoing S wave from a source in the upper crust or an S wave bottoming in the upper crust. At larger distances also arrivals caused by superposition of multiple S-wave reverberations and SV to P and/or P to SV conversions inside the whole crust.
Sb	Either an upgoing S wave from a source in the lower crust or an S wave bottoming in the lower crust (alt: S*)
Sn	Any S wave bottoming in the uppermost mantle or an upgoing S wave from a source in the uppermost mantle
SnSn	Sn free-surface reflection
SgSg	Sg free-surface reflection
SmS	S reflection from the outer side of the Moho
SmSN	SmS multiple free-surface reflection; N is a positive integer. For example, SmS2 is SmSSmS.
SmP	S to P reflection from the outer side of the Moho
Lg	A wave group observed at larger regional distances and caused by superposition of multiple S-wave reverberations and SV to P and/or P to SV conversions inside the whole crust. The maximum energy travels with a group velocity around 3.5 km/s.
Rg	Short-period crustal Rayleigh wave
Mantle Phases	
P	A longitudinal wave, bottoming below the uppermost mantle; also an upgoing longitudinal wave from a source below the uppermost mantle

PP	Free-surface reflection of P wave leaving a source downward
PS	P, leaving a source downward, reflected as an S at the free surface. At shorter distances the first leg is represented by a crustal P wave.
PPP	Analogous to PP
PPS	PP to S converted reflection at the free surface; travel time matches that of PSP
PSS	PS reflected at the free surface
PcP	P reflection from the core-mantle boundary (CMB)
PcS	P to S converted reflection from the CMB
PcPN	PcP multiple free-surface reflection; N is a positive integer. For example PcP2 is PcPPcP.
Pz+P	P reflection from outer side of a discontinuity at depth z; z may be a positive numerical value in km. For example, P660+P is a P reflection from the top of the 660 km discontinuity. (alt: PzP)
Pz-P	P reflection from inner side of discontinuity at depth z. For example, P660-P is a P reflection from below the 660 km discontinuity, which means it is precursory to PP.
Pz+S	P to S converted reflection from outer side of discontinuity at depth z (alt: PzS)
Pz-S	P to S converted reflection from inner side of discontinuity at depth z
PScS	P (leaving a source downward) to ScS reflection at the free surface
Pdif	P diffracted along the CMB in the mantle (old: Pdiff)
S	Shear wave, bottoming below the uppermost mantle; also an upgoing shear wave from a source below the uppermost mantle
SS	Free-surface reflection of an S wave leaving a source downward
SP	S, leaving source downward, reflected as P at the free surface. At shorter distances the second leg is represented by a crustal P wave.
SSS	Analogous to SS
SSP	SS to P converted reflection at the free surface; travel time matches that of SPS.
SPP	SP reflected at the free surface
ScS	S reflection from the CMB
ScP	S to P converted reflection from the CMB
ScSN	ScS multiple free-surface reflection; N is a positive integer. For example ScS2 is ScSScS.
Sz+S	S reflection from outer side of a discontinuity at depth z; z may be a positive numerical value in km. For example S660+S is an S reflection from the top of the 660 km discontinuity. (alt: SzS)
Sz-S	S reflection from inner side of discontinuity at depth z. For example, S660-S is an S reflection from below the 660 km discontinuity, which means it is precursory to SS.
Sz+P	S to P converted reflection from outer side of discontinuity at depth z (alt: SzP)
Sz-P	S to P converted reflection from inner side of discontinuity at depth z
ScSP	ScS to P reflection at the free surface
Sdif	S diffracted along the CMB in the mantle (old: Sdiff)
Core Phases	
PKP	Unspecified P wave bottoming in the core (alt: P')
PKPab	P wave bottoming in the upper outer core; ab indicates the retrograde branch of the PKP caustic (old: PKP2)
PKPbc	P wave bottoming in the lower outer core; bc indicates the prograde branch of the PKP caustic (old: PKP1)
PKPdf	P wave bottoming in the inner core (alt: PKIKP)
PKPpre	A precursor to PKPdf due to scattering near or at the CMB (old: PKhKP)

PKPdif	P wave diffracted at the inner core boundary (ICB) in the outer core
PKS	Unspecified P wave bottoming in the core and converting to S at the CMB
PKSab	PKS bottoming in the upper outer core
PKSbc	PKS bottoming in the lower outer core
PKSdf	PKS bottoming in the inner core
P'P'	Free-surface reflection of PKP (alt: PKPPKP)
P'*N*	PKP reflected at the free surface *N* - 1 times; *N* is a positive integer. For example, P'3 is P'P'P'. (alt: PKP*N*)
P'*z*-P'	PKP reflected from inner side of a discontinuity at depth *z* outside the core, which means it is precursory to P'P'; *z* may be a positive numerical value in km.
P'S'	PKP to SKS converted reflection at the free surface; other examples are P'PKS, P'SKP (alt: PKPSKS)
PS'	P (leaving a source downward) to SKS reflection at the free surface (alt: PSKS)
PKKP	Unspecified P wave reflected once from the inner side of the CMB
PKKPab	PKKP bottoming in the upper outer core
PKKPbc	PKKP bottoming in the lower outer core
PKKPdf	PKKP bottoming in the inner core
P*N*KP	P wave reflected *N* - 1 times from inner side of the CMB; *N* is a positive integer.
PKKPpre	A precursor to PKKP due to scattering near the CMB
PKiKP	P wave reflected from the inner core boundary (ICB)
PK*N*IKP	P wave reflected *N* - 1 times from the inner side of the ICB
PKJKP	P wave traversing the outer core as P and the inner core as S
PKKS	P wave reflected once from inner side of the CMB and converted to S at the CMB
PKKSab	PKKS bottoming in the upper outer core
PKKSbc	PKKS bottoming in the lower outer core
PKKSdf	PKKS bottoming in the inner core
PcPP'	PcP to PKP reflection at the free surface; other examples are PcPS', PcSP', PcSS', PcPSKP, PcSSKP. (alt: PcPPKP)
SKS	unspecified S wave traversing the core as P (alt: S')
SKSac	SKS bottoming in the outer core
SKSdf	SKS bottoming in the inner core (alt: SKIKS)
SPdifKS	SKS wave with a segment of mantleside Pdif at the source and/or the receiver side of the ray path (alt: SKPdifS)
SKP	Unspecified S wave traversing the core and then the mantle as P
SKPab	SKP bottoming in the upper outer core
SKPbc	SKP bottoming in the lower outer core
SKPdf	SKP bottoming in the inner core
S'S'	Free-surface reflection of SKS (alt: SKSSKS)
S'*N*	SKS reflected at the free surface *N* - 1 times; *N* is a positive integer
S'*z*-S'	SKS reflected from inner side of discontinuity at depth *z* outside the core, which means it is precursory to S'S'; *z* may be a positive numerical value in km.
S'P'	SKS to PKP converted reflection at the free surface; other examples are S'SKP, S'PKS. (alt: SKSPKP)
S'P	SKS to P reflection at the free surface (alt: SKSP)
SKKS	Unspecified S wave reflected once from inner side of the CMB
SKKSac	SKKS bottoming in the outer core
SKKSdf	SKKS bottoming in the inner core
S*N*KS	S wave reflected *N* - 1 times from inner side of the CMB; *N* is a positive integer.
SKiKS	S wave traversing the outer core as P and reflected from the ICB
SKJKS	S wave traversing the outer core as P and the inner core as S

SKKP	S wave traversing the core as P with one reflection from the inner side of the CMB and then continuing as P in the mantle
SKKPab	SKKP bottoming in the upper outer core
SKKPbc	SKKP bottoming in the lower outer core
SKKPdf	SKKP bottoming in the inner core
ScSS'	ScS to SKS reflection at the free surface; other examples are ScPS', ScSP', ScPP', ScSSKP, ScPSKP. (alt: ScSSKS)
Near-source Surface reflections (Depth Phases)	
p*Py*	All P-type onsets (P*y*), as defined above, which resulted from reflection of an upgoing P wave at the free surface or an ocean bottom. WARNING: The character *y* is only a wild card for any seismic phase, which could be generated at the free surface. Examples are pP, pPKP, pPP, pPcP, etc.
sP*y*	All Py resulting from reflection of an upgoing S wave at the free surface or an ocean bottom; for example, sP, sPKP, sPP, sPcP, etc.
pS*y*	All S-type onsets (S*y*), as defined above, which resulted from reflection of an upgoing P wave at the free surface or an ocean bottom; for example, pS, pSKS, pSS, pScP, etc.
sS*y*	All Sy resulting from reflection of an upgoing S wave at the free surface or an ocean bottom; for example, sSn, sSS, sScS, sSdif, etc.
pwP*y*	All Py resulting from reflection of an upgoing P wave at the ocean's free surface
pmP*y*	All Py resulting from reflection of an upgoing P wave from the inner side of the Moho
Surface Waves	
L	Unspecified long-period surface wave
LQ	Love wave
LR	Rayleigh wave
G	Mantle wave of Love type
G*N*	Mantle wave of Love type; *N* is integer and indicates wave packets traveling along the minor arcs (odd numbers) or major arc (even numbers) of the great circle
R	Mantle wave of Rayleigh type
R*N*	Mantle wave of Rayleigh type; *N* is integer and indicates wave packets traveling along the minor arcs (odd numbers) or major arc (even numbers) of the great circle
PL	Fundamental leaking mode following P onsets generated by coupling of P energy into the waveguide formed by the crust and upper mantle SPL S wave coupling into the PL waveguide; other examples are SSPL, SSSPL.
Acoustic Phases	
H	A hydroacoustic wave from a source in the water, which couples in the ground
HPg	H phase converted to Pg at the receiver side
HSg	H phase converted to Sg at the receiver side
HRg	H phase converted to Rg at the receiver side
I	An atmospheric sound arrival which couples in the ground
IPg	I phase converted to Pg at the receiver side
ISg	I phase converted to Sg at the receiver side
IRg	I phase converted to Rg at the receiver side
T	A tertiary wave. This is an acoustic wave from a source in the solid earth, usually trapped in a low-velocity oceanic water layer called the SOFAR channel (SOund Fixing And Ranging).
TPg	T phase converted to Pg at the receiver side
TSg	T phase converted to Sg at the receiver side
TRg	T phase converted to Rg at the receiver side
Amplitude Measurement Phases	
A	Unspecified amplitude measurement

AML	Amplitude measurement for local magnitude
AMB	Amplitude measurement for body-wave magnitude
AMS	Amplitude measurement for surface-wave magnitude
END	Time of visible end of record for duration magnitude
Unidentified Arrivals	
x	unidentified arrival (old: i, e, NULL)
rx	unidentified regional arrival (old: i, e, NULL)
tx	unidentified teleseismic arrival (old: i, e, NULL)
Px	unidentified arrival of P type (old: i, e, NULL, (P), P?)
Sx	unidentified arrival of S type (old: i, e, NULL, (S), S?)

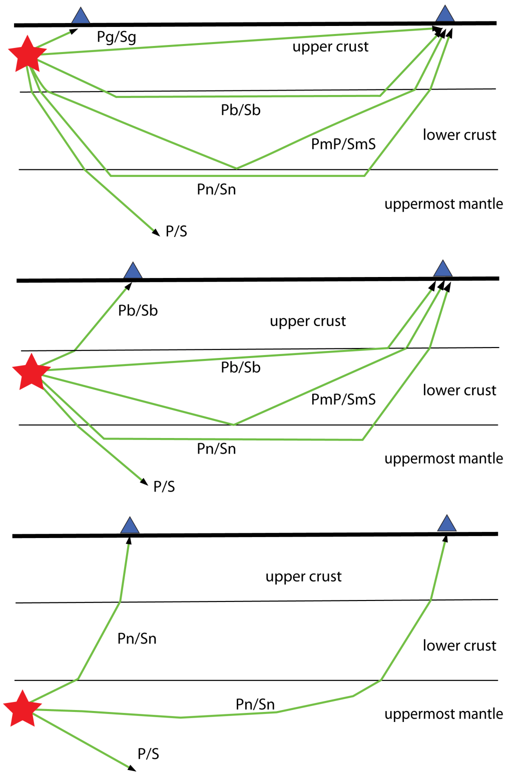

Figure 7.1: Seismic 'crustal phases' observed in the case of a two-layer crust in local and regional distance ranges (0°<D< about 20°) from the seismic source in the: upper crust (top); lower crust (middle); and uppermost mantle (bottom).

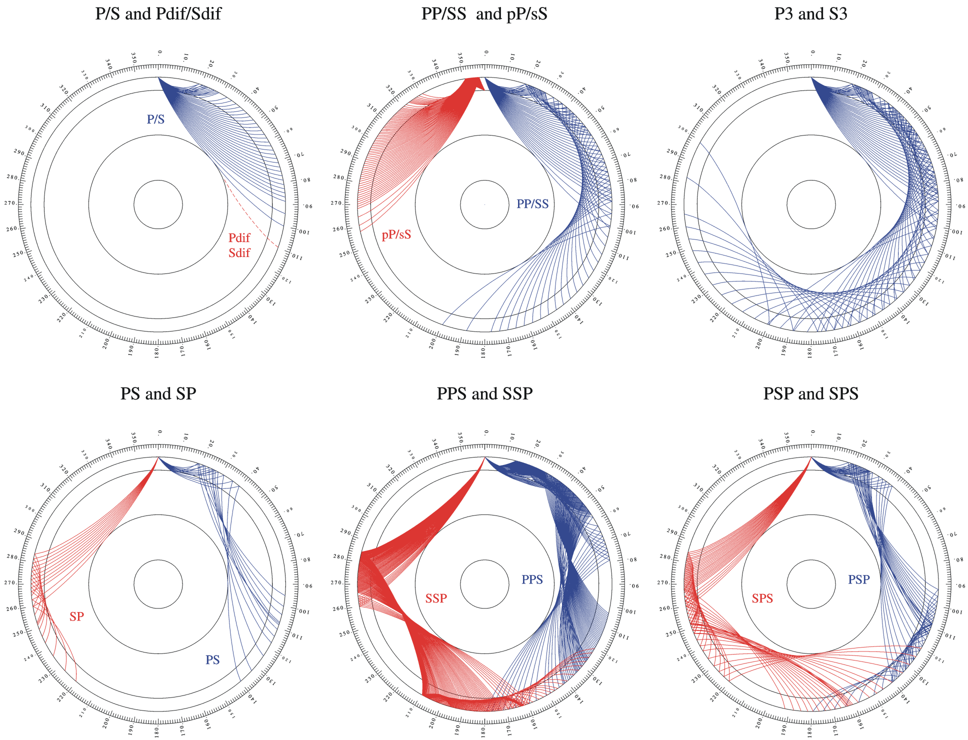

Figure 7.2: Mantle phases observed at the teleseismic distance range $D >$ about 20°.

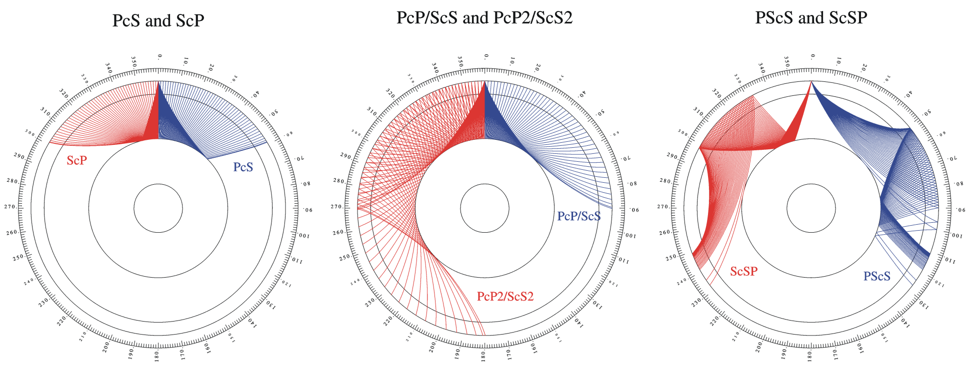

Figure 7.3: Reflections from the Earth's core.

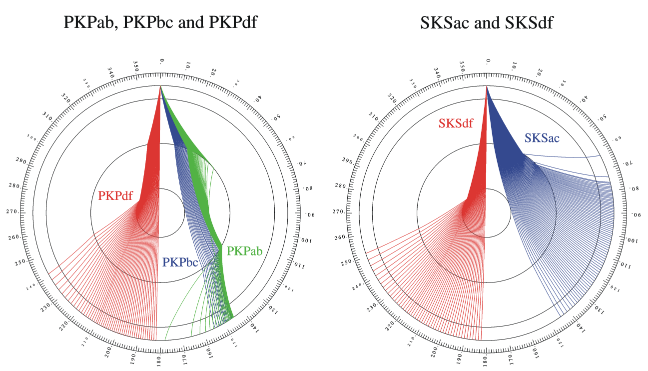

Figure 7.4: Seismic rays of direct core phases.

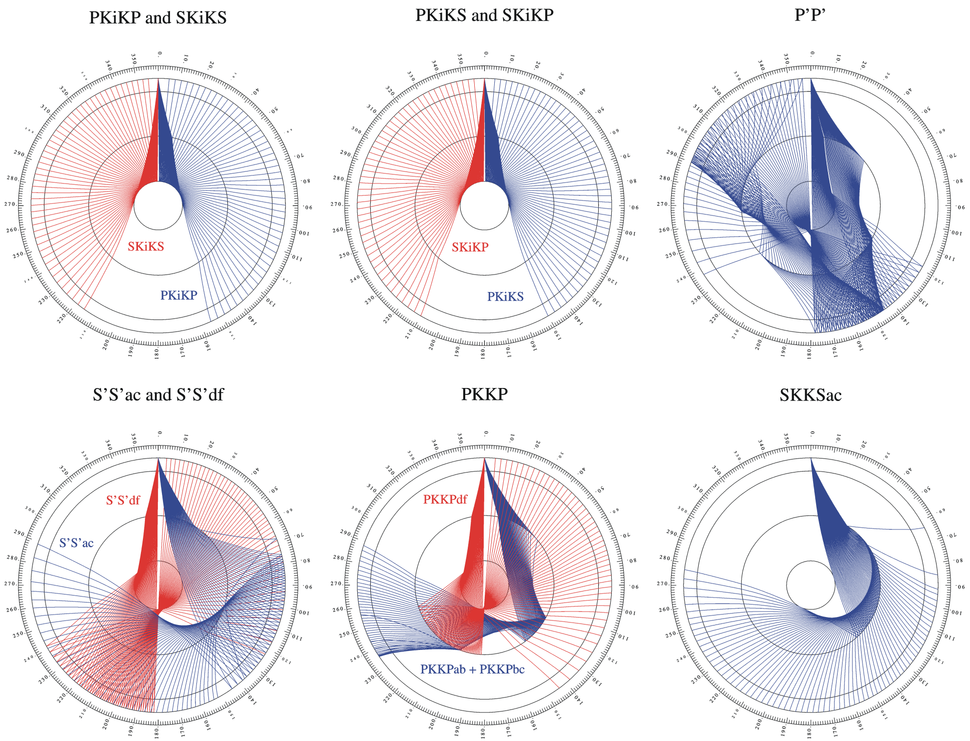

Figure 7.5: Seismic rays of single-reflected core phases.

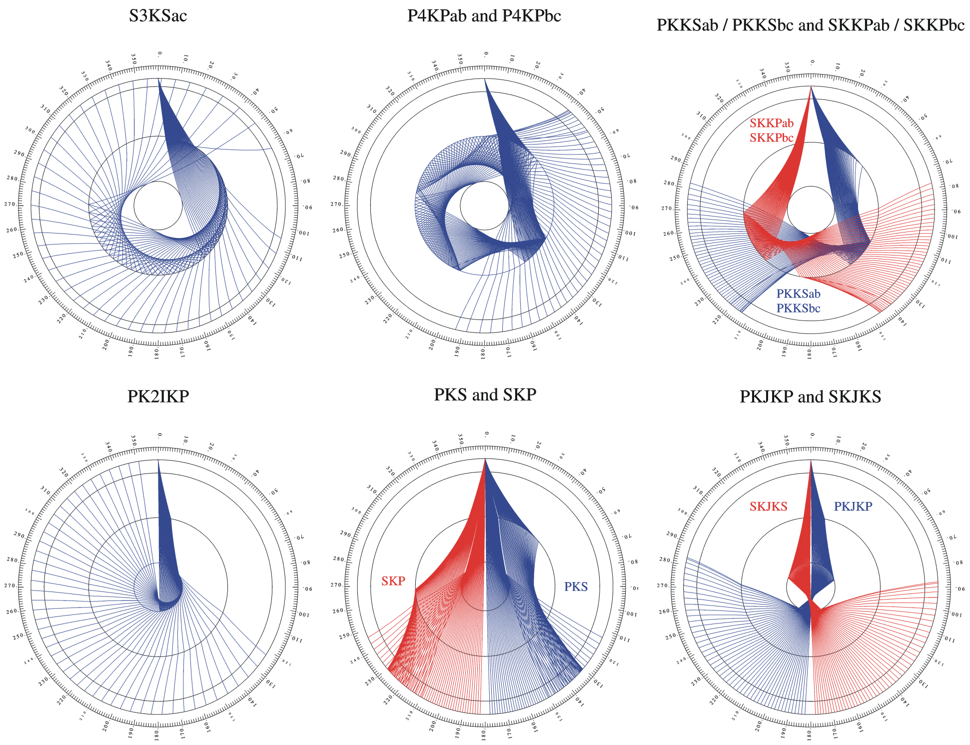

Figure 7.6: Seismic rays of multiple-reflected and converted core phases.

7.2 Flinn-Engdahl regions

The Flinn-Engdahl regions were first proposed by *Flinn and Engdahl* (1965), with the standard defined by *Flinn et al.* (1974). The latest version of the schema published by *Young et al.* (1996), divides the Earth into 50 seismic regions (figure 7.7), which are further subdivided producing a total of 754 geographical regions (listed below). The geographic regions are numbered 1 to 757 with regions 172, 299 and 550 no longer in use. The boundaries of these regions are defined at one-degree intervals.

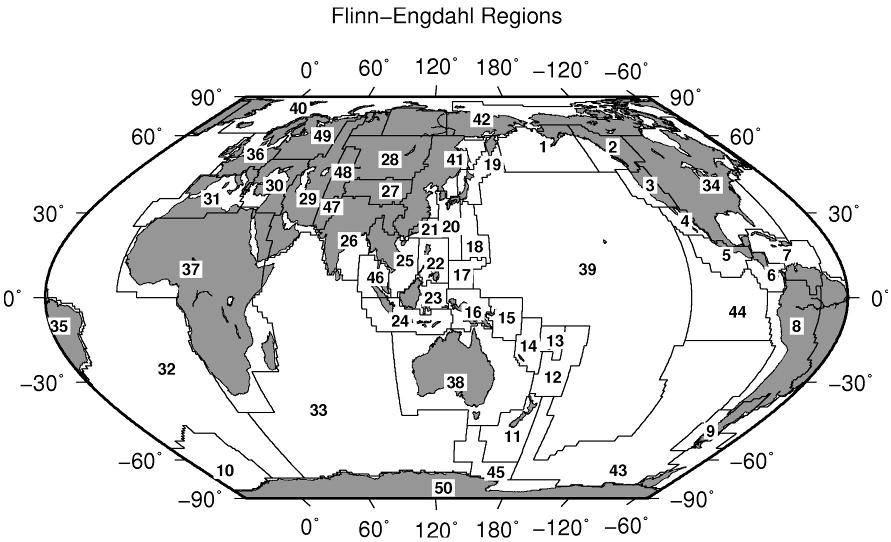

Figure 7.7: Map of all Flinn-Engdahl seismic regions.

Seismic Region 1
Alaska-Aleutian Arc
1. Central Alaska
2. Southern Alaska
3. Bering Sea
4. Komandorsky Islands region
5. Near Islands
6. Rat Islands
7. Andreanof Islands
8. Pribilof Islands
9. Fox Islands
10. Unimak Island region
11. Bristol Bay
12. Alaska Peninsula
13. Kodiak Island region
14. Kenai Peninsula
15. Gulf of Alaska
16. South of Aleutian Islands
17. South of Alaska

Seismic Region 2
Eastern Alaska to Vancouver Island
18. Southern Yukon Territory
19. Southeastern Alaska
20. Off coast of southeastern Alaska
21. West of Vancouver Island
22. Queen Charlotte Islands region
23. British Columbia
24. Alberta
25. Vancouver Island region
26. Off coast of Washington
27. Near coast of Washington
28. Washington-Oregon border region
29. Washington

Seismic Region 3
California-Nevada Region
30. Off coast of Oregon
31. Near coast of Oregon
32. Oregon
33. Western Idaho
34. Off coast of northern California
35. Near coast of northern California
36. Northern California
37. Nevada
38. Off coast of California
39. Central California
40. California-Nevada border region
41. Southern Nevada
42. Western Arizona
43. Southern California
44. California-Arizona border region
45. California-Baja California border region
46. Western Arizona-Sonora border region

Seismic Region 4
Lower California and Gulf of California
47. Off west coast of Baja California
48. Baja California
49. Gulf of California

50. Sonora
51. Off coast of central Mexico
52. Near coast of central Mexico

Seismic Region 5
Mexico-Guatemala Area
53. Revilla Gigedo Islands region
54. Off coast of Jalisco
55. Near coast of Jalisco
56. Near coast of Michoacan
57. Michoacan
58. Near coast of Guerrero
59. Guerrero
60. Oaxaca
61. Chiapas
62. Mexico-Guatemala border region
63. Off coast of Mexico
64. Off coast of Michoacan
65. Off coast of Guerrero
66. Near coast of Oaxaca
67. Off coast of Oaxaca
68. Off coast of Chiapas
69. Near coast of Chiapas
70. Guatemala
71. Near coast of Guatemala
730. Northern East Pacific Rise

Seismic Region 6
Central America
72. Honduras
73. El Salvador
74. Near coast of Nicaragua
75. Nicaragua
76. Off coast of central America
77. Off coast of Costa Rica
78. Costa Rica
79. North of Panama
80. Panama-Costa Rica border region
81. Panama
82. Panama-Colombia border region
83. South of Panama

Seismic Region 7
Caribbean Loop
84. Yucatan Peninsula
85. Cuba region
86. Jamaica region
87. Haiti region
88. Dominican Republic region
89. Mona Passage
90. Puerto Rico region
91. Virgin Islands
92. Leeward Islands
93. Belize
94. Caribbean Sea
95. Windward Islands
96. Near north coast of Colombia
97. Near coast of Venezuela
98. Trinidad
99. Northern Colombia
100. Lake Maracaibo
101. Venezuela
731. North of Honduras

Seismic Region 8
Andean South America
102. Near west coast of Colombia
103. Colombia
104. Off coast of Ecuador
105. Near coast of Ecuador
106. Colombia-Ecuador border region
107. Ecuador
108. Off coast of northern Peru
109. Near coast of northern Peru
110. Peru-Ecuador border region
111. Northern Peru
112. Peru-Brazil border region
113. Western Brazil
114. Off coast of Peru
115. Near coast of Peru
116. Central Peru
117. Southern Peru
118. Peru-Bolivia border region
119. Northern Bolivia
120. Central Bolivia
121. Off coast of northern Chile
122. Near coast of northern Chile
123. Northern Chile
124. Chile-Bolivia border region
125. Southern Bolivia
126. Paraguay
127. Chile-Argentina border region
128. Jujuy Province
129. Salta Province
130. Catamarca Province
131. Tucuman Province
132. Santiago del Estero Province
133. Northeastern Argentina
134. Off coast of central Chile
135. Near coast of central Chile
136. Central Chile
137. San Juan Province
138. La Rioja Province
139. Mendoza Province
140. San Luis Province
141. Cordoba Province
142. Uruguay

Seismic Region 9
Extreme South America
143. Off coast of southern Chile
144. Southern Chile
145. Southern Chile-Argentina border region
146. Southern Argentina

Seismic Region 10
Southern Antilles
147. Tierra del Fuego
148. Falkland Islands region
149. Drake Passage
150. Scotia Sea
151. South Georgia Island region
152. South Georgia Rise
153. South Sandwich Islands region
154. South Shetland Islands
155. Antarctic Peninsula
156. Southwestern Atlantic Ocean
157. Weddell Sea
732. East of South Sandwich Islands

Seismic Region 11
New Zealand Region
158. Off west coast of North Island
159. North Island
160. Off east coast of North Island
161. Off west coast of South Island
162. South Island
163. Cook Strait
164. Off east coast of South Island
165. North of Macquarie Island
166. Auckland Islands region
167. Macquarie Island region
168. South of New Zealand

Seismic Region 12
Kermadec-Tonga-Samoa Area
169. Samoa Islands region

170. Samoa Islands
171. South of Fiji Islands
172. West of Tonga Islands (REGION NOT IN USE)
173. Tonga Islands
174. Tonga Islands region
175. South of Tonga Islands
176. North of New Zealand
177. Kermadec Islands region
178. Kermadec Islands
179. South of Kermadec Islands

Seismic Region 13
Fiji Area
180. North of Fiji Islands
181. Fiji Islands region
182. Fiji Islands

Seismic Region 14
Vanuatu (New Hebrides)
183. Santa Cruz Islands region
184. Santa Cruz Islands
185. Vanuatu Islands region
186. Vanuatu Islands
187. New Caledonia
188. Loyalty Islands
189. Southeast of Loyalty Islands

Seismic Region 15
Bismarck and Solomon Islands
190. New Ireland region
191. North of Solomon Islands
192. New Britain region
193. Bougainville - Solomon Islands region
194. D'Entrecasteaux Islands region
195. South of Solomon Islands

Seismic Region 16
New Guinea
196. Irian Jaya region
197. Near north coast of Irian Jaya
198. Ninigo Islands region
199. Admiralty Islands region
200. Near north coast of New Guinea
201. Irian Jaya
202. New Guinea
203. Bismarck Sea
204. Aru Islands region
205. Near south coast of Irian Jaya
206. Near south coast of New Guinea
207. Eastern New Guinea region
208. Arafura Sea

Seismic Region 17
Caroline Islands to Guam
209. Western Caroline Islands
210. South of Mariana Islands

Seismic Region 18
Guam to Japan
211. Southeast of Honshu
212. Bonin Islands region
213. Volcano Islands region
214. West of Mariana Islands
215. Mariana Islands region
216. Mariana Islands

Seismic Region 19
Japan-Kurils-Kamchatka
217. Kamchatka Peninsula
218. Near east coast of Kamchatka Peninsula
219. Off east coast of Kamchatka Peninsula
220. Northwest of Kuril Islands
221. Kuril Islands
222. East of Kuril Islands
223. Eastern Sea of Japan
224. Hokkaido region
225. Off southeast coast of Hokkaido
226. Near west coast of eastern Honshu
227. Eastern Honshu
228. Near east coast of eastern Honshu
229. Off east coast of Honshu
230. Near south coast of eastern Honshu

Seismic Region 20
Southwestern Japan and Ryukyu Islands
231. South Korea
232. Western Honshu
233. Near south coast of western Honshu
234. Northwest of Ryukyu Islands
235. Kyushu
236. Shikoku
237. Southeast of Shikoku
238. Ryukyu Islands
239. Southeast of Ryukyu Islands
240. West of Bonin Islands
241. Philippine Sea

Seismic Region 21
Taiwan
242. Near coast of southeastern China
243. Taiwan region
244. Taiwan
245. Northeast of Taiwan
246. Southwestern Ryukyu Islands
247. Southeast of Taiwan

Seismic Region 22
Philippines
248. Philippine Islands region
249. Luzon
250. Mindoro
251. Samar
252. Palawan
253. Sulu Sea
254. Panay
255. Cebu
256. Leyte
257. Negros
258. Sulu Archipelago
259. Mindanao
260. East of Philippine Islands

Seismic Region 23
Borneo-Sulawesi
261. Borneo
262. Celebes Sea
263. Talaud Islands
264. North of Halmahera
265. Minahassa Peninsula, Sulawesi
266. Northern Molucca Sea
267. Halmahera
268. Sulawesi
269. Southern Molucca Sea
270. Ceram Sea
271. Buru
272. Seram

Seismic Region 24
Sunda Arc
273. Southwest of Sumatera
274. Southern Sumatera

275. Java Sea
276. Sunda Strait
277. Jawa
278. Bali Sea
279. Flores Sea
280. Banda Sea
281. Tanimbar Islands region
282. South of Jawa
283. Bali region
284. South of Bali
285. Sumbawa region
286. Flores region
287. Sumba region
288. Savu Sea
289. Timor region
290. Timor Sea
291. South of Sumbawa
292. South of Sumba
293. South of Timor

Seismic Region 25
Myanmar and Southeast Asia
294. Myanmar-India border region
295. Myanmar-Bangladesh border region
296. Myanmar
297. Myanmar-China border region
298. Near south coast of Myanmar
299. Southeast Asia (REGION NOT IN USE)
300. Hainan Island
301. South China Sea
733. Thailand
734. Laos
735. Kampuchea
736. Vietnam
737. Gulf of Tongking

Seismic Region 26
India-Xizang-Szechwan-Yunnan
302. Eastern Kashmir
303. Kashmir-India border region
304. Kashmir-Xizang border region
305. Western Xizang-India border region
306. Xizang
307. Sichuan
308. Northern India
309. Nepal-India border region
310. Nepal
311. Sikkim
312. Bhutan
313. Eastern Xizang-India border region
314. Southern India
315. India-Bangladesh border region
316. Bangladesh
317. Northeastern India
318. Yunnan
319. Bay of Bengal

Seismic Region 27
Southern Xinjiang to Gansu
320. Kyrgyzstan-Xinjiang border region
321. Southern Xinjiang
322. Gansu
323. Western Nei Mongol
324. Kashmir-Xinjiang border region
325. Qinghai

Seismic Region 28
Alma-Ata to Lake Baikal
326. Southwestern Siberia
327. Lake Baykal region
328. East of Lake Baykal
329. Eastern Kazakhstan
330. Lake Issyk-Kul region
331. Kazakhstan-Xinjiang border region
332. Northern Xinjiang
333. Tuva-Buryatia-Mongolia border region
334. Mongolia

Seismic Region 29
Western Asia
335. Ural Mountains region
336. Western Kazakhstan
337. Eastern Caucasus
338. Caspian Sea
339. Northwestern Uzbekistan
340. Turkmenistan
341. Iran-Turkmenistan border region
342. Turkmenistan-Afghanistan border region
343. Turkey-Iran border region
344. Iran-Armenia-Azerbaijan border region
345. Northwestern Iran
346. Iran-Iraq border region
347. Western Iran
348. Northern and central Iran
349. Northwestern Afghanistan
350. Southwestern Afghanistan
351. Eastern Arabian Peninsula
352. Persian Gulf
353. Southern Iran
354. Southwestern Pakistan
355. Gulf of Oman
356. Off coast of Pakistan

Seismic Region 30
Middle East-Crimea-Eastern Balkans
357. Ukraine - Moldova - Southwestern Russia region
358. Romania
359. Bulgaria
360. Black Sea
361. Crimea region
362. Western Caucasus
363. Greece-Bulgaria border region
364. Greece
365. Aegean Sea
366. Turkey
367. Turkey-Georgia-Armenia border region
368. Southern Greece
369. Dodecanese Islands
370. Crete
371. Eastern Mediterranean Sea
372. Cyprus region
373. Dead Sea region
374. Jordan - Syria region
375. Iraq

Seismic Region 31
Western Mediterranean Area
376. Portugal
377. Spain
378. Pyrenees
379. Near south coast of France
380. Corsica
381. Central Italy
382. Adriatic Sea
383. Northwestern Balkan Peninsula
384. West of Gibraltar
385. Strait of Gibraltar
386. Balearic Islands
387. Western Mediterranean Sea

388. Sardinia
389. Tyrrhenian Sea
390. Southern Italy
391. Albania
392. Greece-Albania border region
393. Madeira Islands region
394. Canary Islands region
395. Morocco
396. Northern Algeria
397. Tunisia
398. Sicily
399. Ionian Sea
400. Central Mediterranean Sea
401. Near coast of Libya

Seismic Region 32
Atlantic Ocean
402. North Atlantic Ocean
403. Northern Mid-Atlantic Ridge
404. Azores Islands region
405. Azores Islands
406. Central Mid-Atlantic Ridge
407. North of Ascension Island
408. Ascension Island region
409. South Atlantic Ocean
410. Southern Mid-Atlantic Ridge
411. Tristan da Cunha region
412. Bouvet Island region
413. Southwest of Africa
414. Southeastern Atlantic Ocean
738. Reykjanes Ridge
739. Azores-Cape St. Vincent Ridge

Seismic Region 33
Indian Ocean
415. Eastern Gulf of Aden
416. Socotra region
417. Arabian Sea
418. Lakshadweep region
419. Northeastern Somalia
420. North Indian Ocean
421. Carlsberg Ridge
422. Maldive Islands region
423. Laccadive Sea
424. Sri Lanka
425. South Indian Ocean
426. Chagos Archipelago region
427. Mauritius - Reunion region
428. Southwest Indian Ridge
429. Mid-Indian Ridge
430. South of Africa
431. Prince Edward Islands region
432. Crozet Islands region
433. Kerguelen Islands region
434. Broken Ridge
435. Southeast Indian Ridge
436. Southern Kerguelen Plateau
437. South of Australia
740. Owen Fracture Zone region
741. Indian Ocean Triple Junction
742. Western Indian-Antarctic Ridge

Seismic Region 34
Eastern North America
438. Saskatchewan
439. Manitoba
440. Hudson Bay
441. Ontario
442. Hudson Strait region
443. Northern Quebec
444. Davis Strait
445. Labrador
446. Labrador Sea
447. Southern Quebec
448. Gaspe Peninsula
449. Eastern Quebec
450. Anticosti Island
451. New Brunswick
452. Nova Scotia
453. Prince Edward Island
454. Gulf of St. Lawrence
455. Newfoundland
456. Montana
457. Eastern Idaho
458. Hebgen Lake region, Montana
459. Yellowstone region
460. Wyoming
461. North Dakota
462. South Dakota
463. Nebraska
464. Minnesota
465. Iowa
466. Wisconsin
467. Illinois
468. Michigan
469. Indiana
470. Southern Ontario
471. Ohio
472. New York
473. Pennsylvania
474. Vermont - New Hampshire region
475. Maine
476. Southern New England
477. Gulf of Maine
478. Utah
479. Colorado
480. Kansas
481. Iowa-Missouri border region
482. Missouri-Kansas border region
483. Missouri
484. Missouri-Arkansas border region
485. Missouri-Illinois border region
486. New Madrid region, Missouri
487. Cape Girardeau region, Missouri
488. Southern Illinois
489. Southern Indiana
490. Kentucky
491. West Virginia
492. Virginia
493. Chesapeake Bay region
494. New Jersey
495. Eastern Arizona
496. New Mexico
497. Northwestern Texas-Oklahoma border region
498. Western Texas
499. Oklahoma
500. Central Texas
501. Arkansas-Oklahoma border region
502. Arkansas
503. Louisiana-Texas border region
504. Louisiana
505. Mississippi
506. Tennessee
507. Alabama
508. Western Florida
509. Georgia
510. Florida-Georgia border region
511. South Carolina
512. North Carolina
513. Off east coast of United States
514. Florida Peninsula
515. Bahama Islands
516. Eastern Arizona-Sonora border region
517. New Mexico-Chihuahua

border region
518. Texas-Mexico border region
519. Southern Texas
520. Near coast of Texas
521. Chihuahua
522. Northern Mexico
523. Central Mexico
524. Jalisco
525. Veracruz
526. Gulf of Mexico
527. Bay of Campeche

Seismic Region 35
Eastern South America
528. Brazil
529. Guyana
530. Suriname
531. French Guiana

Seismic Region 36
Northwestern Europe
532. Eire
533. United Kingdom
534. North Sea
535. Southern Norway
536. Sweden
537. Baltic Sea
538. France
539. Bay of Biscay
540. The Netherlands
541. Belgium
542. Denmark
543. Germany
544. Switzerland
545. Northern Italy
546. Austria
547. Czech and Slovak Republics
548. Poland
549. Hungary

Seismic Region 37
Africa
550. Northwest Africa (REGION NOT IN USE)
551. Southern Algeria
552. Libya
553. Egypt
554. Red Sea
555. Western Arabian Peninsula
556. Chad region
557. Sudan
558. Ethiopia
559. Western Gulf of Aden
560. Northwestern Somalia
561. Off south coast of northwest Africa
562. Cameroon
563. Equatorial Guinea
564. Central African Republic
565. Gabon
566. Congo
567. Zaire
568. Uganda
569. Lake Victoria region
570. Kenya
571. Southern Somalia
572. Lake Tanganyika region
573. Tanzania
574. Northwest of Madagascar
575. Angola
576. Zambia
577. Malawi
578. Namibia
579. Botswana
580. Zimbabwe
581. Mozambique
582. Mozambique Channel
583. Madagascar
584. South Africa
585. Lesotho
586. Swaziland
587. Off coast of South Africa
743. Western Sahara
744. Mauritania
745. Mali
746. Senegal - Gambia region
747. Guinea region
748. Sierra Leone
749. Liberia region
750. Cote d'Ivoire
751. Burkina Faso
752. Ghana
753. Benin - Togo region
754. Niger
755. Nigeria

Seismic Region 38
Australia
588. Northwest of Australia
589. West of Australia
590. Western Australia
591. Northern Territory
592. South Australia
593. Gulf of Carpentaria
594. Queensland
595. Coral Sea
596. Northwest of New Caledonia
597. New Caledonia region
598. Southwest of Australia
599. Off south coast of Australia
600. Near coast of South Australia
601. New South Wales
602. Victoria
603. Near southeast coast of Australia
604. Near east coast of Australia
605. East of Australia
606. Norfolk Island region
607. Northwest of New Zealand
608. Bass Strait
609. Tasmania region
610. Southeast of Australia

Seismic Region 39
Pacific Basin
611. North Pacific Ocean
612. Hawaiian Islands region
613. Hawaiian Islands
614. Eastern Caroline Islands region
615. Marshall Islands region
616. Enewetak Atoll region
617. Bikini Atoll region
618. Gilbert Islands region
619. Johnston Island region
620. Line Islands region
621. Palmyra Island region
622. Kiritimati region
623. Tuvalu region
624. Phoenix Islands region
625. Tokelau Islands region
626. Northern Cook Islands
627. Cook Islands region
628. Society Islands region
629. Tubuai Islands region
630. Marquesas Islands region
631. Tuamotu Archipelago region
632. South Pacific Ocean

Seismic Region 40
Arctic Zone
633. Lomonosov Ridge
634. Arctic Ocean
635. Near north coast of Kalaallit Nunaat
636. Eastern Kalaallit Nunaat
637. Iceland region
638. Iceland
639. Jan Mayen Island region
640. Greenland Sea
641. North of Svalbard
642. Norwegian Sea

643. Svalbard region
644. North of Franz Josef Land
645. Franz Josef Land
646. Northern Norway
647. Barents Sea
648. Novaya Zemlya
649. Kara Sea
650. Near coast of northwestern Siberia
651. North of Severnaya Zemlya
652. Severnaya Zemlya
653. Near coast of northern Siberia
654. East of Severnaya Zemlya
655. Laptev Sea

Seismic Region 41
Eastern Asia
656. Southeastern Siberia
657. Priamurye-Northeastern China border region
658. Northeastern China
659. North Korea
660. Sea of Japan
661. Primorye
662. Sakhalin Island
663. Sea of Okhotsk
664. Southeastern China
665. Yellow Sea
666. Off east coast of southeastern China

Seismic Region 42
Northeastern Asia, Northern Alaska to Greenland
667. North of New Siberian Islands
668. New Siberian Islands
669. Eastern Siberian Sea
670. Near north coast of eastern Siberia
671. Eastern Siberia
672. Chukchi Sea
673. Bering Strait
674. St. Lawrence Island region
675. Beaufort Sea
676. Northern Alaska
677. Northern Yukon Territory
678. Queen Elizabeth Islands
679. Northwest Territories
680. Western Kalaallit Nunaat
681. Baffin Bay
682. Baffin Island region

Seismic Region 43
Southeastern and Antarctic Pacific Ocean
683. Southeastcentral Pacific Ocean
684. Southern East Pacific Rise
685. Easter Island region
686. West Chile Rise
687. Juan Fernandez Islands region
688. East of North Island
689. Chatham Islands region
690. South of Chatham Islands
691. Pacific-Antarctic Ridge
692. Southern Pacific Ocean
756. Southeast of Easter Island

Seismic Region 44
Galapagos Area
693. Eastcentral Pacific Ocean
694. Central East Pacific Rise
695. West of Galapagos Islands
696. Galapagos Islands region
697. Galapagos Islands
698. Southwest of Galapagos Islands
699. Southeast of Galapagos Islands
757. Galapagos Triple Junction region

Seismic Region 45
Macquarie Loop
700. South of Tasmania
701. West of Macquarie Island
702. Balleny Islands region

Seismic Region 46
Andaman Islands to Sumatera
703. Andaman Islands region
704. Nicobar Islands region
705. Off west coast of northern Sumatera
706. Northern Sumatera
707. Malay Peninsula
708. Gulf of Thailand

Seismic Region 47
Baluchistan
709. Southeastern Afghanistan
710. Pakistan
711. Southwestern Kashmir
712. India-Pakistan border region

Seismic Region 48
Hindu Kush and Pamir
713. Central Kazakhstan
714. Southeastern Uzbekistan
715. Tajikistan
716. Kyrgyzstan
717. Afghanistan-Tajikistan border region
718. Hindu Kush region
719. Tajikistan-Xinjiang border region
720. Northwestern Kashmir

Seismic Region 49
Northern Eurasia
721. Finland
722. Norway-Murmansk border region
723. Finland-Karelia border region
724. Baltic States - Belarus - Northwestern Russia
725. Northwestern Siberia
726. Northern and central Siberia

Seismic Region 50
Antarctica
727. Victoria Land
728. Ross Sea
729. Antarctica

7.3 Magnitudes - draft by Peter Bormann

The ISC determines itself, receives (from other seismological agencies, networks and stations) and publishes a diversity of magnitude data. Although trying to be as complete and specific as possible, preference is given in future (from 2012 onwards ??) to magnitudes determined according to standard procedures recommended by the Working Group on Magnitude Measurements of the IASPEI Commission on Seismological Observation and Interpretation (CoSOI). So far, such standards have been agreed upon for the local magnitude ML and two kinds each of body-wave (mb and mB_{BB}) and surface-wave magnitudes (Ms_{20} and Ms_{BB}). BB stands for direct measurement on unfiltered velocity broadband records in a wide range of periods, whereas mb and Ms_{20} are based on narrowband amplitude measurements around periods of 1 s and 20 s, respectively. The measurement standards aim at reducing the data scatter due to procedural differences and to increase the value of magnitude as well as related amplitude and period data for research and application. The nomenclature of these magnitudes has been chosen so as to be unique and to fit into the IASPEI Seismic Format (ISF) for magnitude data transmission, archiving and reporting. These symbols should only be used for magnitude data measured according to the respective standards or with slightly modified procedures that do not significantly bias the results in the considered magnitude range. Agency or station magnitudes of similar type that is commonly biased by more than 0.1 magnitude unit with respect to the magnitude produced by an IASPEI Standard Procedure should be identified by nomenclature that is distinct from the IASPEI magnitude nomenclature (see NMSOP-2, IS 3.2). Some of those complementary magnitudes, which are also reproduced in the ISC bulletin, are listed and defined under Abbreviations and Contractions.

ML is consistent with the original definition of the local magnitude by Richter (1935) and mB_{BB} in close agreement with the original definition of medium-period body-wave magnitude mB measured in a wide range of periods between some 2 to 20 s and calibrated with the Gutenberg (1945) Q-function for vertical-component P waves. Similarly, Ms_{BB} is best tuned to the unbiased use of the IASPEI (1967) recommended standard magnitude formula for surface-wave amplitudes in a wide range of periods and distances, as proposed by its authors Vaněk et al. (1962). In contrast, mb and Ms_{20} are chiefly based on measurement standards defined by US agencies in the 1960s in conjunction with the global deployment of the World-Wide Standard Seismograph Network (WWSSN). Some modifications were made in the 1970s to account for IASPEI recommendations on extended measurement time windows for mb. Although not being optimal for calibrating narrow-band spectral amplitudes measured around 1 s and 20 s only, mb and Ms_{20} use until now the same original calibrations functions as mB_{BB} and Ms_{BB}. But mb and Ms_{20} data constitute as of now by far the largest available magnitude data set. Therefore it has to be continued into the future and consciously used, knowing about both its advantages (e.g., mb is by far the most frequently measured teleseismic magnitude and often the only available (and then reasonable good) magnitude estimator for small earthquakes) and shortcomings (see Bormann et al., 2009).

Abbreviated descriptions of the standard procedures for ML, mb, mB_{BB} and Ms_{BB} are summarized below. For more details, including also the transfer functions of the simulation filters to be used, see http://www.iaspei.org/commissions/CSOI.html and Dewey & Bormann et al. (2011?). All standard magnitudes are determined via measurements of amplitudes (A for displacement or V for velocity) and for mb and Ms_{20} also of the related periods T. Although ML and the velocity-based standard magnitudes do not required to know the associated dominating period, T has to be measured, reported and preserved together with Vmax in bulletin databases since it is an important complementary parameter related to the seismic source process and/or the station site and wave-propagation effects.

All amplitudes used in the magnitude formulas below are to be measured as one-half of the absolute maximum peak-to-adjacent-trough (sometimes called 'peak-to-peak') deflection of the seismogram trace and to be corrected (with the exception of the trace amplitude for ML) for the displacement or velocity magnification at the measured period. The periods are to be measured as twice the time intervals separating the peak and adjacent-trough from which the amplitudes are measured. The amplitude-phase arrival-times have to be measured and reported too as the time of the zero-crossing between the peak and adjacent-trough from which the amplitudes are measured.

Note that the commonly known classical calibration relationships have been modified below to be consistent with displacements measured in nm, and velocities in nm/s, which is now common with high-resolution digital data and analysis tools. With these general definitions of the measurement parameters and R - hypocentral distance in km (typically less than 1000 km), Δ - epicental distance in degrees (1° = 111,2 km) and h - hypocenter depth in km, the standard formulas and procedures read as follows:

ML: For **crustal earthquakes** in regions with attenuative properties similar to those of Southern California, and with A being the **maximum trace amplitude** in nm that is measured on output from a **horizontal-component** instrument that is filtered so as to replicate that of a Wood-Anderson standard seismograph (but with a static magnification of 1) the proposed standard equation is:

$$ML = \log_{10}(A) + 1.11 \log_{10} R + 0.00189R - 2.09 \tag{7.1}$$

Note that for seismographic stations containing two horizontal components, amplitudes are measured independently from each horizontal component and each amplitude is treated as a single datum. No vector average is calculated! Moreover, for crustal earthquakes in regions with attenuative properties that are different from than those of coastal California and for measuring magnitudes with vertical-component seismographs the constants in the above equation have to be re-determined to adjust for the different regional attenuation as well as for systematic differences between amplitudes measured on horizontal and vertical seismographs.

mb:

$$mb = \log_{10}(A/T) + Q(\Delta, h) - 3.0 \tag{7.2}$$

where A = **vertical component P-wave ground amplitude in nm** measured **at distances 20° ≤ Δ ≤ 100°** and calculated from the maximum trace-amplitude with **T < 3 s** in the entire P-phase train (time spanned by P, pP, sP, and possibly PcP and their codas, and ending preferably before PP). A is measured on output from an instrument that is filtered so that the overall frequency response **synthesizes a WWSSN short-period seismograph**.

mB_{BB}:

$$mB_{BB} = \log_{10}(Vmax/2\pi) + Q(\Delta, h) - 3.0 \tag{7.3}$$

where **Vmax = vertical component ground velocity in nm/s** at periods **between 0.2 s < T < 30 s**, measured **in the range 20° ≤ Δ ≤ 100°**. Vmax is calculated from the maximum trace-amplitude in the entire P-phase train (see mb), as recorded on a seismogram that is proportional to velocity at least in the period range of measurements.

Ms_{20}:

$$Ms_{20} = \log_{10}(A/T) + 1.66\log_{10}\Delta + 0.3 \tag{7.4}$$

where A = **vertical-component ground displacement in nm** measured from the maximum trace amplitude of a surface-wave phase having a period T **between 18 s and 22 s** on a waveform that has been filtered so that the frequency response of the seismograph/filter simulates a WWSSN long-period seismograph. Ms_{20} is calculated only for events with a **focal depth** h **< 60 km recorded at 20° ≤ Δ ≤ 160°**.

Ms_{BB}:

$$Ms_{BB} = \log_{10}(Vmax/2\pi) + 1.66\log_{10} + 0.3 \tag{7.5}$$

where **Vmax = vertical-component ground velocity in nm/s** associated with the maximum trace-amplitude in the surface-wave train at periods between **3 s < T < 60 s** as recorded **at distances 2° ≤ Δ ≤ 160°** on a seismogram that is proportional to velocity at least in that range of considered periods. Ms_{BB} is calculated for events with a **focal depth** h **< 60 km recorded at 2° ≤ Δ ≤ 160°**.

Mw: Moment magnitude Mw is calculated from data of the scalar seismic moment M_0. There exist no measurement standards yet for M_0. However, IASPEI recommends the following standard formula for calculating Mw from M_0 (when given in Nm)

$$Mw = \frac{2}{3}(\log_{10} M_0 - 9.1) \tag{7.6}$$

7.4 The IASPEI Standard Format (ISF)

The ISF is the IASPEI approved standard format for the exchange of parametric seismological data (hypocentres, magnitudes, phase arrivals, moment tensors etc.) and is one of the formats used by the ISC. It was adopted as standard in August 2001 and is an extension of the International Monitoring System 1.0 (IMS1.0) standard, which was developed for exchanging data used to monitor the Comprehensive Test Ban Treaty. An example of the ISF is shown in Example 7.8.

Bulletin data which use the ISF, comprise of origin and arrival information, which is provided in a series of data blocks. These include: a bulletin title block; an event title block; an origin block; a magnitude sub-block; an effect block; a reference block; and a phase block.

Within these blocks an important extension of the IMS1.0 standard is the ability to add additional comments and thus provide further parametric information. The ISF comments are distinguishable within the open parentheses required for IMS1.0 comments by beginning with a hash mark (#) followed by a keyword identifying the type of formatted comment. Each additional line required in the ISF comment begins with the hash (within the comment parantheses) and followed by blank spaces at least as long as the keyword. Optional lines within the comment are signified with a plus sign (+) instead of a hash mark. The keywords include `PRIME` (to designate a prime origin of a hypocentre); `CENTROID` (to indicate the centroid origin); `MOMTENS` (moment tensor solution); `FAULT_PLANE` (fault plane solution); `PRINAX` (principal axes); `PARAM` (an origin parameter e.g. hypocentre depth given by a depth phase).

The full documentation for the ISF is maintained at the ISC and can be downloaded from www.isc.ac.uk/doc/code/isf/isf.pdf. The documentation for the IMS1.0 standard can be downloaded from www.isc.ac.uk/doc/code/isf/ims1_0.pdf.

```
DATA_TYPE BULLETIN IMS1.0:short
ISC Comprehensive Bulletin
Event 12343211 Carlsberg Ridge

2007/01/01 00:31:35.60        1.400   0.2400   66.5700                  10.0              44                          BJI        8197245
2007/01/01 00:31:42.72   1.18 1.291   1.2248   67.0882 7.040 4.573 152   6.3  7.33  285  403   37  10.11  93.23 m i se ISCJB     10861269
 (#PARAM pP_DEPTH=29.06914)
2007/01/01 00:31:43.00   1.33         1.2490   67.0200 7.700 4.900 109  10.0        112                               MOS        9869872
2007/01/01 00:31:43.78   0.62 0.820   1.2152   67.2227 17.80 13.40 145  0.0f         30       94  26.27 145.19     uk IDC       10017155
2007/01/01 00:31:45.00   0.10         0.8800   67.2600 1.112 1.112  -1  12.0f       253   87                          GCMT       8834611
 (#MOMTENS sc    M0 fCLVD    MRR    MTT    MPP    MRT    MTP    MPR NST1 NST2 Author   )
 (#             eM0 eCLVD    eRR    eTT    ePP    eRT    eTP    ePR NCO1 NCO2 Duration )
 (#        17 1.663       -1.190 -0.153  1.350 -0.163 -1.270 -0.015   50   87 GCMT     )
 (#                        0.035  0.030  0.030  0.091  0.027  0.081   80  173     1.20 )
 (#FAULT_PLANE Typ Strike   Dip    Rake  NP  NS Plane Author   )
 (#            BDC 351.00 48.00  -60.00               GCMT     )
 (+                130.00 50.00 -119.00                        )
 (#PRINAX sc  T_val T_azim  T_pl  B_val B_azim  B_pl  P_val P_azim  P_pl Author    )
 (#       17  2.076 240.00  1.00 -0.818 150.00 22.00 -1.251 333.00 68.00 GCMT      )

 (nsta1 refers to body waves, cutoff=40s. nsta2 refers to surface waves, cutoff=50s.)
2007/01/01 00:31:45.02   0.29 1.370   1.2320   67.1170 8.400 7.000   4  10.0f       138       42  10.10 150.43     se NEIC       9896327
2007/01/01 00:31:46.75        1.490   1.2320   67.0620 75.00 52.00 167  20.7  3.52  298  270                       ke EHB       14149655
2007/01/01 00:31:50.90                2.6790   67.7860                  33.0f                                         SZGRF      8830531
 (Carlsberg Ridge)
2007/01/01 00:31:46.30   1.33 1.252   1.2398   67.1213 6.908 4.587 153  15.1  8.19  285  403   37  10.11  93.24 m i se ISC       10650944
 (#PRIME)
 (#PARAM pP_DEPTH=27+5)
Ms     5.2          BJI        8197245
Msz    5.0          BJI        8197245
mB     5.3          BJI        8197245
mb     4.8          BJI        8197245
MS     5.1      134 ISCJB     10861269
mb     4.9      118 ISCJB     10861269
MS     4.8        9 MOS        9869872
mb     5.2       46 MOS        9869872
MS     4.9 0.1   25 IDC       10017155
Ms1    4.9 0.1   25 IDC       10017155
mb     4.5 0.1   24 IDC       10017155
mb1    4.5 0.1   24 IDC       10017155
mb1mx  4.5 0.1   30 IDC       10017155
mbtmp  4.5 0.1   24 IDC       10017155
ms1mx  4.7 0.1   39 IDC       10017155
MW     5.4       87 GCMT       8834611
MS     5.2       93 NEIC       9896327
mb     5.1       67 NEIC       9896327
mb     5.8          SZGRF      8830531
MS     5.1      134 ISC       10650944
mb     4.9      118 ISC       10650944

DGAR   10.11 148.3 Pn       00:34:11.1     0.1                           T__                        _e                   1
DGAR   10.11 148.3 Pn       00:34:11.08    0.1                           T__                        _e                   1
TRD    12.17  53.3 Pn       00:34:37.73  -1.52                           T__                        _e                   1
TRD    12.17  53.3 AMB      00:34:47.35                                  ___            64.9  1.13  __                   1
AJM    26.12  15.5 P        00:37:20.85    1.1                           T__                        _e                   1
ATD    26.17 294.0 P        00:37:22.5     2.1 113.1         3.40        T__   8.7      47.2  1.05  __ mb      5.0       1
ATD    26.17 294.0 LR       00:45:24.786       256.2        31.30        ___          1681.1 19.24  __ MS      4.6       1
OPO    27.78 223.9 P        00:37:36.96    2.1  39.3         7.80        T__   4.0       3.9  0.91  __ mb      4.0       1
OPO    27.78 223.9 S        00:42:18.5     1.2 180.0        20.20        T__  43.9       1.4  0.23  __                   1
BOK    28.87  37.6 P        00:37:44.52    0.0                           T__                        _e                   1
NDI    28.94  18.6 P        00:37:47.13    2.0                           T__                        _e                   1
NDI    28.94  18.6 AMB      00:37:48.59                                  ___             9.1  2.15  __ mb      4.1       1

STOP
```

Example 7.8: Example of the IASPEI Standard Format (ISF) for a single event, including an origin block, a magnitude sub-block and a phase block with ISF comments also included (see text). Note: the bulletin has been modified from this event's actual ISC Bulletin.

7.5 Ground Truth (GT) events

Accurate locations are crucial in testing Earth models derived from body and surface wave tomography as well as in location calibration studies. 'Ground Truth' (GT) events are well-established source locations and origin times. A database of IASPEI reference events (GT earthquakes and explosions) is hosted at the ISC (www.isc.ac.uk). A full description of GT selection criteria can be found in *Bondár and McLaughlin* (2009b).

The events are coded by category GT0, GT1, GT2 or GT5, where the epicentre of a GTX event is known to within X km to a 95% confidence level. A map of all IASPEI reference events is shown in Figure 7.9 and the types of event are categorised in Figure 7.10. GT0 are explosions with with announced locations and origin times. GT1 and GT2 are typically explosions, mine blasts or rock bursts either associated to explosion phenomenology located upon overhead imagery with seismically determined origin times or precisely located by in-mine seismic networks. GT1-2 events are assumed to be shallow, but depth is unknown.

The database consists of nuclear explosions of GT0–5 quality, adopted from the Nuclear Explosion Database (*Bennett et al.*, 2010); GT0–5 chemical explosions, rock bursts, mine-induced events, as well as a few earthquakes, inherited from the reference event set by *Bondár et al.* (2004); GT5 events (typically earthquakes with crustal depths) which have been identified using either the method of *Bondár et al.* (2008) (2,275 events) or *Bondár and McLaughlin* (2009b) (updated regularly from the EHB catalogue (*Engdahl et al.*, 1998)), which uses the following criteria:

- 10 or more stations within 150 km from the epicentre
- one or more stations within 10 km
- $\Delta U \leq 0.35$
- a secondary azimuthal gap $\leq 160°$

where ΔU is the network quality metric defined as the mean absolute deviation between the best-fitting uniformly distributed network of stations and the actual network:

$$\Delta U = \frac{4 \sum |esaz_i - (unif_i + b)|}{360N}, 0 \leq \Delta U \leq 1 \tag{7.7}$$

where N is the number of stations, $esaz_i$ is the ith event-to-station azimuth, $unif_i = 360i/N$ for $i = 0$, ..., $N - 1$, and $b = avg\,(esaz_i) - avg\,(unif_i)$. ΔU is normalised so that it is 0 when the stations are uniformly distributed in azimuth and 1 when all the stations are at the same azimuth.

The seismological community is invited to participate in this project by nominating seismic events for the reference event database. Submitters may be contacted for further confirmation and for arrival time data. The IASPEI Reference Event List will be periodically published both in written and electronic form with proper acknowledgement of all submitters.

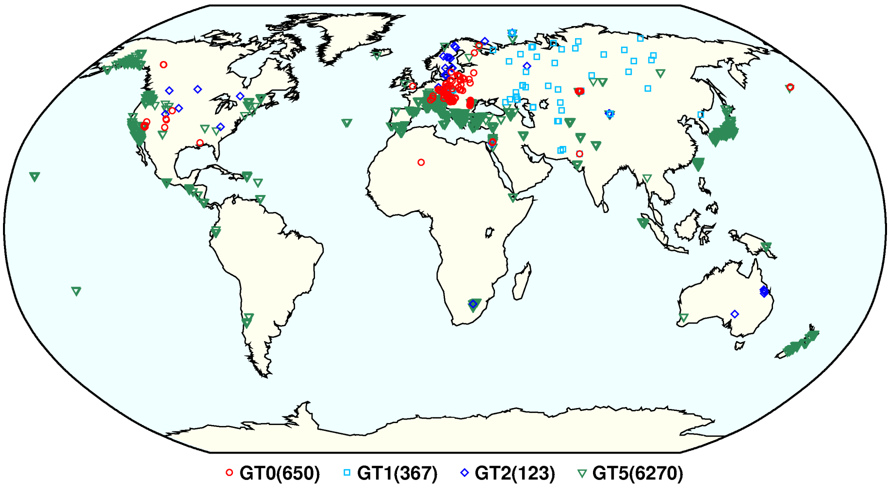

Figure 7.9: Map of all IASPEI Reference Events.

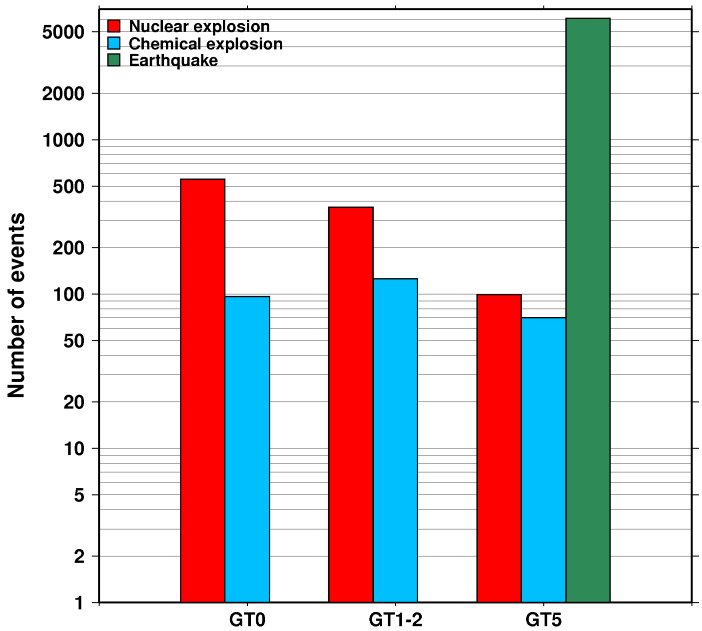

Figure 7.10: Histogram showing the event types within the IASPEI Reference Event list.

7.6 Nomenclature of event types

8

Addendum & announcements

Adapt current addendum.

- Specific changes to procedures.
- Comment or small article about new agency?

9

Notable event

9.1 The Darfield (Canterbury) New Zealand M_W 7.1 earthquake of September 2010, and Christchurch, New Zealand M_W 6.2 earthquake of February 2011 - example article by John Ristau (GNS, j.ristau@gns.cri.nz)

On 4 September 2010 at 04:35 New Zealand standard time (3 September 16:35 UTC) the moment magnitude (M_W) 7.1 Darfield earthquake occurred in the Canterbury region of New Zealand approximately 10 km southeast of the town of Darfield and 40 km west of Christchurch, New Zealand's second largest city with a population of approximately 380 000 (Figure 9.1). The earthquake was widely felt throughout the South Island and the lower North Island with over 7300 felt reports received, and caused significant damage in Christchurch. Extensive liquefaction and lateral spreading was observed throughout Christchurch which contributed significantly to structural damage. Through a fortunate combination of strict building codes and the earthquake occurring at night when the streets were largely deserted there were no deaths and only two serious injuries reported. Most of the damage was confined to unreinforced brick and masonry structures including toppled chimneys and parapets, failure of gables, and damage to masonry frames. Modern buildings and light timber frame structures performed well with little structural damage.

Less than six months later on 22 February 2011 at 12:51 NZDT (21 February 23:51 UTC) a M_W 6.2 aftershock occurred approximately 10 km SE of Christchurch (Figure 9.1). The Christchurch earthquake caused heavy damage to the city including the central business district. In stark contrast to the Darfield earthquake, the Christchurch earthquake occurred during the lunch hour on a weekday when the central business district (CBD) was at its most crowded. As a result there were more than 180 fatalities with over half occurring with the complete collapse of the six-story Canterbury Television (CTV) building. Around 900 buildings in the CBD are expected to be demolished with another 300 buildings in the suburbs suffering the same fate.

GeoNet, on behalf of GNS Science, operates a dense network of seismometers, strong-motion accelerometers and GPS sites in the Canterbury region which has resulted in a large data set of vital information (*Petersen et al.*, 2011) (Figure 9.1). Of particular interest is the Canterbury network of nearly 40 seismic instruments which includes a number of strong-motion accelerometers (*Avery et al.*, 2004). After both the Darfield and Christchurch earthquakes GNS immediately sent teams of technicians to Christchurch and the Canterbury region to install a number a temporary seismometers and accelerometers to better record the aftershocks. As a re-

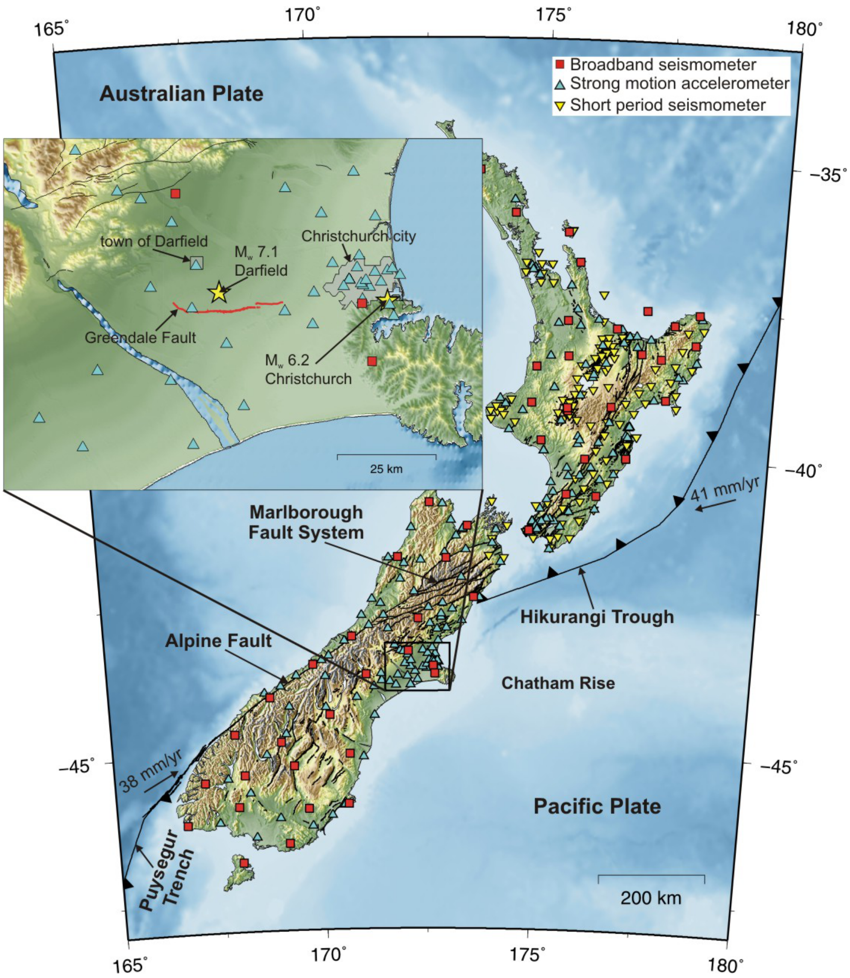

Figure 9.1: Tectonic setting of New Zealand and the Canterbury region, and the GeoNet seismometer and accelerometer network. (inset) Epicentres of the Darfield and Christchurch earthquakes (yellow stars), the previously unknown Greendale fault surface trace (red line), and the locations of the town of Darfield and Christchurch cite.

sult the Darfield and Christchurch earthquakes are two of the best recorded major earthquakes anywhere in the world.

Prior to the Darfield earthquake the Canterbury region had a relatively low level of seismic activity compared with many other parts of New Zealand. New Zealand straddles the boundary of the Pacific and Australian plates. In the South Island the Alpine Fault, which runs along the west coast, accommodates the vast majority of the relative plate motion. A number of M > 6–7 earthquakes have occurred in the foothills west of Christchurch in the past 150 years, but there were no mapped active faults in the Canterbury plains. The Darfield earthquake demonstrates that the zone of active deformation in the eastern South Island extends beyond the visible range front.

The most obvious physical feature of the Darfield earthquake is a 29.5 km long surface rupture on the previously unknown Greendale Fault (Figure 9.1). The Greendale Fault was buried beneath deposits from the last glacial period 18000–20 000 years ago (*Forsyth et al.*, 2008). The fault cut across mainly well cultivated farmland which made the fault trace relatively easy to map. Movement was predominantly right-lateral strike-slip with an average horizontal displacement of ∼2.5 m, and maximum displacements of ∼5 m horizontally and 1.5 m vertically (*Quigley et al.*, 2010). The Darfield earthquake has, however, been shown to be much more complex than a simple strike-slip event.

The hypocentre has been very well constrained (within at most ± 0.5 km) to be about 4 km north of the surface trace of the Greendale Fault (*Gledhill et al.*, 2011). This cannot be explained by location uncertainty or by a shallow-dipping fault as a strike-slip mechanism will be near-vertical. Another important piece of information comes from various estimates of the focal mechanism. Moment tensor solutions using teleseismic data give a strike-slip focal mechanism in agreement with the Greendale Fault trace. The regional moment tensor and first-motion source mechanisms are in close agreement and show reverse faulting. The USGS broadband energy solution also indicates a complex event with at least two subevents.

Preliminary results from the strong-motion accelerometer data suggest that there were at least three distinct fault ruptures in the sequence. The earthquake began north of the Greendale Fault on a blind reverse fault (M_W 6.3) which continued along the Greendale Fault which ruptured the surface (M_W 6.9). Finally, the Greendale Fault triggered another blind reverse fault at the western end of the Greendale Fault (M_W 6.5) and possibly a third blind reverse fault at the eastern end. Preliminary geodetic modelling (*Beavan et al.*, 2010) also requires several fault segments to be active during the earthquake including an initial rupture on a blind reverse fault which triggered the Greendale fault where the majority of the moment release occurred. A number of other reverse faults were also active giving M_W 7.1 for all modelled segments.

A vigorous aftershock sequence followed the Darfield and Christchurch earthquakes with over 6300 located events (Figure 9.2) - 27 being $M_L \geq 5.0$. The aftershock distribution shows a NNW-SSE oriented ‘finger’ of aftershocks off the main alignment. The aftershock focal mechanisms show a variety of faulting styles, providing additional evidence for the complex nature of the rupture process. There is a cluster of aftershocks at the western end of the fault trace where the focal mechanisms are predominantly reverse faulting. Additionally near-source strong-motion stations show unusually high vertical accelerations that require an initial reverse component to the event.

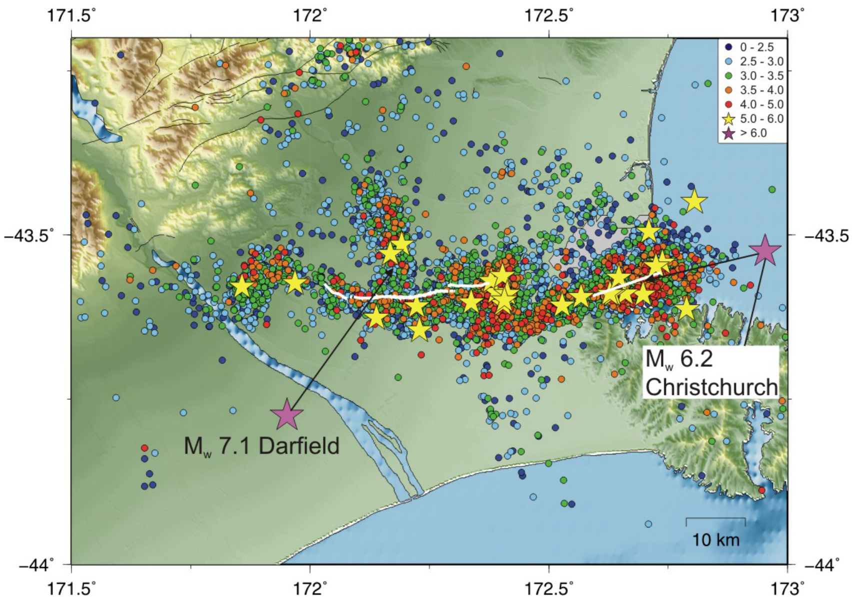

Figure 9.2: Map of preliminary aftershock locations. Yellow stars are $M_L \geq 5.0$ aftershocks and the purple stars point to the epicentres of the Darfield and Christchurch earthquakes. More than 6300 aftershocks have been located through 31 May 2011. Note the 'finger' of aftershocks trending north from the epicentre of the Darfield earthquake and the cluster of aftershocks at the western end of the Greendale fault trace (white line).

The Christchurch earthquake was a reverse faulting mechanism on an ENE-WSW striking fault plane. The M_W 6.2 Christchurch earthquake had a much larger impact on Christchurch than the M_W 7.1 Darfield earthquake for several reasons.

1. Most obvious is the Christchurch earthquake hypocentre being only 10 km from Christchurch compared with 40 km for the Darfield earthquake.

2. The energy release for both events was also quite high. The USGS energy magnitude (M_E) was M_E 6.7 for the Christchurch events and M_E 7.4 for the Darfield event. The crustal structure is extremely strong in the Canterbury region resulting in high stress drops and high fault friction for both events.

3. The direction of the radiated energy for the Christchurch earthquake was directly towards Christchurch.

4. A recently discovered trampoline or 'slapdown' effect beneath Christchurch. As seismic energy travels beneath Christchurch the weaker upper layers travelled farther upwards than the stronger lower layers, and so separated from them. The upper layers than fell back and 'slapped' against the lower layers which were on their way back up. This resulted in high impacts and high vertical accelerations. Peak vertical ground accelerations reached

> 2.20g for the February event compared with 1.26g for the September event. This also helps to explain the widespread liquefaction observed throughout Christchurch during the earthquake.

Considerable research is still required to fully characterize the complexity of the Darfield earthquake and the relationship between the Darfield and Christchurch earthquakes. This will involve a full multi-disciplinary study involving seismology, geodesy, finite-element source-modelling, and geology to constrain the rupture process. However, preliminary modelling has shown that the Darfield sequence began as a steeply dipping reverse-faulting event, continued by triggering the Greendale fault as a right-lateral strike-slip event which accommodated the majority of the moment release, and also involved several other reverse faulting events at either end of the Greendale fault.

Extensive look at any significant earthquakes that occurred within the 4 month time period. A **guest author** can contribute a short description of the earthquake, including the tectonic setting, historical seismicity and any possible research conducted in the region.

BD:

- Historical seismicity maps
- Historical moment tensor solutions
- Histogram of historical magnitudes - Gutenberg & Richter FMD; show the magnitude of completeness
- Histogram showing aftershocks with time.
- List of agency contributors
- Map of stations reporting
- Change in agencies reporting from the region with time.
- Phases reported - comparison with predicted arrival-times; map of residuals.

10

Data collection and statistics

Data reports at the ISC are filed by the ISCs automated parser....

With data constantly being reported to the ISC, even after the ISC has published its review, the total data shown as collected, within this section, is limited to 2 years after the time of the associated reading or event. i.e. any hypocentre data collected two years after the event are not reflected in the figures below.

10.1 Summary of reports to the ISC

As stated in the ISC procedures, a total of 114 agencies have reported data for September 2008 to December 2008. The parsing of these reports into the ISC database is summarised in Table 10.1.

The reports which contained phase data are summarised in Table 10.2, with the stations contributing these data shown in Figure 10.2. The large increase in phase data reported to the ISC since 1999, when emailed reports began being parsed automatically, is shown in Figure 10.1.

10.1: Table summarising the parsing of reports received by the ISC from a total of 114 agencies, containing data for September 2008 to December 2008.

	Number of reports
Total collected	2551
Automatically parsed	2150
Manually parsed	400
Deleted	1

10.2 Phase readings

10.2: Table summarising the reports containing phase readings.

Reports with phase arrivals	2 209
Reports with phase arrivals including amplitudes	538
Reports with only phase arrivals (no hypocentres reported)	339
Total phase arrivals received	3 196 138
Total phase arrival-times received	3 015 421
Number of duplicate phase arrival-times	693 927 (23%)
Number of amplitudes received	935 254
Average phase arrivals per report	1 447
Stations reporting phase arrivals	4 982
Stations reporting phase arrivals with amplitudes data	2 155
Max number of stations per report	2063
Min number of stations per report	
Average number of stations per report	27

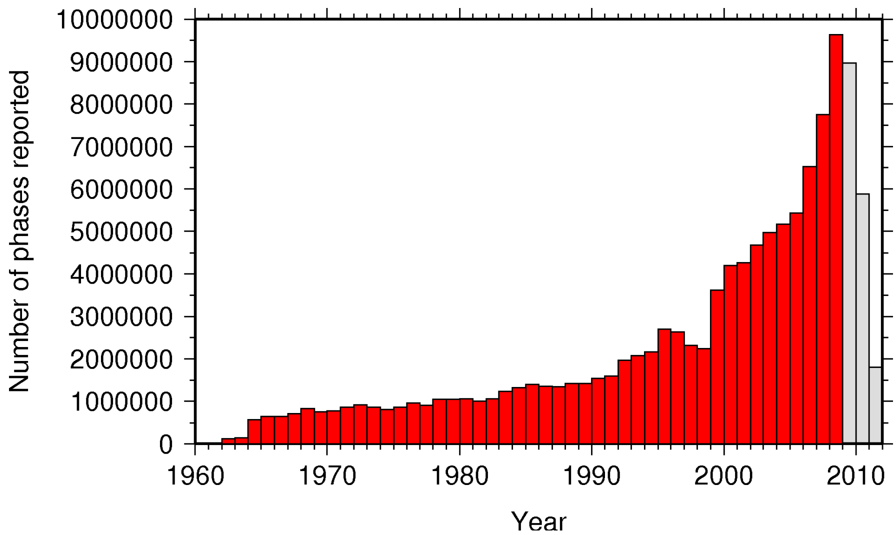

Figure 10.1: Histogram showing the number of phases collected by the ISC for events each month since 1999.

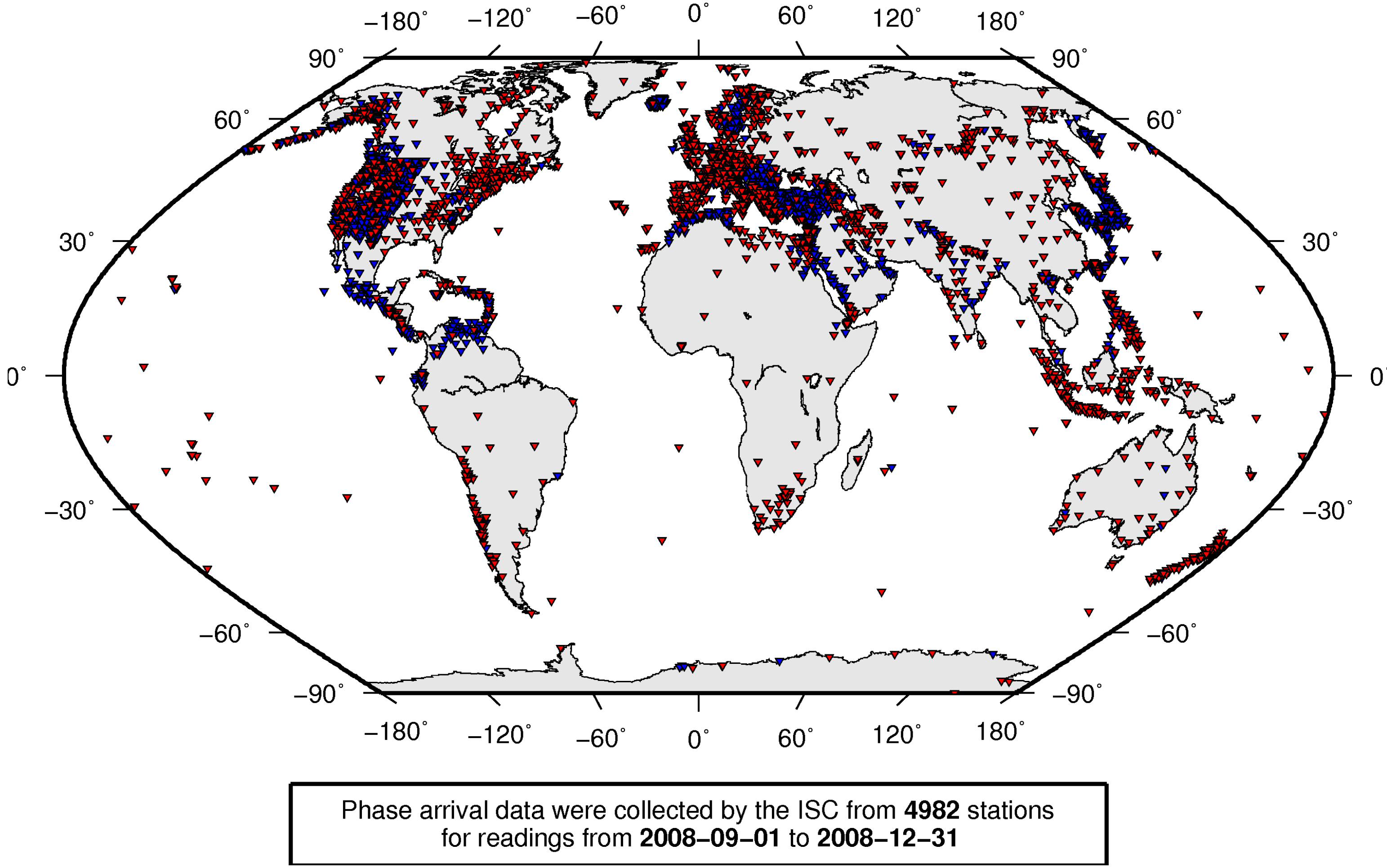

Figure 10.2: Stations contributing phase data to the ISC for events from September 2008 to the end of December 2008. Stations in blue reported phase arrival-time readings without amplitude data; stations in red provided both phase arrival-time and amplitude readings.

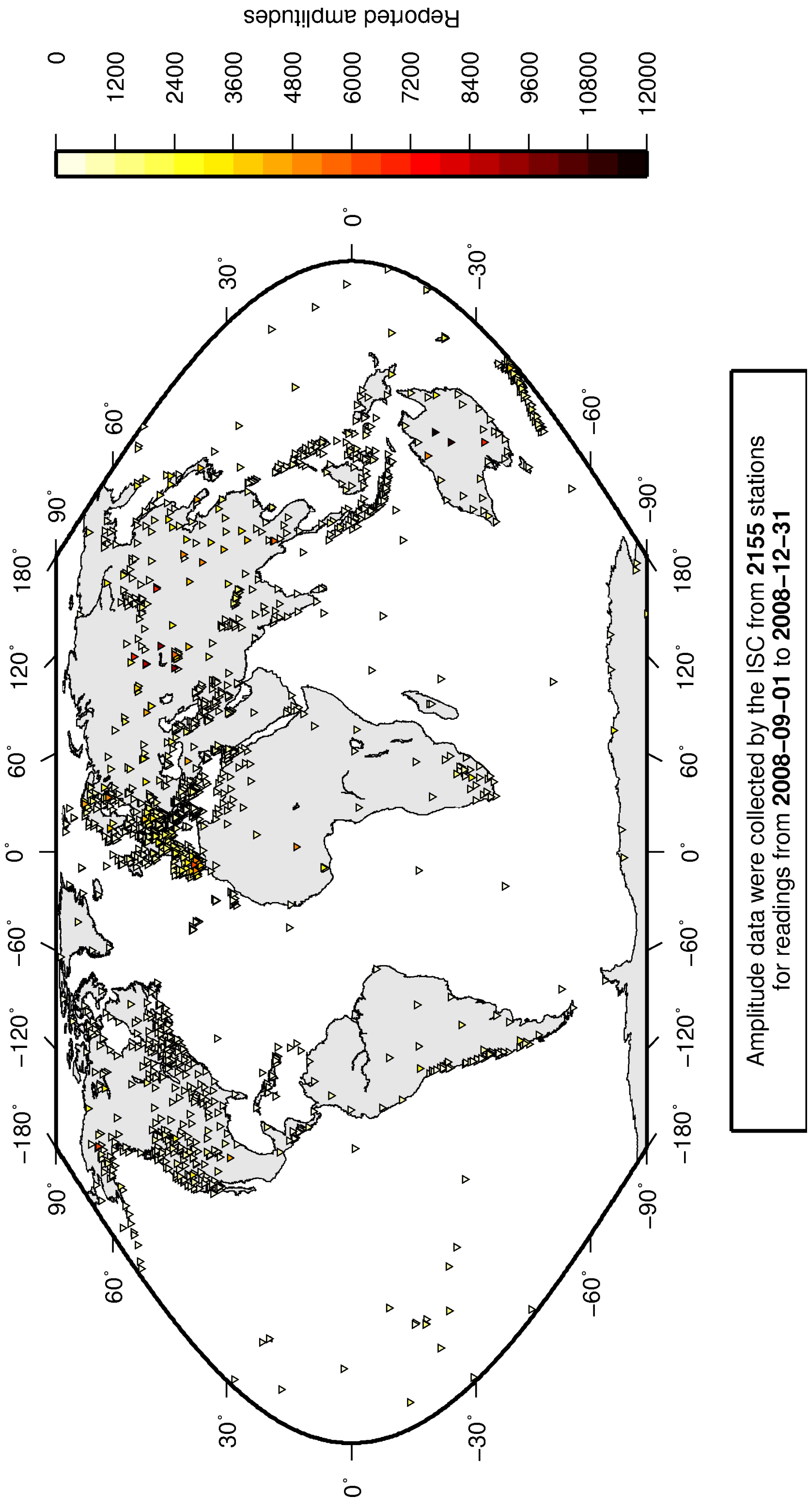

Figure 10.3: Stations contributing amplitude data to the ISC. The total number of amplitude readings reported by each station are shown.

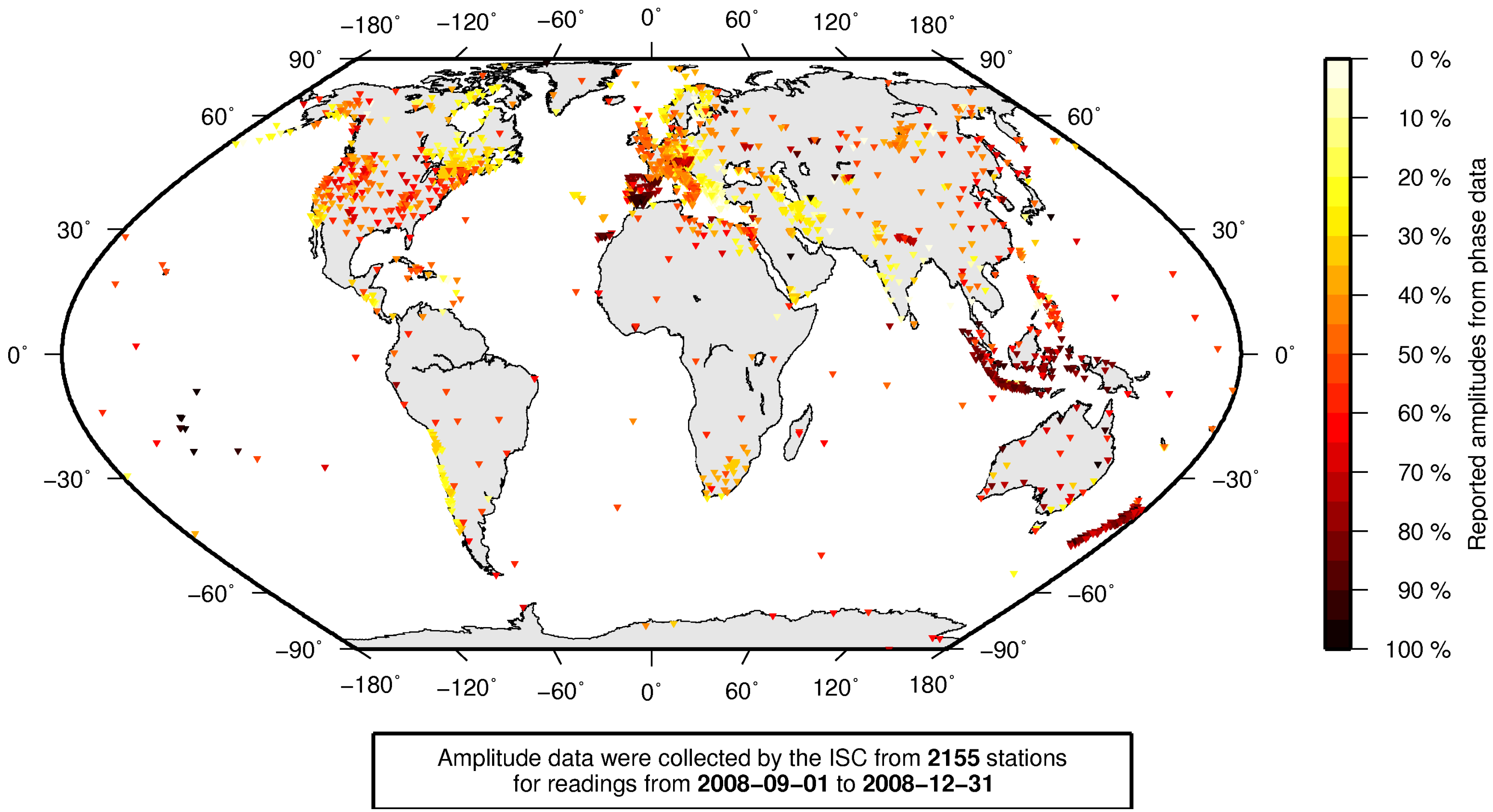

Figure 10.4: The percentage of amplitude data reported to the ISC compared to the total number of phase arrivals reported by each station.

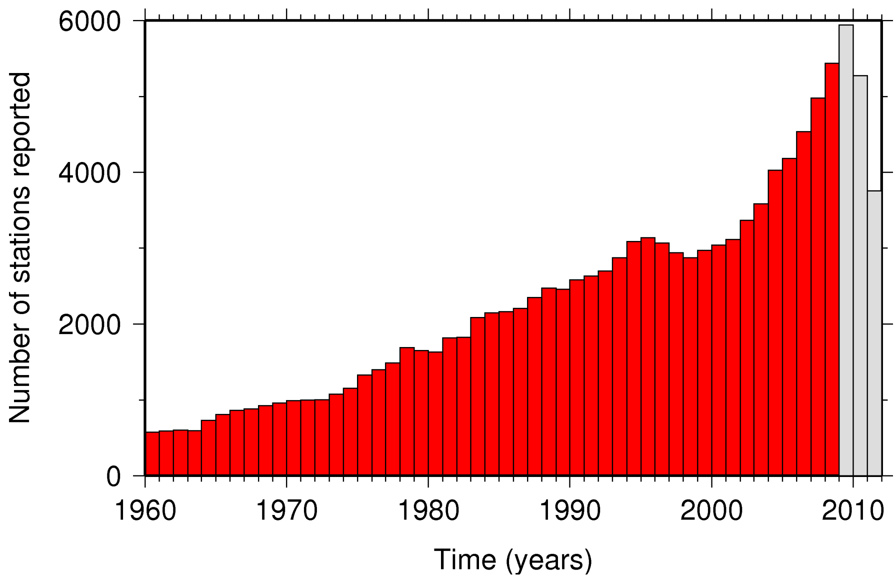

Figure 10.5: Histogram showing the number of stations collected by the ISC for data each year since 1960. The data in grey covers the current period where station information is still being collected before the ISC review takes place and is accurate at the time of publication.

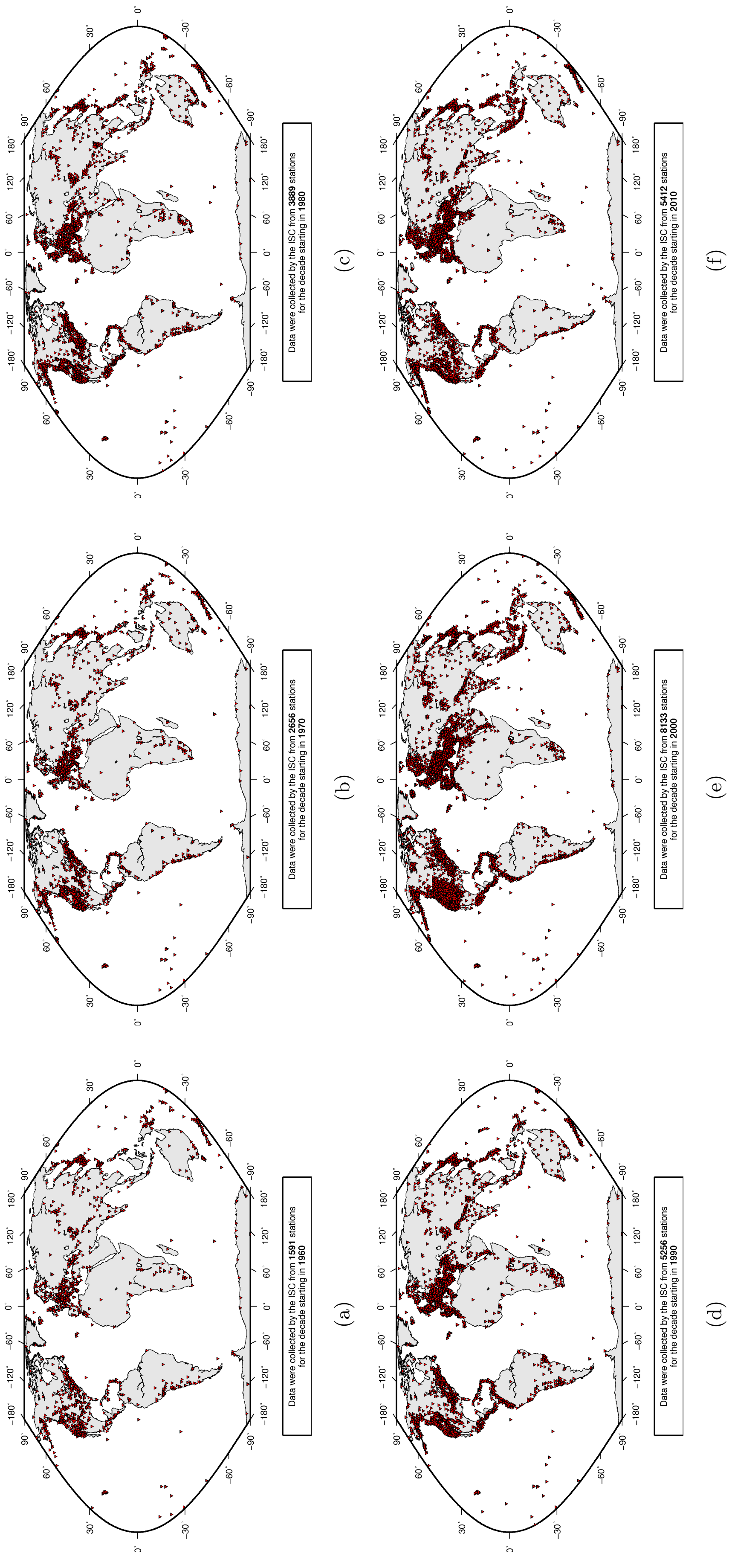

Figure 10.6: Maps showing the stations that reported to the ISC for each decade since 1960.

10.3 Hypocentres collected

The reports containing hypocentres are summarised in Table 10.3. The number of hypocentres collected by the ISC has also increased since 1999, as shown in Figure 10.7. A map of all hypocentres reported to the ISC for September 2008 to the end of December 2008 is shown in Figure 10.8. Where a network magnitude was reported with the hypocentre, this is also shown on the map, with preference given to reported values, first of M_W followed by M_S, m_b and M_L respectively (where more than one network magnitude was reported). The distribution of the network magnitudes displayed on the map is shown in the histogram in Figure 10.9.

10.3: Table summarising the reports containing hypocentres.

Reports with hypocentres	2212
Reports of only hypocentres (no phase readings)	342
Total hypocentres received	205539
Number of duplicate hypocentres	40801 (20%)
Unique agencies contributing hypocentres	138

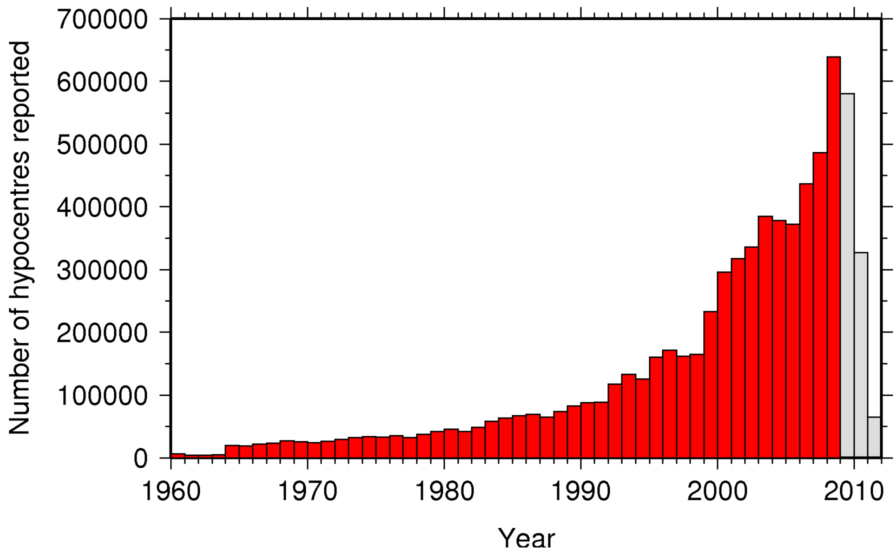

Figure 10.7: Histogram showing the number of hypocentres collected by the ISC for events each year since 1960. For each event, multiple hypocentres are reported.

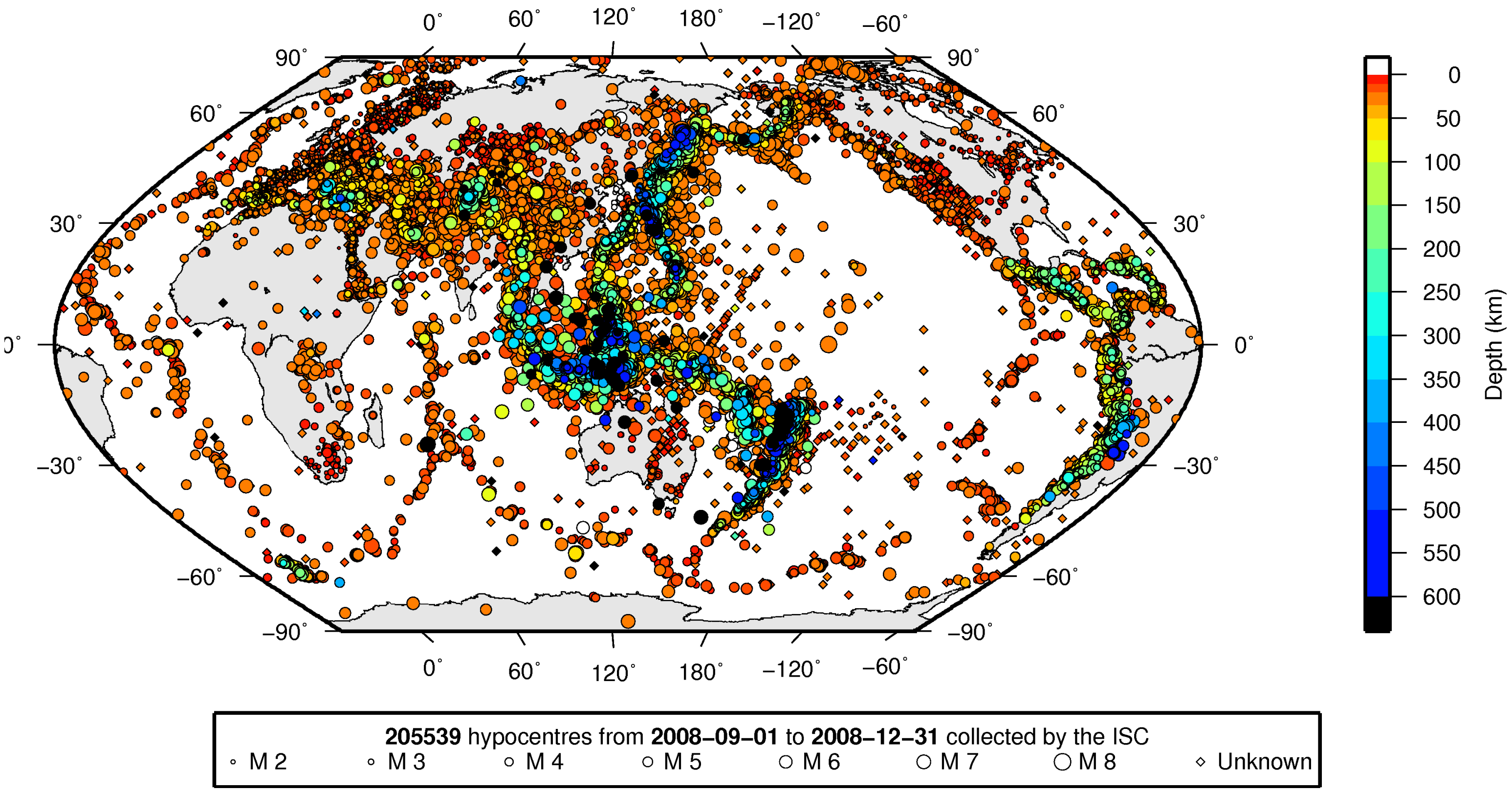

Figure 10.8: Map of all hypocentres collected by the ISC. The scatter shows the large variation of the multiple hypocentres that are reported for each event. The distribution of magnitudes are shown in Figure 10.9. The magnitude corresponds with the reported network magnitude. If more than one network magnitude type was reported, preference was given to values of M_W, M_S, m_b and M_L respectively.

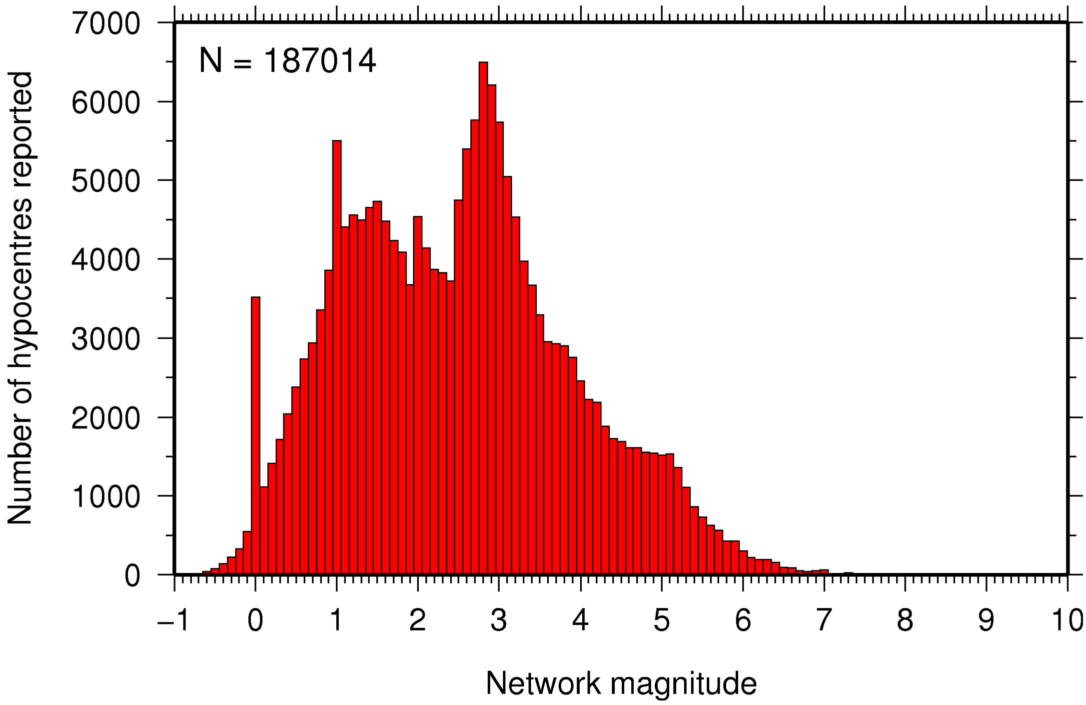

Figure 10.9: Histogram of network magnitudes for hypocentres reported to the ISC. Hypocentres which were reported without a network magnitude are not included in the histogram. The geographical distribution of hypocentres are shown in Figure 10.8. If more than one network magnitude type was reported, preference was given to values of M_W, M_S, m_b and M_L respectively.

10.4 Association of phases with hypocentres

From all the hypocentres reported (Table 10.3), the phases associated by the ISC to those hypocentres (not including ISC authored hypocentres) are summarised in Table 10.4.

10.4: Table summarising the association of phases with hypocentres by the ISC.

Total hypocentres with isc associated phases	88678
Total hypocentres with isc associated IASPEI standard phases	7417
Total hypocentres with isc associated non-standard/unmatched phases	82441
Total number of associated IASPEI standard phases	122677
Unique phase names from the associated IASPEI standard phases	41
Total number of associated non-standard/unmatched phases	1259003
Unique phase names from the associated non-standard/unmatched phases	72
UNFINISHED TABLE	UNFINISHED

10.5: Table of standard phase names associated with hypocentres by the ISC. This does not include ISC authored hypocentres - more phases will be associated to these hypocentres. Only agencies reporting more than 10% of the phases are shown. Those phase names not matching any *IASPEI* standard phase or that differ significantly from the theoretical travel-time are shown seperately in table 10.6.

Phase name	Total associated	Agency (total reported)
AMB	134	SKHL (99%)

10.5: (continued)

Phase name	Total associated	Agency (total reported)
AML	2052	GUC (78%)
AMS	1	SKHL (100%)
Lg	3	NNC (100%)
LR	1592	IDC (89%)
P	11215	IDC (87%)
Pb	3500	WEL (22%), CSEM (13%), NEIC (10%)
PcP	130	IDC (88%)
Pdif	5	NEIC (20%), HEL (20%), IDC (20%), NNC (20%), BJI (20%)
PG	10	PRU (100%)
Pg	13482	CSEM (22%), WBNET (18%)
PKiKP	1	IDC (100%)
PKKPbc	1	NDI (100%)
PKP	2	BER (100%)
PKPab	80	IDC (95%)
PKPbc	930	IDC (95%)
PKPdf	419	IDC (86%)
PKPpre	19	IDC (95%)
pmax	430	MOS (95%)
Pn	48859	WEL (23%), NEIC (16%)
pP	88	IDC (59%), NEIC (25%), MOS (11%)
PP	6	BJI (100%)
pPKPbc	8	IDC (75%), NEIC (12%), MOS (12%)
pPKPdf	9	IDC (67%), NEIC (22%), MOS (11%)
Px	11	DJA (55%)
rx	12	SKHL (100%)
S	985	WBNET (40%), WEL (21%), IDC (20%)
Sb	3363	CSEM (13%), GUC (12%), NEIC (10%)
ScP	9	IDC (89%), NEIC (11%)
Sg	11716	CSEM (22%), WBNET (21%)
SG	17	PRU (100%)
SKKSac	1	BJI (100%)
SKPbc	1	IDC (100%)
SKSdf	1	BJI (100%)
smax	1396	BJI (100%)
Sn	22150	NEIC (16%), MEX (15%)
sP	4	BJI (75%), IDC (25%)
SS	3	BJI (100%)
sS	2	BJI (100%)
Sx	3	BYKL (67%), IDC (33%)
x	27	CASC (52%), NDI (22%), PRU (15%)

10.6: Table of agency phase names associated with hypocentres by the ISC. These phases include phases whose name or travel-time could not be mapped to an appropriate IASPEI standard phase. Only agencies reporting more than 10% of the phases are shown. Those phase names that do match an *IASPEI* standard phase are shown in Table 10.5.

Phase name	Total reported	Agency (total reported)
(Pg)	1	BGR (100%)
A	5434	INMG (77%), SVSA (19%)
AMB	15	SKHL (100%)
AMb	3	BER (67%), KISR (33%)
AML	12088	GUC (48%), PRE (30%), BER (10%)
AMP	521	NOU (81%), HLW (19%)
AMS	9	PRE (100%)
e	1	WAR (100%)
EPg	1	HYB (100%)
L	1	BGR (100%)
Lg	50749	MDD (57%), CSEM (35%)
LG	455	OTT (100%)
LMZ	1	WAR (100%)

10.6: (continued)

Phase name	Total reported	Agency (total reported)
LQ	9	PPT (100%)
max	232	BYKL (100%)
mb	27	OTT (100%)
ml	40	OMAN (100%)
MPN	2	HEL (100%)
MSG	11909	HEL (100%)
MSN	9	HEL (100%)
P	393585	JMA (33%), TAP (14%), CSEM (12%)
P*	9442	WEL (99%)
P*P	2	ZUR (100%)
P1	13	ZUR (100%)
Pb	18836	IRIS (72%), CSEM (27%)
PB	6745	ATH (88%), HEL (12%)
PFAKE	1	NEIC (100%)
PG	11833	PRU (28%), HEL (25%), ATH (21%), WEL (18%)
Pg	116495	CSEM (45%), MDD (20%), ROM (13%)
Pgmax	106	NERS (100%)
PgPg	14	BYKL (100%)
PKP	2	NAO (50%), BER (50%)
PKPdf	2	NAO (100%)
PKS	1	BJI (100%)
Pmax	885	BYKL (99%)
PmP	54	LEDBW (56%), BGR (39%)
Pn	55466	CSEM (49%), NEIC (13%), MDD (10%)
PN	41004	WEL (59%), ATH (27%)
pP	22	BJI (55%), IDC (36%)
PP	3	BJI (100%)
pPcP	4	NEIC (50%), IDC (50%)
pPg	20	SKHL (100%)
pPKPbc	1	IDC (100%)
pPn	4	SKHL (100%)
Px	43	LEDBW (100%)
Rg	906	CSEM (69%), NNC (15%)
RG	1635	HEL (100%)
rx	3	SKHL (100%)
S	341055	JMA (38%), TAP (13%), CSEM (11%)
S*	3782	WEL (99%)
Sb	22178	IRIS (82%), CSEM (18%)
SB	5138	ATH (75%), HEL (25%)
Sg	72948	CSEM (50%), ROM (15%)
SG	18404	HEL (54%), PRU (29%)
Sgmax	167	NERS (100%)
SgSg	8	BYKL (100%)
SKS	1	BJI (100%)
Smax	1186	BYKL (100%)
smax	479	MOS (67%), BJI (33%)
SmS	75	LEDBW (64%), BGR (36%)
Sn	32814	CSEM (40%), MDD (18%), NEIC (10%)
SN	14520	WEL (47%), ATH (36%), OTT (13%)
sP	16	BJI (81%), SKHL (12%)
sPg	6	SKHL (100%)
sPKP	2	BJI (100%)
SS	4	BJI (100%)
sS	2	BJI (100%)
Sx	43	LEDBW (100%)
T	62	PPT (42%), IDC (24%), TRN (16%)
Trac	2230	OTT (100%)
UNKNOWN	5109	LJU (34%), TEH (30%), ECX (15%)
x	140	NDI (48%), PRU (46%)

10.5 Collection of network magnitude data

Magnitudes calculated from individual networks, associated with reported hypocentres are summarised in Table 10.7. The number of unique agencies reporting different sized hypocentres is displayed in Figure 10.10. This is subdivided into various magnitude types in Figures 10.11–10.15. The distribution of hypocentres (nb. not events) with magnitude value for the different magnitudes reported are shown in Figures 10.16–10.20.

Various magnitude types are reported by different agencies. These are listed in full in Table 10.8.

10.7: Table summarising the magnitude values reported for inidividual stations.

Hypocentres the ISC received network magnitude data for	187014
Total number of network magnitudes collected	266435
Total number of unique magnitude types collected	41
Average number of unique magnitude types per hypocentre	1.4
Agencies providing network magnitude data	137
Average number of network magnitude values for each hypocentre	??

10.5.1 Agencies reporting magnitudes

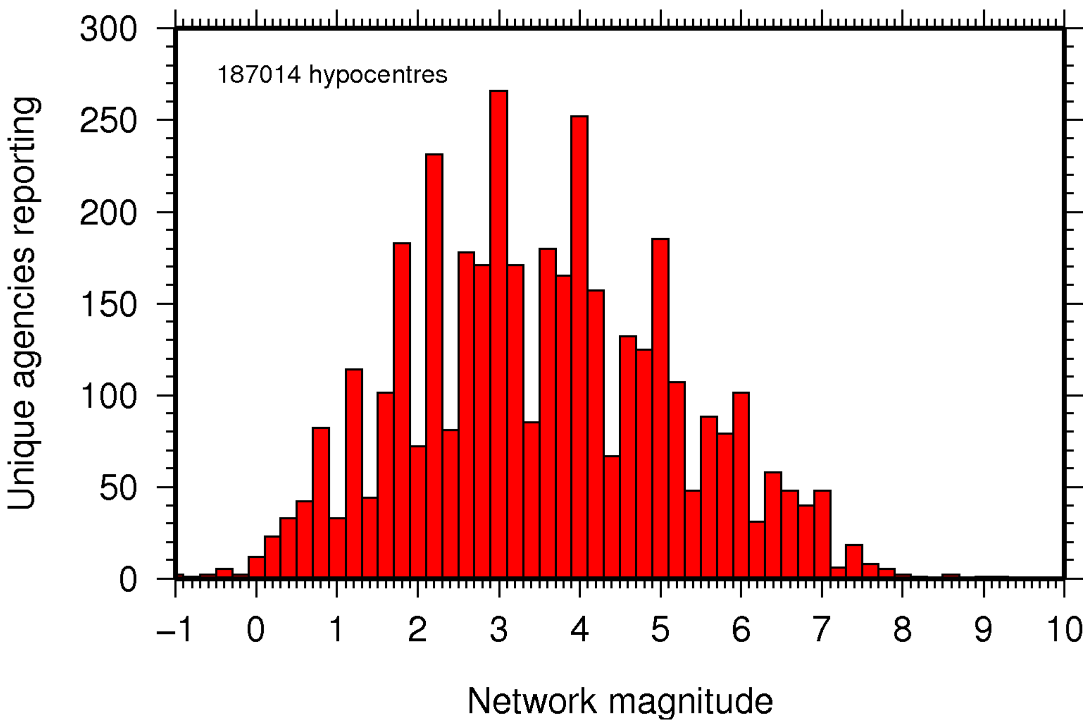

Figure 10.10: Histogram showing the number of unique agencies that reported network magnitude values. All magnitude types are included.

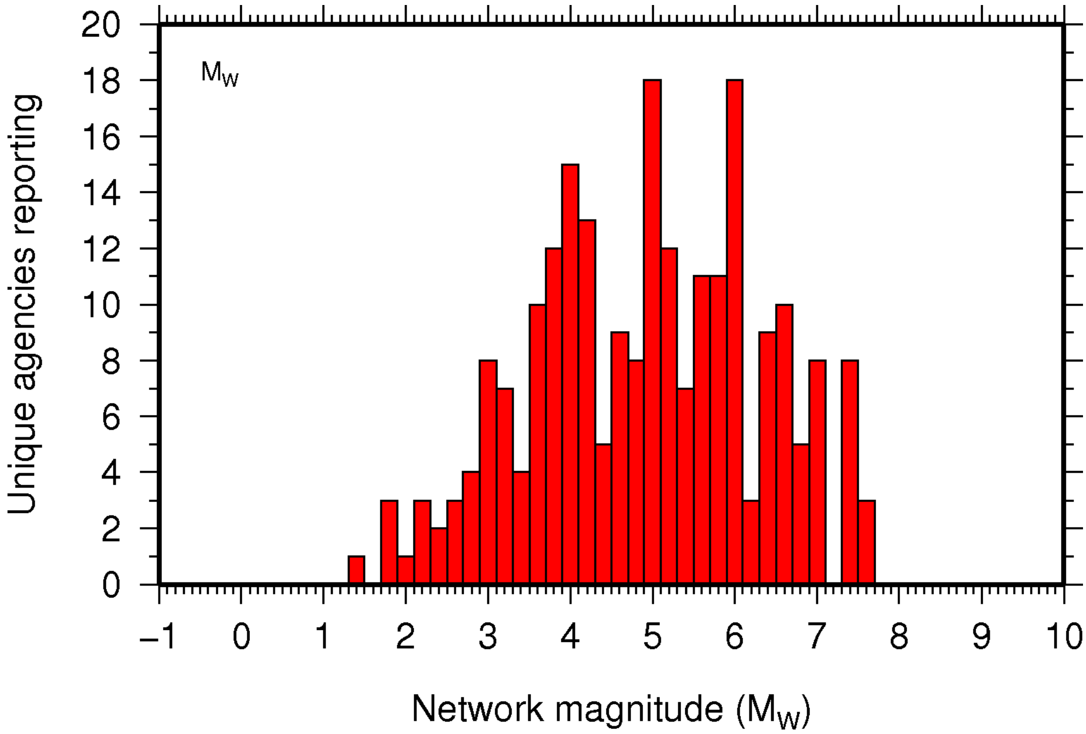

Figure 10.11: Histogram showing the number of unique agencies that reported network magnitude values of M_W. The figure shows unfeasibly small values of M_W being reported.

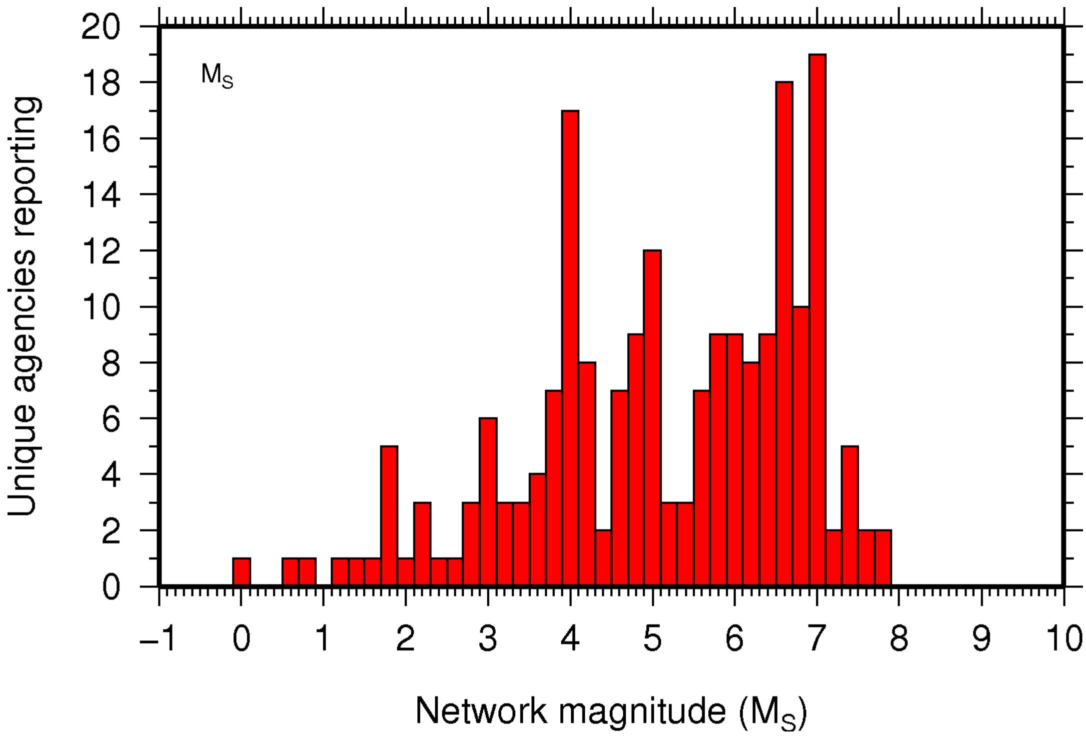

Figure 10.12: Histogram showing the number of unique agencies that reported network magnitude values of M_S. The figure shows unfeasibly small values of M_S being reported.

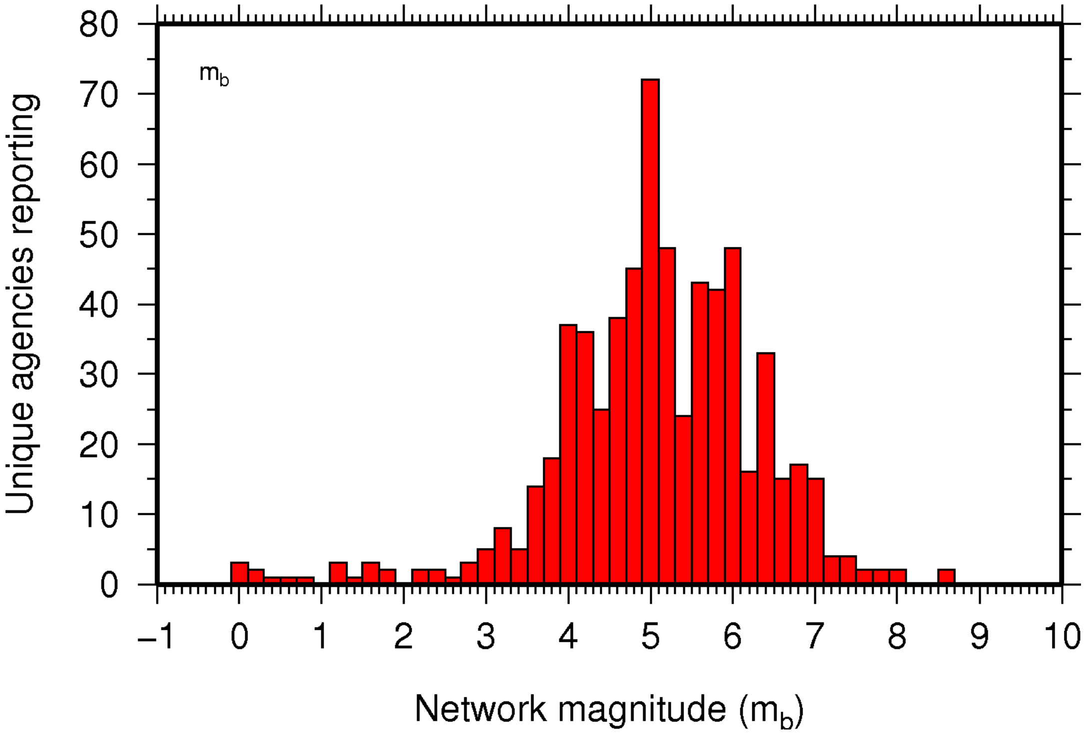

Figure 10.13: Histogram showing the number of unique agencies that reported network magnitude values of m_b. This includes both m_b and m_B.

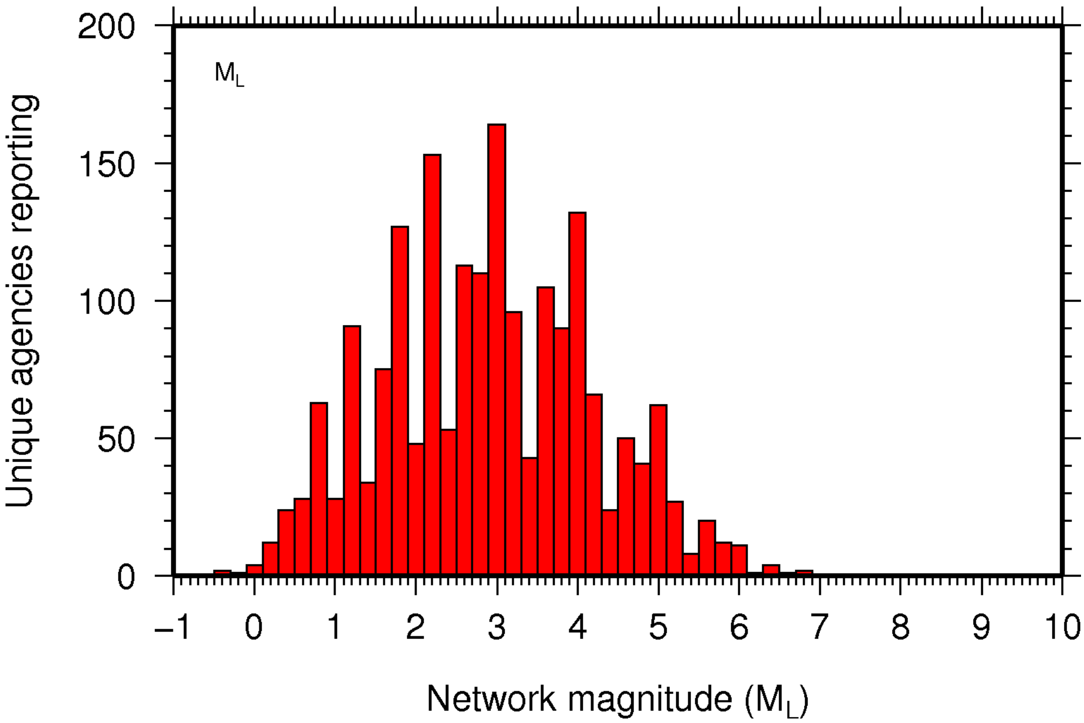

Figure 10.14: Histogram showing the number of unique agencies that reported network magnitude values of M_L.

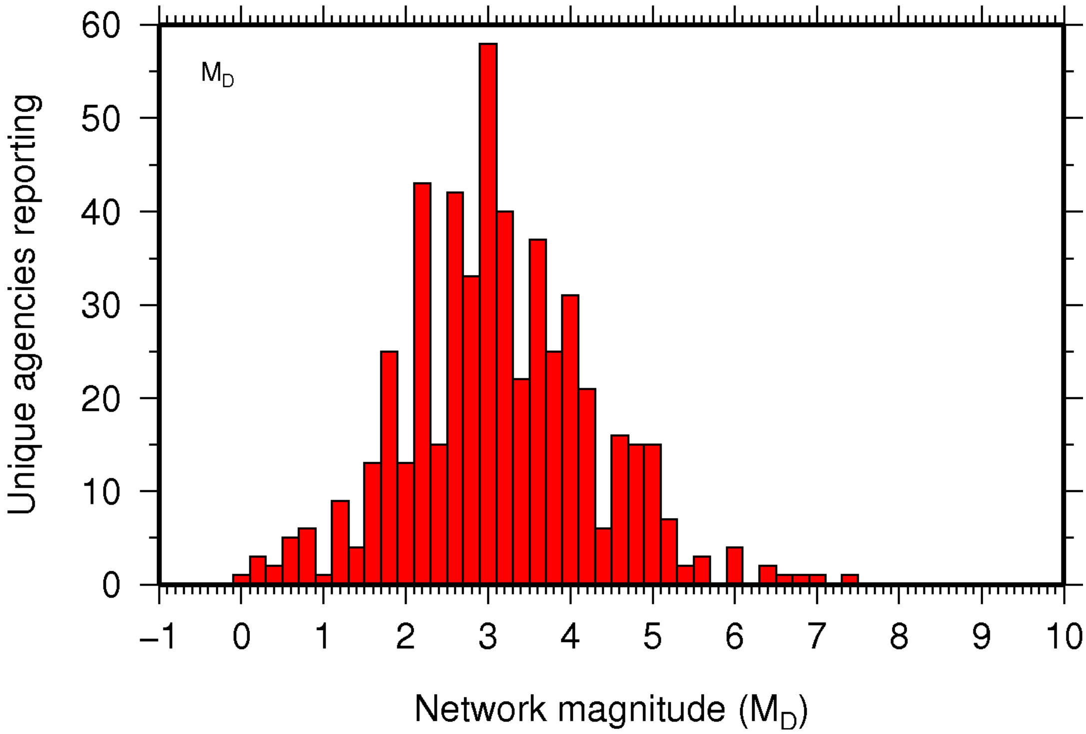

Figure 10.15: Histogram showing the number of unique agencies that reported network magnitude values of M_D.

10.5.2 Network magnitude types

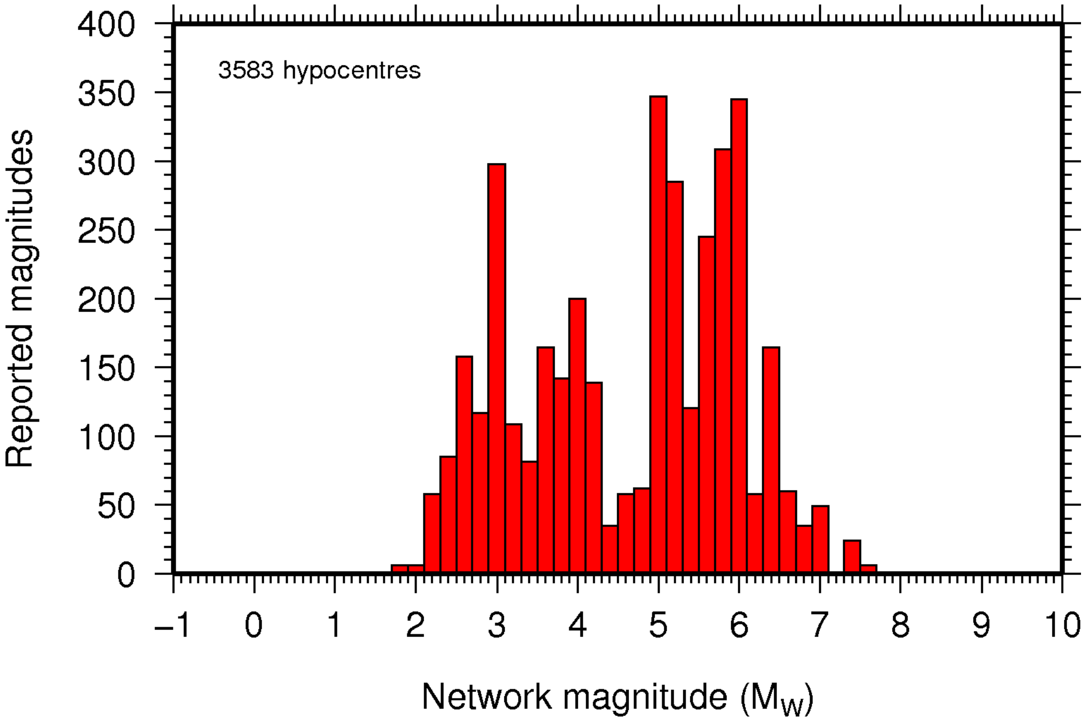

Figure 10.16: Histogram to show the number of reported M_W network magnitudes to the ISC for all corresponding hypocentres.

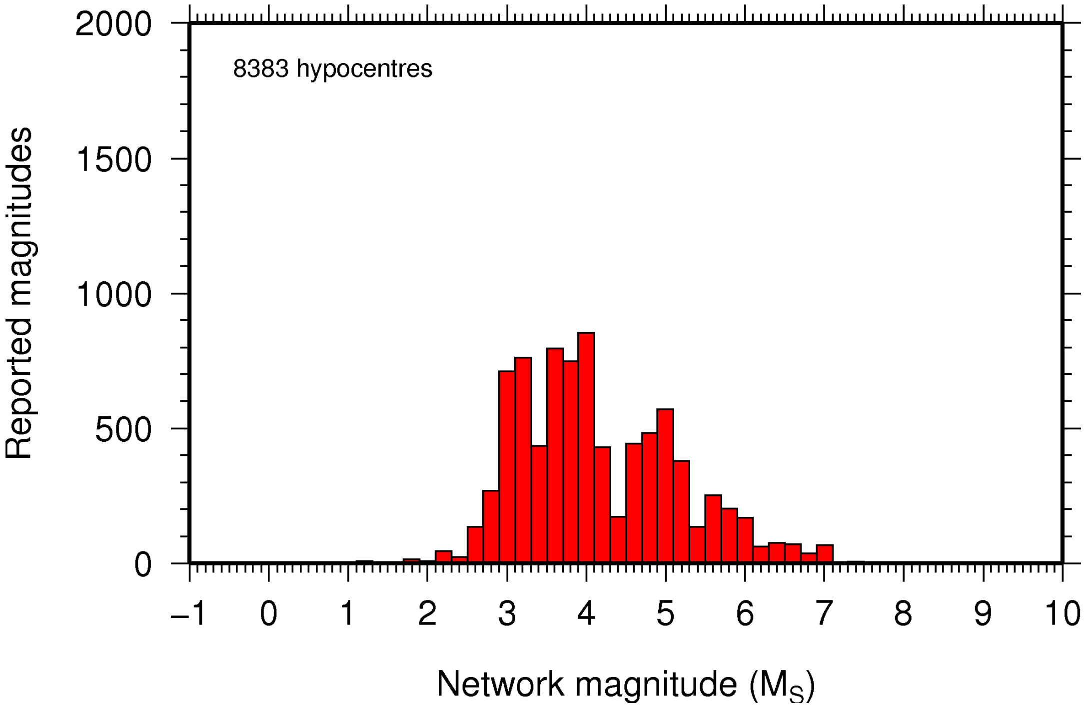

Figure 10.17: Histogram to show the number of reported M_S network magnitudes to the ISC for all corresponding hypocentres.

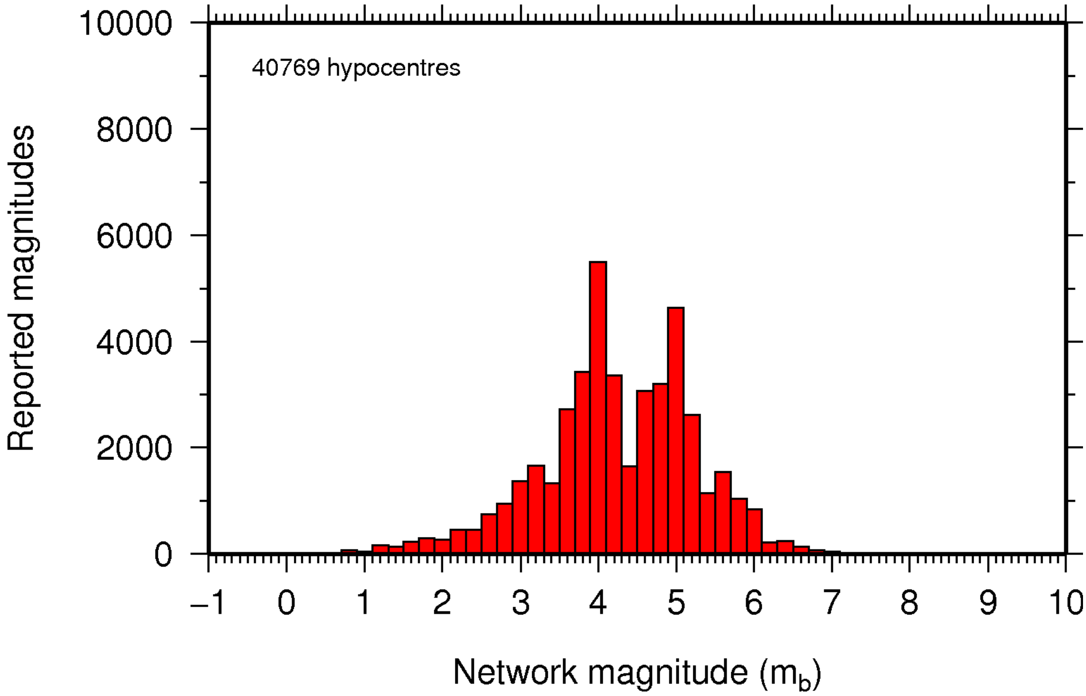

Figure 10.18: Histogram to show the number of reported m_b network magnitudes to the ISC for all corresponding hypocentres. This includes both m_b and m_B.

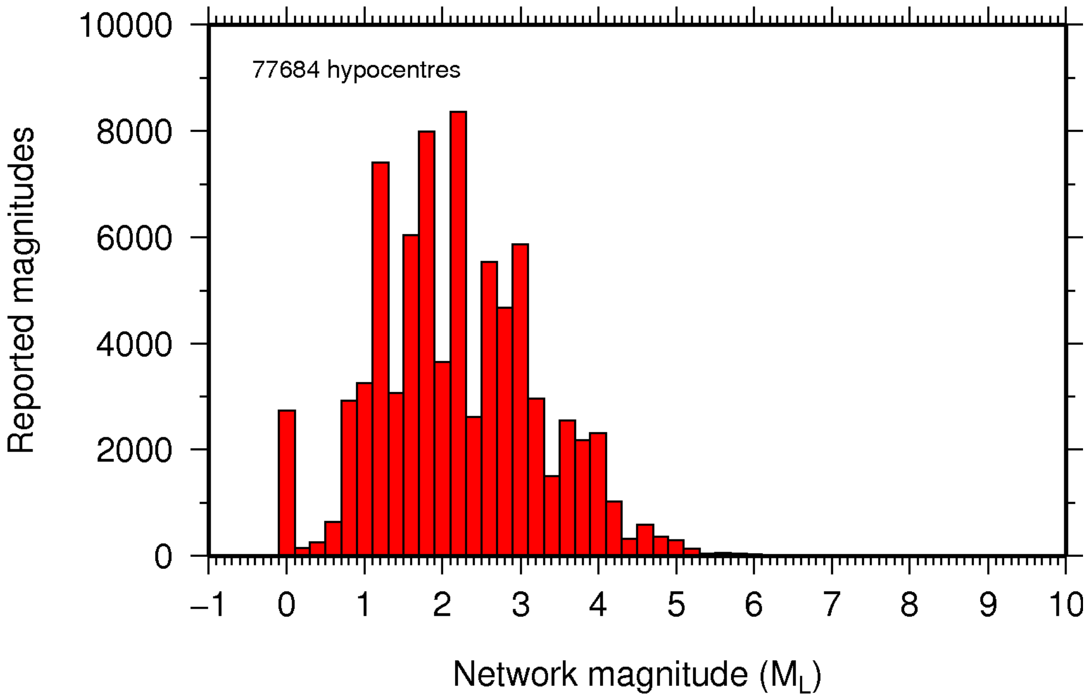

Figure 10.19: Histogram to show the number of reported M_L network magnitudes to the ISC for all corresponding hypocentres.

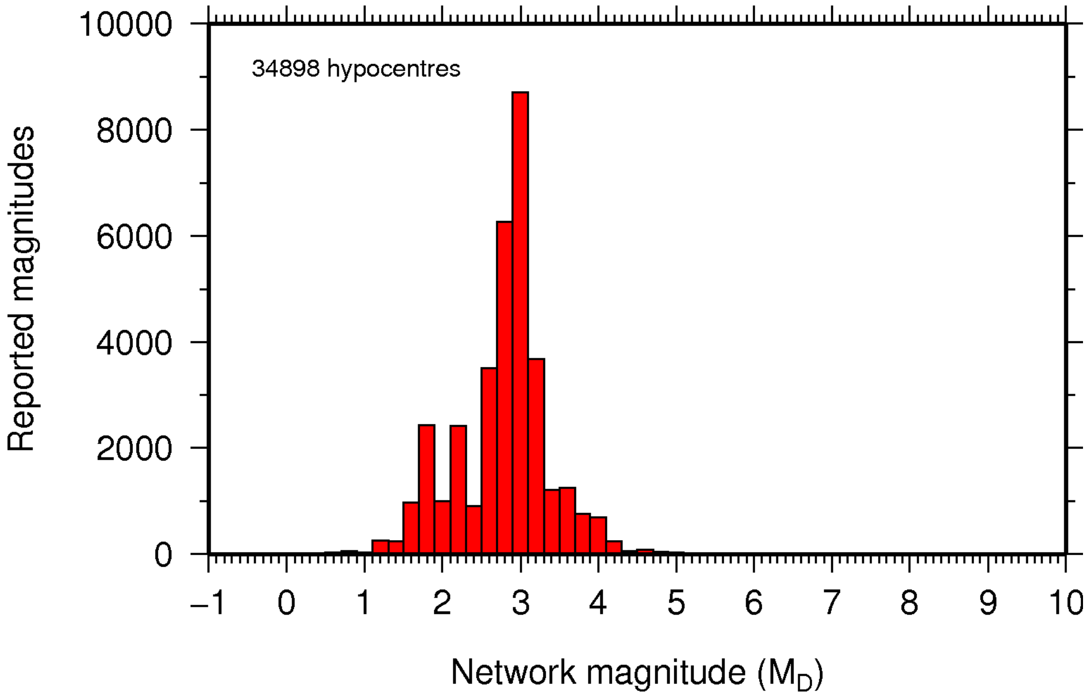

Figure 10.20: Histogram to show the number of reported M_D network magnitudes to the ISC for all corresponding hypocentres.

10.6 Timing of data collection

Here we present the timing of reports to the ISC. In Figure 10.21 the reports are grouped into one of six categories - from within 3 days of an event, to over one year. The histogram shows the distribution with magnitude (for hypocentres where a network magnitude was reported) for each category, whilst the map shows the geographic distribution of the reported hypocentre.

The absolute timing of all hypocentre reports, regardless of magnitude is shown in Figure 10.22.

10.8: Table of all network magnitude types reported. The agencies reporting at least 10% of the corresponding magnitude type are listed.

Network magnitude	Total reported	Agency (percent reported)
LG	3	OTT (33%), NEIC (33%), MDD (33%)
M	3001	NEIC (48%), DJA (33%), SKO (11%)
mB	3393	BJI (41%), DJA (33%), NEIC (26%)
mb	40255	IDC (25%), NEIC (24%), NNC (15%)
mb1	10232	IDC (100%)
mb1mx	10232	IDC (100%)
mbh	16	SKHL (100%)
mbLg	2980	MDD (100%)
mbtmp	10231	IDC (100%)
mbv	16	SKHL (100%)
Mc	125	NSSC (58%), CSEM (38%)
MD	34911	DDA (18%), CSEM (17%), ATH (14%), ISK (13%), ROM (11%)
ME	58	NEIC (100%)
MG	443	JMA (33%), AEIC (28%), GUC (14%), MDD (12%)
ML	79520	CSEM (14%)
MLG	2	NEIC (100%)
MLv	3130	DJA (100%)
Mm	60	NIC (100%)
Mn	428	OTT (49%), MDD (23%), TEH (21%)
MPV	5808	NNC (100%)
MS	8383	IDC (48%), NEIC (13%), BJI (13%)
Ms1	3984	IDC (100%)
ms1mx	3984	IDC (100%)
Ms7	1099	BJI (100%)
msh	48	SKHL (100%)
msha	14	SKHL (100%)
MW	3771	NEIC (22%), GCMT (21%), FUNV (20%), NIED (15%)
Mw(mB)	1125	DJA (100%)
Mwp	18	DJA (100%)
UNKNOWN	39165	JMA (100%)

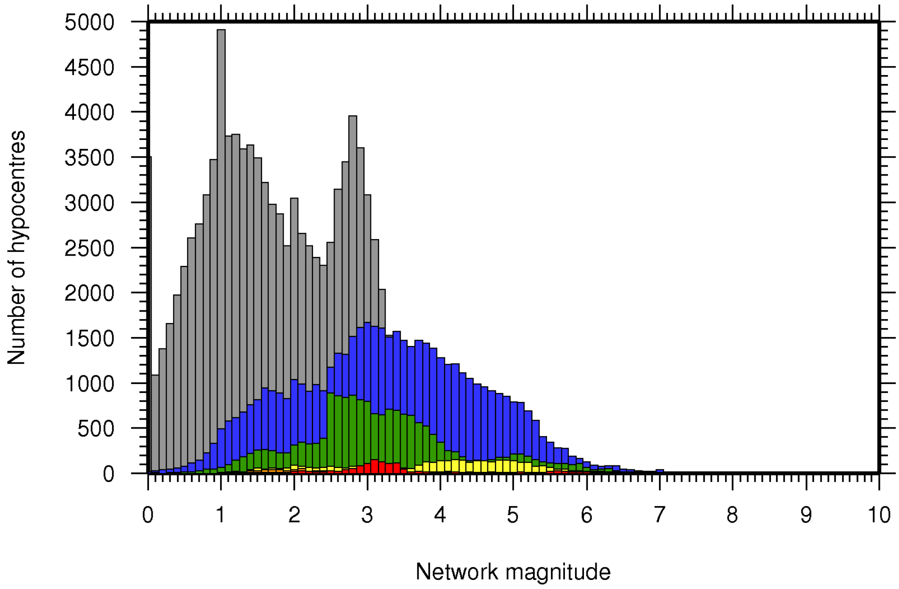

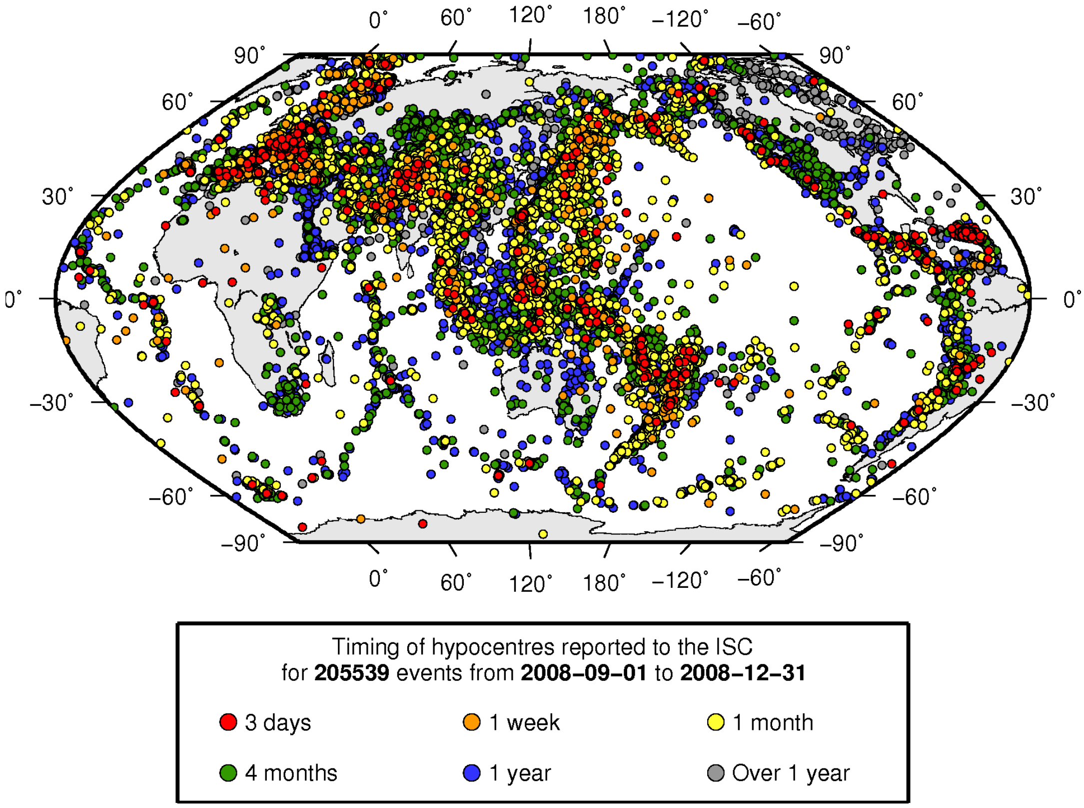

Figure 10.21: Timing of hypocentres reported to the ISC. The colours show the time after the origin time, that the corresponding hypocentre was reported. The histogram shows the distribution with magnitude - only hypocentres with a reported network magnitude (see Figure 10.9) are included in the histogram - if more than one network magnitude was reported, preference was given to a value of M_W followed by M_S, m_b and M_L respectively; all reported hypocentres are included on the map. Note: early reported hypocentres are plotted above later reported arrivals, on both the map and histogram.

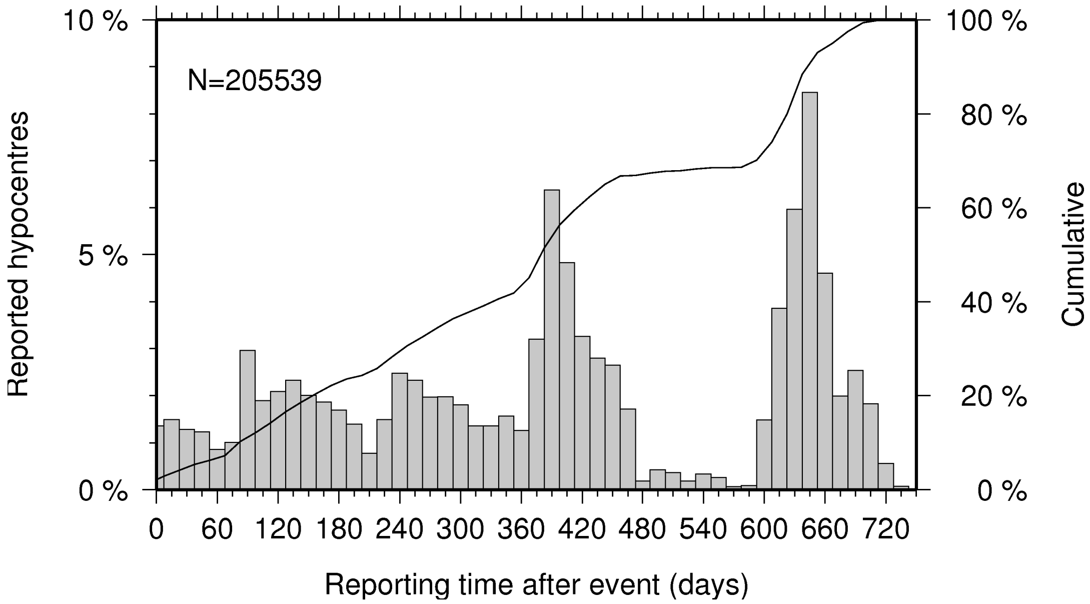

Figure 10.22: Histogram showing the timing of reports of the hypocentres (total of N) to the ISC. The cumulative frequency is shown by the solid line.

10.7 Moment Tensors

A summary of moment tensors reported to the ISC is summarised in Table ...

11

Agencies

11.1 Contributing agencies

The number of agencies which report directly to the ISC is shown in Chapter 5. Some agencies reporting to the ISC, also provide data from additional agencies, which do not report directly to the ISC but are still contributing to the Bulletin. A list of agencies reporting both directly and indirectly is shown in table 11.1 and are shown in figure 11.2. The number of agencies contributing (both directly and indirectly) since 1960 is shown in figure 11.1.

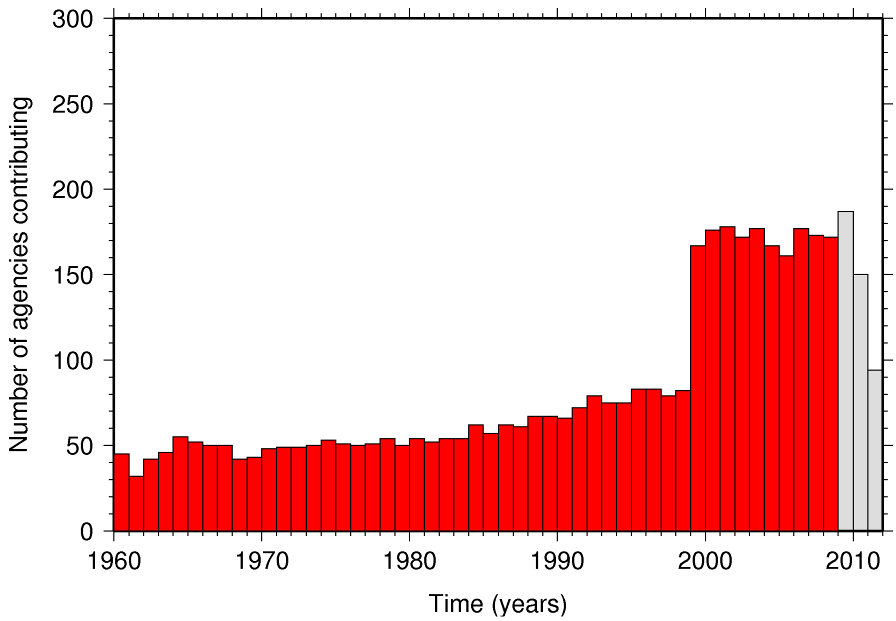

Figure 11.1: Histogram showing the number of agencies contributing to the ISC Bulletin with data from each year since 1960.

11.2 Report types

Data collected by the ISC can consist of multiple data types. They can contain a 'catalogue' of hypocentres, without any associated phase readings labelled; or lists of 'unassociated phase data', without a hypocentre labelled as directly associated with the reading. Of course, some reports may contain any number of these different data types. In table 11.1, the number of different data types reported to the ISC by each agency is listed.

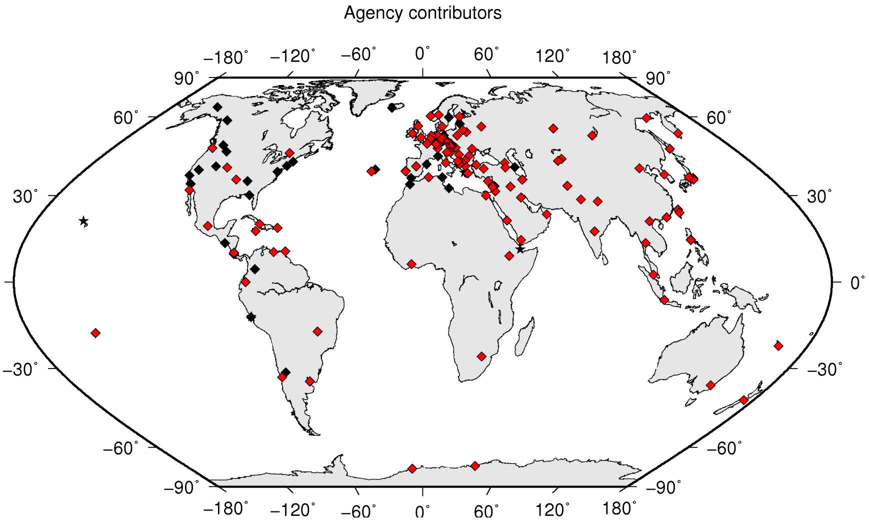

Figure 11.2: Map of agencies that have contributed data to the ISC for this issue of the ISC Bulletin. Agencies that have reported directly to the ISC are shown in red. Those who have reported indirectly (via another agency) are shown in black. Any new/renewed agencies, since the last Bulletin summary, are shown by a star. Each agency is listed in table 11.1.

11.1: Table listing all agencies reporting to the ISC for this summary period. Agencies in bold are either new or renewed reporting since the last summary. The number of each data type reported by each agency is also listed. Agencies reporting indirectly may have 'hypocentres with associated phases' but no associated phases listed - this is due to the association being made by the agency reporting directly to the ISC. A summary map of the agencies and the types of data reported is shown in figure 11.3.

Agency	Country	Directly or indirectly reporting	Hypocentres with associated phases	Hypocentres w/o associated phases	Associated phases	Unassociated phases	Moment Tensor solutions
AAE	Ethiopia	DIRECT	0	0	0	477	0
AEIC	U.S.A.	INDIRECT	17	99	0	0	0
ANF	U.S.A.	INDIRECT	2149	282	0	0	0
ARE	**Peru**	**INDIRECT**	**0**	**2**	**0**	**0**	**0**
ARO	**Djibouti**	**INDIRECT**	**0**	**2**	**0**	**0**	**0**
ASIES	Chinese Taipei	DIRECT	0	19	0	0	0
ASRS	Russia	DIRECT	6	0	73	0	0
ATH	Greece	DIRECT	3275	3087	45208	2914	0
AUST	Australia	DIRECT	0	42	0	10109	0
AWI	Germany	DIRECT	0	0	0	5498	0
AZER	Azerbaijan	INDIRECT	0	57	0	0	0
BELR	Republic of Belarus	DIRECT	0	0	0	2099	0
BEO	Serbia	DIRECT	1029	583	10733	26	0
BER	Norway	DIRECT	811	548	10471	271	0
BGR	Germany	DIRECT	258	363	17745	25	0
BGS	United Kingdom	DIRECT	169	54	5519	5703	0
BJI[1]	China	DIRECT	1963	56	104349	14145	0
BKK	Thailand	DIRECT	0	0	0	2068	0
BNS	Germany	INDIRECT	5	36	0	0	0
BRA	Republic of Slovakia	DIRECT	0	0	0	8636	0
BRG	Germany	DIRECT	0	0	0	3696	0
BUC	Romania	DIRECT	385	53	4437	20149	0
BUD	Hungary	DIRECT	0	31	0	1334	0
BUG	Germany	INDIRECT	26	0	0	0	0
BUT	U.S.A.	INDIRECT	77	9	0	0	0
BYKL	Russia	DIRECT	119	1	7464	0	0

[1]China Earthquake Administration only reports sesimic arrivals from a set of 24 stations designated for International Data Exchange

11.1: (continued)

Agency	Country	Directly or indirectly reporting	Hypocentres with associated phases	Hypocentres w/o associated phases	Associated phases	Unassociated phases	Moment Tensor solutions
CAR	Venezuela	INDIRECT	0	1	0	0	0
CASC	Costa Rica	DIRECT	346	7	8769	0	0
CERI	U.S.A.	INDIRECT	0	1	0	0	0
CLL	Germany	DIRECT	127	0	3735	7220	0
CNRM	Morocco	INDIRECT	0	82	0	0	0
CRAAG	Algeria	DIRECT	281	125	1936	510	0
CSEM	France	DIRECT	19233	41	415434	0	0
DBN	Netherlands	DIRECT	0	0	0	609	0
DDA	Turkey	DIRECT	3620	2627	34846	11282	0
DHMR	Yemen	DIRECT	198	109	2076	2361	0
DIAS	Ireland	DIRECT	0	0	0	163	0
DJA	Indonesia	DIRECT	2139	2191	35050	0	0
DMN	Nepal	DIRECT	1323	35	12808	0	0
DNK	Denmark	DIRECT	0	26	0	4299	0
ECX	Mexico	DIRECT	310	5	4326	0	0
EST	**Estonia**	**INDIRECT**	**0**	**5**	**0**	**0**	**0**
FUNV	Venezuela	DIRECT	737	0	12072	0	0
GCMT	U.S.A.	INDIRECT	0	627	0	0	581
GEN	Italy	INDIRECT	0	374	0	0	0
GFZ	Germany	INDIRECT	7	0	0	0	0
GII	Israel	DIRECT	10	1	216	0	0
GRAL	Lebanon	DIRECT	220	76	1218	483	0
GUC	Chile	DIRECT	2095	38	31091	393	0
HDC	Costa Rica	INDIRECT	0	1	0	0	0
HEL	Finland	DIRECT	3175	2044	50102	2802	0
HKC	Hong Kong	DIRECT	0	0	0	82	0
HLW	Egypt	DIRECT	211	146	3301	0	0
HYB	India	DIRECT	1	0	966	292	0
IDC	Austria	DIRECT	10237	49	176841	0	0
IGIL	Portugal	DIRECT	294	0	1226	15	0
IGQ	Ecuador	DIRECT	0	69	0	2341	0
INMG	Portugal	DIRECT	630	629	27201	999	0
IPEC	Czech Republic	INDIRECT	1	336	0	0	0
IRIS	U.S.A.	DIRECT	0	0	210776	0	0
ISK	Turkey	DIRECT	7	5398	0	40733	0
ISN	Iraq	DIRECT	0	0	0	1264	0
JEN	Germany	DIRECT	0	0	0	1619	0
JMA	Japan	DIRECT	40137	368	280779	327	0
JSN	Jamaica	DIRECT	81	0	478	2	0
JSO	Jordan	DIRECT	532	70	6332	1	0
KISR	Kuwait	DIRECT	303	263	5485	901	0
KLM	Malaysia	DIRECT	0	0	0	2627	0
KMA	Republic of Korea	DIRECT	20	0	489	0	0
KNET	Kyrgyzstan	DIRECT	1298	1	13090	8	0
KRSC	Russia	DIRECT	323	0	6381	11	0
LDG	France	DIRECT	1892	1778	47089	3241	0
LDO	U.S.A.	INDIRECT	0	4	0	0	0
LEDBW	Germany	DIRECT	51	8	1299	0	0
LIB	Libya	INDIRECT	0	57	0	0	0
LIC	Ivory Coast	DIRECT	197	0	591	0	0
LIM	Peru	INDIRECT	0	4	0	0	0
LIS	Portugal	INDIRECT	0	2	0	0	0
LIT	Lithuania	DIRECT	191	47	1223	336	0
LJU	Republic of Slovenia	DIRECT	555	355	6842	4879	0
LPA	Argentina	DIRECT	0	0	0	112	0
LVSN	Latvia	INDIRECT	0	89	0	0	0
MAN	Philippines	DIRECT	0	608	0	10929	0
MAT	Japan	DIRECT	0	0	0	3972	0
MDD	Spain	DIRECT	3166	2254	85702	0	0
MEX	Mexico	DIRECT	674	26	10769	0	0
MOLD	Republic of Moldova	DIRECT	0	0	0	1172	0
MOS	Russia	DIRECT	1814	488	273567	0	0

11.1: (continued)

Agency	Country	Directly or indirectly reporting	Hypocentres with associated phases	Hypocentres w/o associated phases	Associated phases	Unassociated phases	Moment Tensor solutions
MRB	Spain	INDIRECT	0	2	0	0	0
MSSP	Pakistan	DIRECT	0	0	0	1278	0
NAO	Norway	DIRECT	1845	876	3857	0	0
NCEDC	U.S.A.	INDIRECT	9	71	0	0	0
NDI	India	DIRECT	494	0	12912	7700	0
NEIC	U.S.A.	DIRECT	13749	4583	425164	0	418
NERS	Russia	DIRECT	23	0	805	0	0
NIC	Cyprus	DIRECT	69	75	553	199	0
NIED	Japan	DIRECT	0	449	0	0	0
NNC	Kazakhstan	DIRECT	6017	166	36269	36	0
NOU	New Caledonia	DIRECT	377	0	3231	1717	0
NSSC	Syria	DIRECT	70	73	932	0	0
NSSP	Armenia	DIRECT	22	24	447	0	0
OMAN	Oman	DIRECT	504	144	4836	0	0
OTT	Canada	DIRECT	302	14	10968	0	0
PAS	U.S.A.	INDIRECT	62	17	0	0	0
PDA	Portugal	INDIRECT	343	296	0	0	0
PDG	Montenegro	DIRECT	176	177	3717	0	0
PGC	Canada	INDIRECT	566	20	6910	0	0
PLV	Vietnam	DIRECT	16	0	171	0	0
PNSN	U.S.A.	DIRECT	2	45	0	0	0
PPT	French Polynesia	DIRECT	833	4	6050	226	0
PRE	South Africa	DIRECT	670	0	13209	36	0
PRU	Czech Republic	DIRECT	2347	1334	22141	191	0
PTWC	**U.S.A.**	**INDIRECT**	**0**	**1**	**0**	**0**	**0**
QCP	Philippines	DIRECT	0	0	0	133	0
REN	U.S.A.	INDIRECT	14	30	0	0	0
REY	Iceland	INDIRECT	0	17	0	0	0
ROM	Italy	DIRECT	2333	1796	30258	0	0
RSNC	Colombia	INDIRECT	0	3	0	0	0
RSPR	U.S.A.	DIRECT	1336	14	15172	0	0
SCEDC	U.S.A.	INDIRECT	62	74	0	0	0
SEA	U.S.A.	INDIRECT	0	42	0	0	0
SFS	Spain	INDIRECT	0	103	0	0	0
SGS	Saudi Arabia	DIRECT	696	363	3930	0	0
SIO	U.S.A.	DIRECT	1	29	2229	0	0
SJA	Argentina	INDIRECT	0	2	0	0	0
SKHL	Russia	DIRECT	96	96	3287	0	0
SKO	Republic of Macedonia	DIRECT	723	132	3498	1022	0
SLC	U.S.A.	INDIRECT	25	0	0	0	0
SNET	El Salvador	INDIRECT	0	2	0	0	0
SOF	Bulgaria	DIRECT	120	90	941	2052	0
SSNC	Cuba	DIRECT	8	1	71	22	0
SSS	El Salvador	INDIRECT	0	1	0	0	0
STR	France	DIRECT	644	670	7046	637	0
SVSA	Portugal	DIRECT	0	0	5074	2343	0
SYO	Japan	DIRECT	0	0	0	1326	0
SZGRF	Germany	INDIRECT	385	15	0	0	0
TAP	Chinese Taipei	DIRECT	5174	2	115219	0	0
TEH	Iran	DIRECT	624	223	15325	0	0
THE	Greece	DIRECT	3425	3259	59637	3511	0
THR	Iran	DIRECT	154	385	1427	0	0
TIF	Georgia	DIRECT	0	265	0	9628	0
TIR	Albania	DIRECT	183	157	1447	925	0
TRI	Italy	DIRECT	0	0	0	2675	0
TRN	Trinidad and Tobago	DIRECT	2	556	0	12576	0
TUN	Tunisia	INDIRECT	0	9	0	0	0
UCC	Belgium	DIRECT	0	32	0	2487	0
UCR	Costa Rica	INDIRECT	0	3	0	0	0
UNK	Unknown	INDIRECT	7	3	0	0	0
UPA	Panama	INDIRECT	0	2	0	0	0
UPP	Sweden	INDIRECT	0	1199	0	0	0

11.1: (continued)

Agency	Country	Directly or indirectly reporting	Hypocentres with associated phases	Hypocentres w/o associated phases	Associated phases	Unassociated phases	Moment Tensor solutions
UPSL	**Greece**	**INDIRECT**	**0**	**22**	**0**	**0**	**0**
USGS	U.S.A.	DIRECT	0	6	0	0	6
VAO	Brazil	DIRECT	0	0	0	432	0
VIE	Austria	DIRECT	920	648	10547	298	0
WAR	Poland	DIRECT	0	470	0	9944	0
WBNET	**Czech Republic**	**DIRECT**	**4083**	**6**	**62342**	**95**	**0**
WEL	New Zealand	DIRECT	2977	4	70231	3741	0
WES	U.S.A.	INDIRECT	0	2	0	0	0
ZAG	Croatia	DIRECT	0	1	0	5769	0
ZUR	Switzerland	DIRECT	223	209	2046	0	0

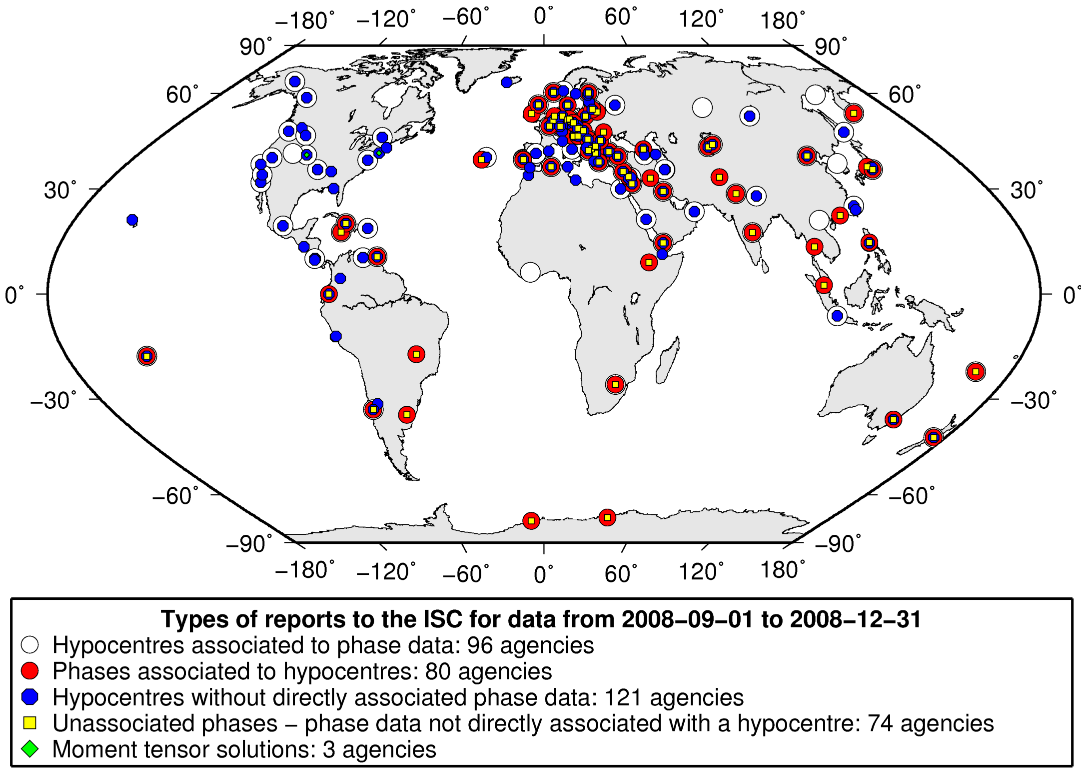

Figure 11.3: Map of the different data types reported by agencies to the ISC. A full list of the data types reported by each agency is shown in table 11.1.

12

ISC Bulletin data

This section provides an overview of the data contained within the ISC Bulletin. Hypocentre estimates have been grouped into events and ....

12.1 Events

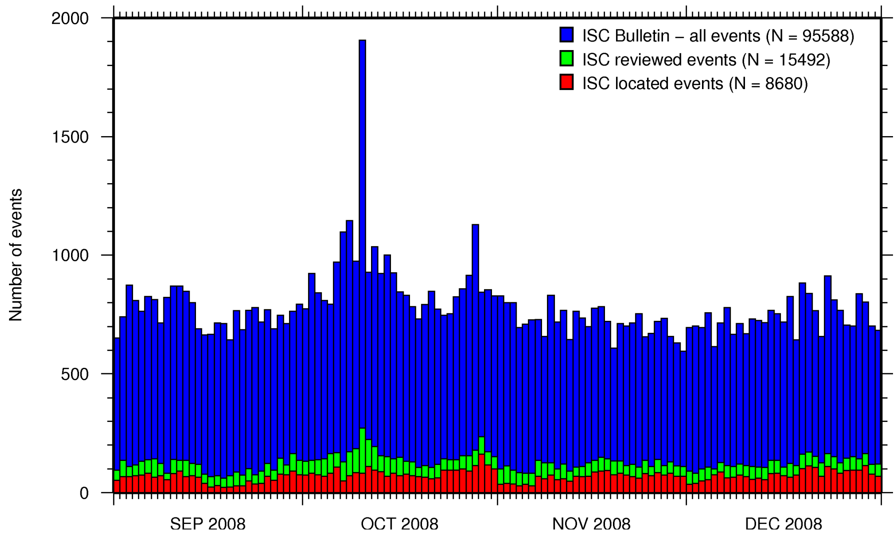

Figure 12.1: Histogram showing the number of events within the bulletin for the current summary period.

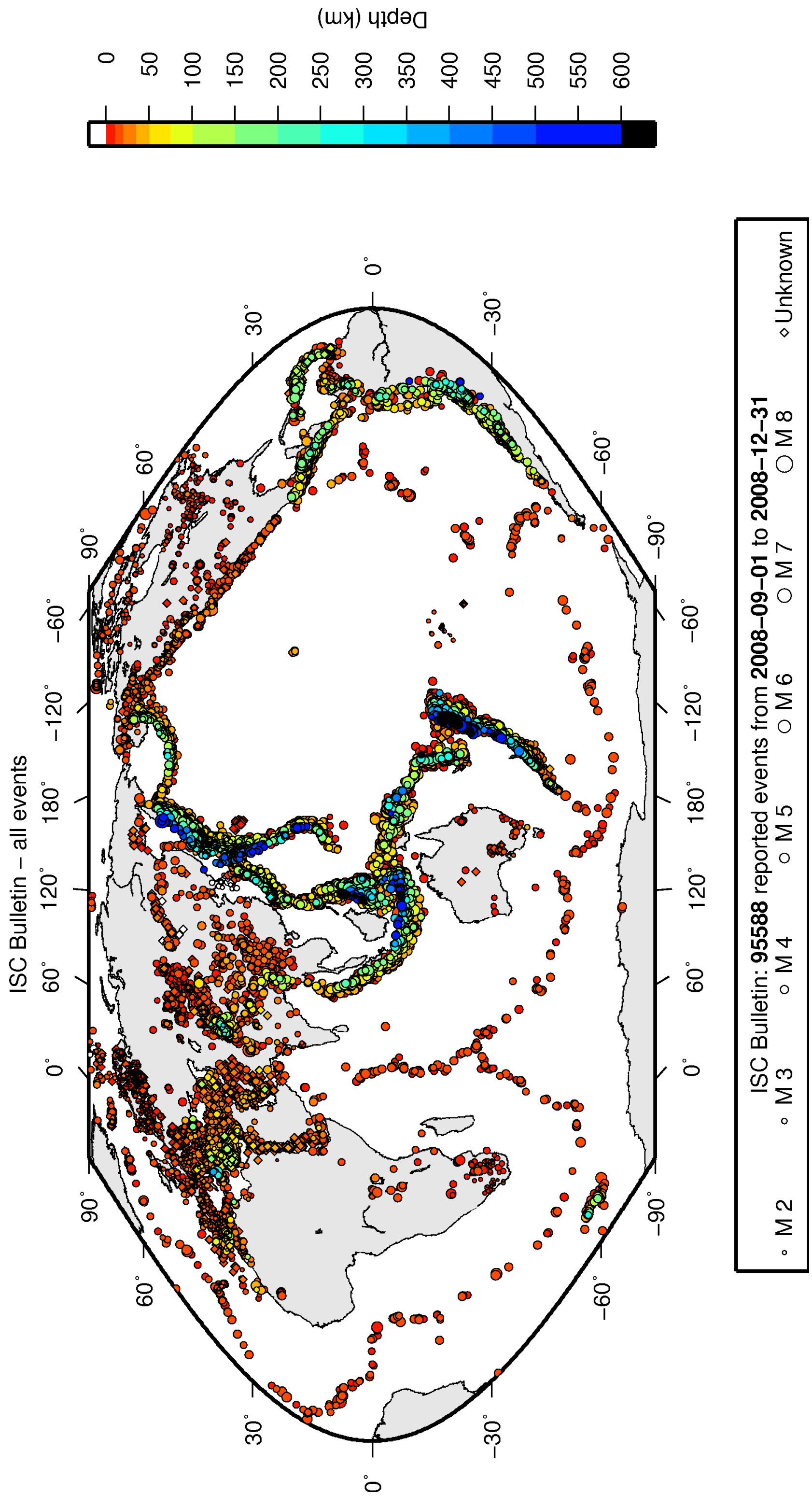

Figure 12.2: Map of all events within the ISC bulletin. Locations show the prime hypocentre.

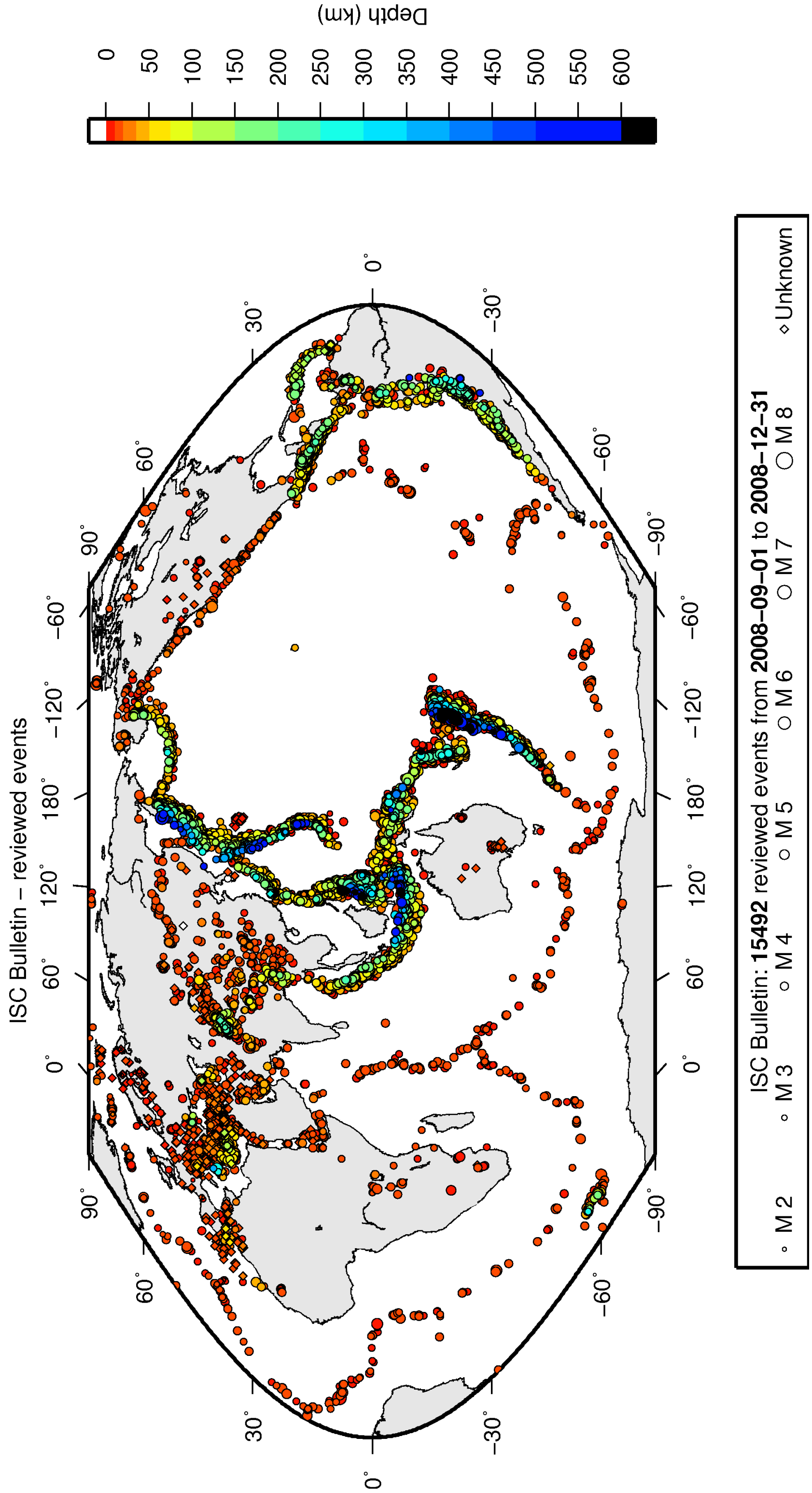

Figure 12.3: Map of all events reviewed by the ISC for this time period. Locations show the prime hypocentre.

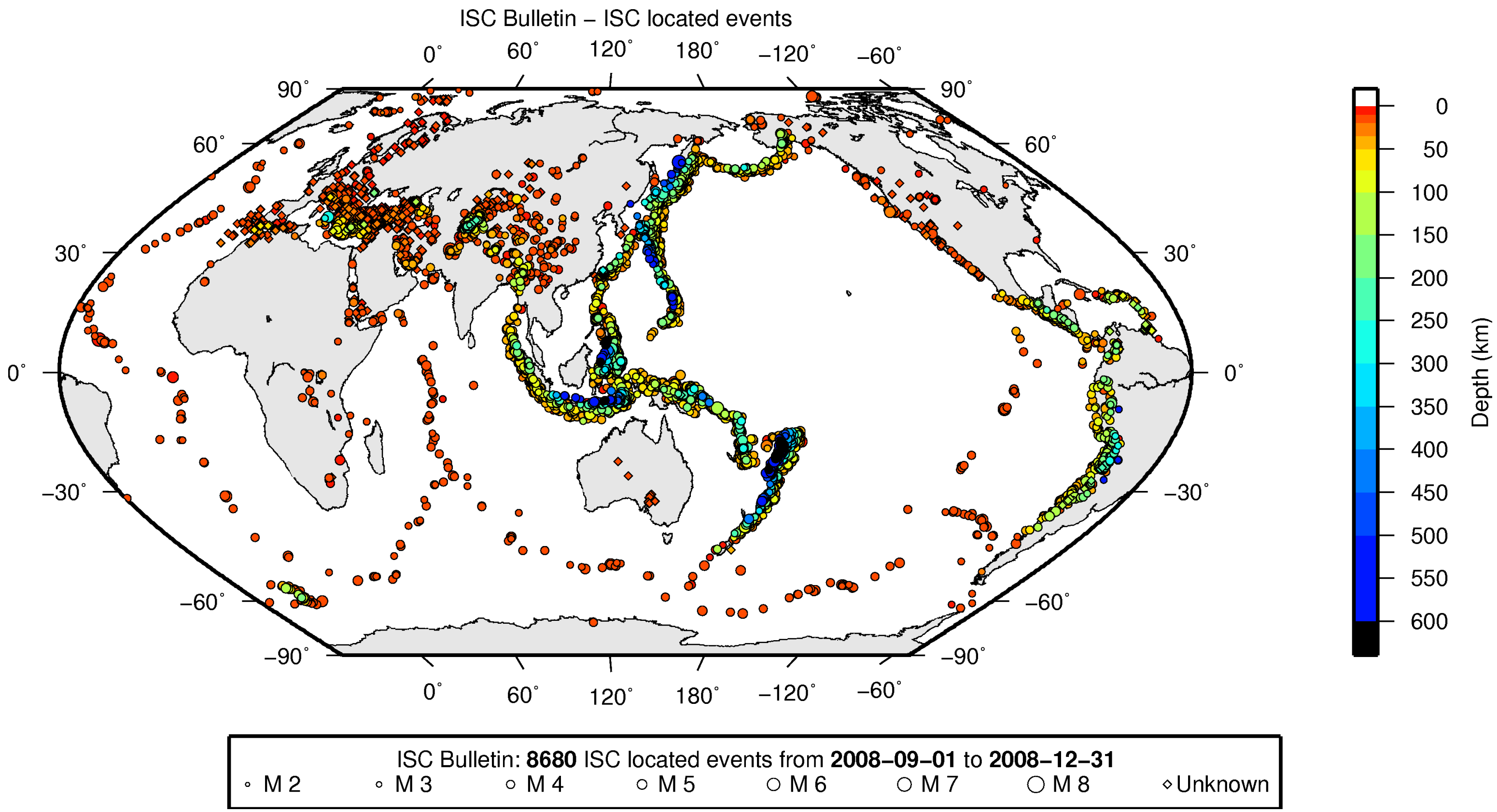

Figure 12.4: Map of all events located by the ISC for this time period. Locations show the ISC determined hypocentre.

12.2 Completeness of the ISC Bulletin

Figures showing the completeness of the bulletin

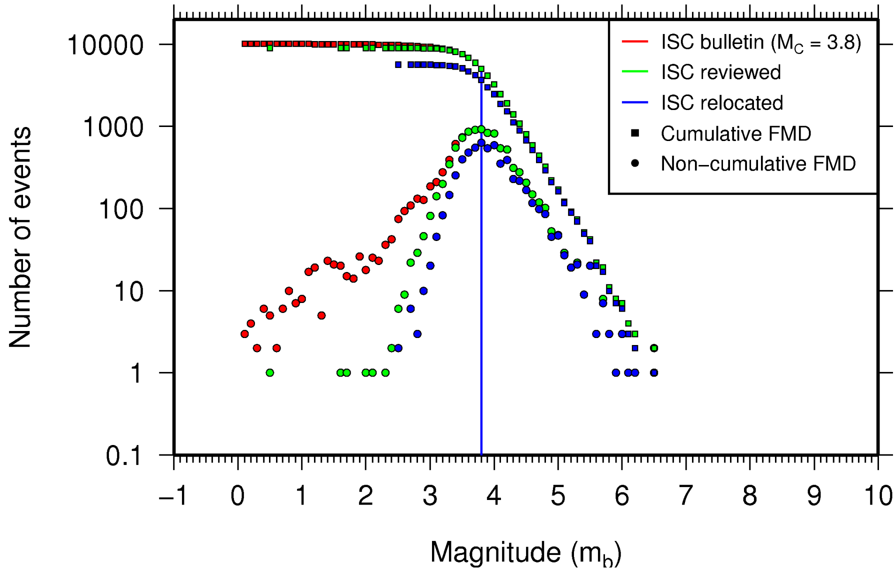

Figure 12.5: Frequency magnitude distribution (FMD) for all events in the ISC bulletin, ISC reviewed events and events located by the ISC. The magnitude of completeness (M_C) is shown in all cases. Note: only events with values of m_b are represented in the figure.

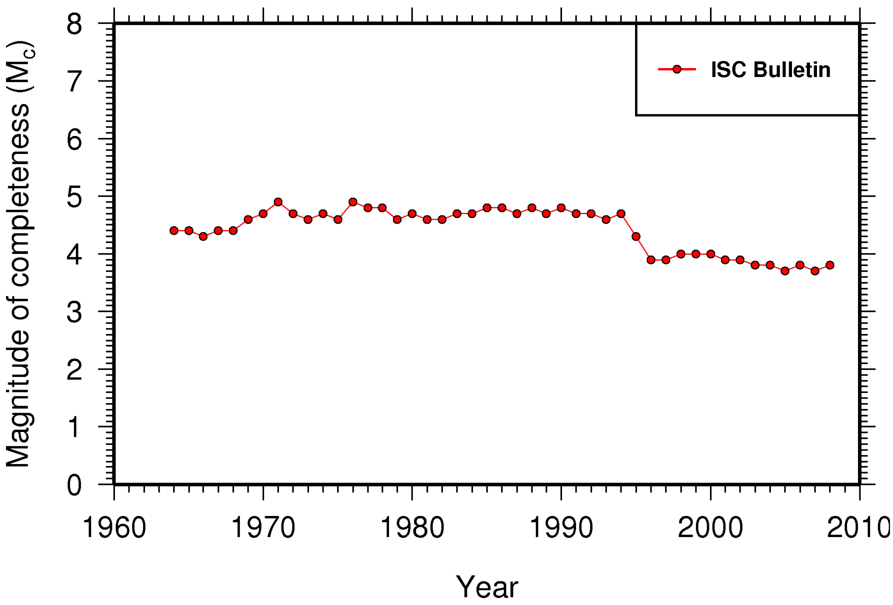

Figure 12.6: Variation of magnitude of completeness (M_C) for each year in the ISC bulletin. Note: M_C is calculated only using those events with values of m_b.

12.3 Comparison of ISC determined depths with reported depths

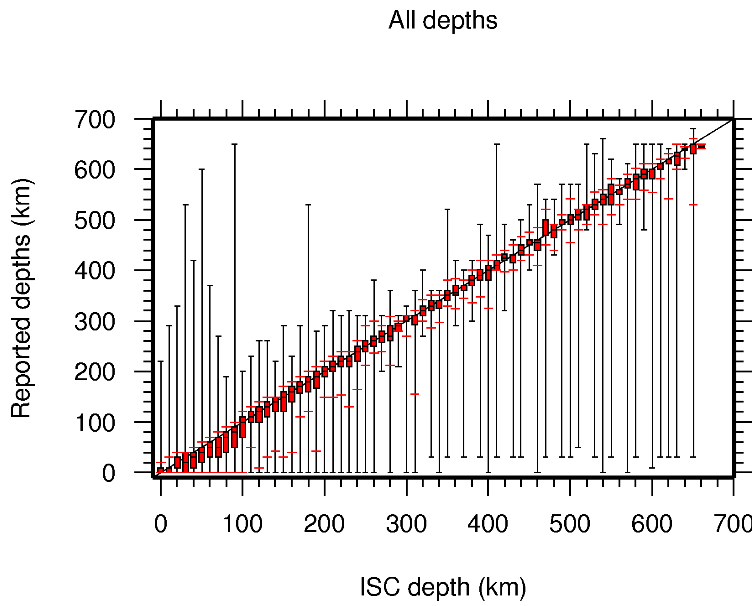

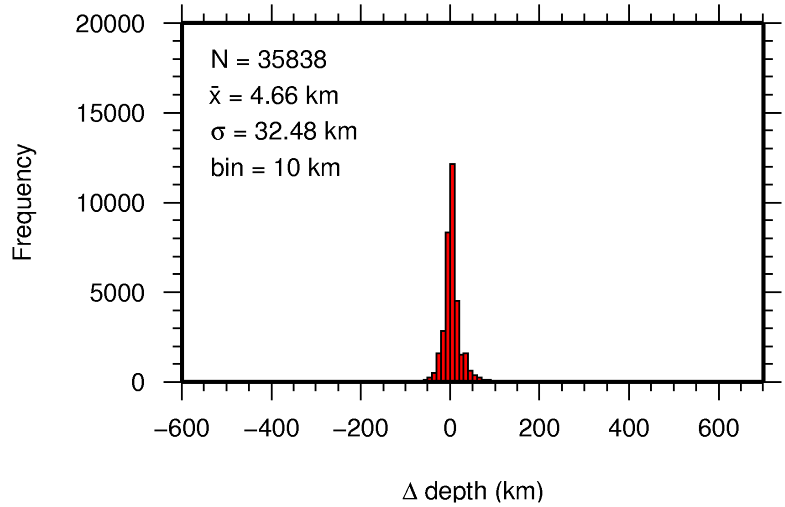

Figure 12.7: Comparison of depths for events with an ISC solution. Top: box-and-whisker plot summarising the differences with depth. The error bars show the maximum and minimum values with red horizontal lines showing the 10th and 90th percentiles; the box shows the interquartile range (25%–75%), with the median value displayed as a horizontal line. All depths are binned to the nearest 10 km. Bottom: histogram showing the differences with the ISC determined depth for all events and at all depths. Δ depth is the *ISC depth − reported depth*.

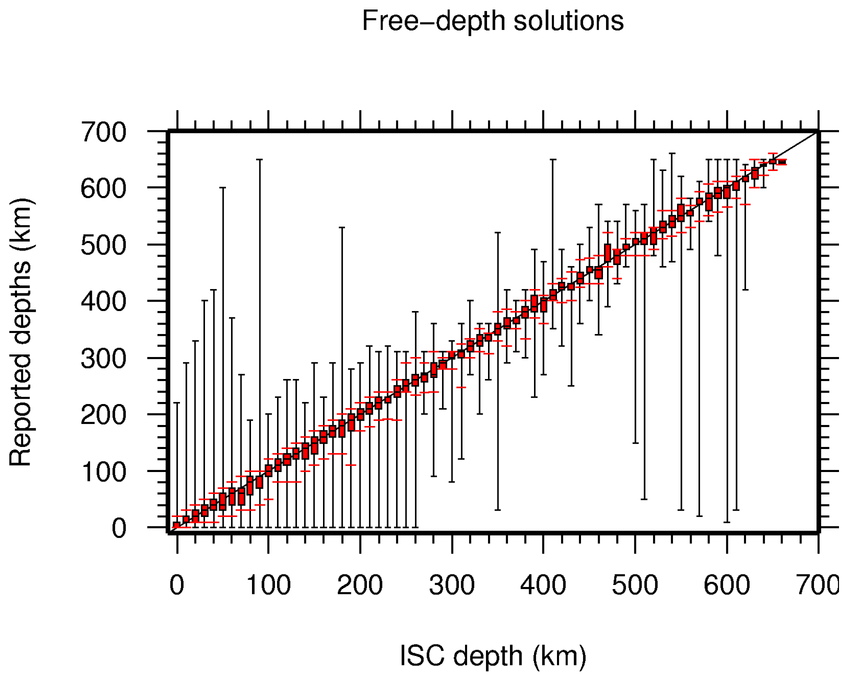

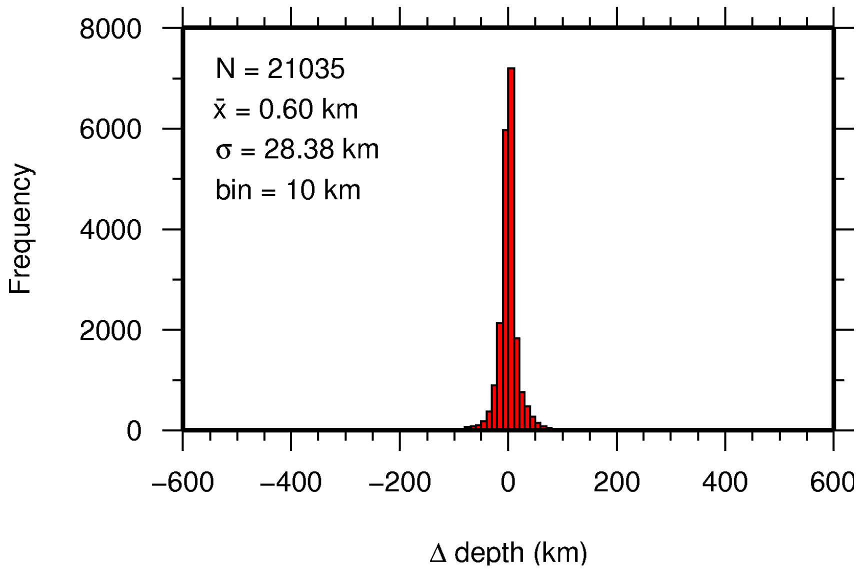

Figure 12.8: Comparison of free-depths for events with an ISC solution. These include depth-phase solutions. Top: box-and-whisker plot summarising the differences at different ISC depths. The error bars show the maximum and minimum values with red horizontal lines showing the 10th and 90th percentiles; the box shows the interquartile range (25%–75%), with the median value displayed as a horizontal line. All depths are binned to the nearest 10 km. Bottom: histogram showing the differences with the ISC determined depth for all events with a free depth and at all ISC depths. Δ depth is the *ISC depth − reported depth*.

12.4 Comparison of epicentres with ISC location

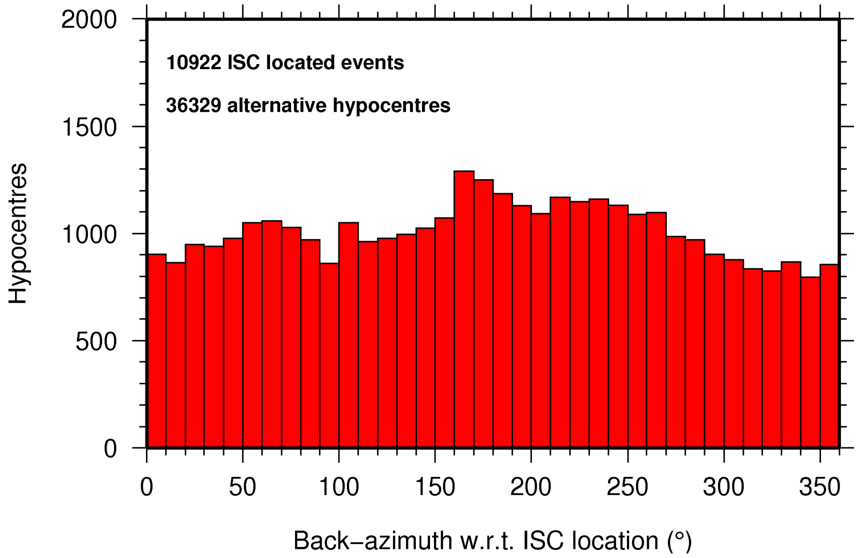

(a)

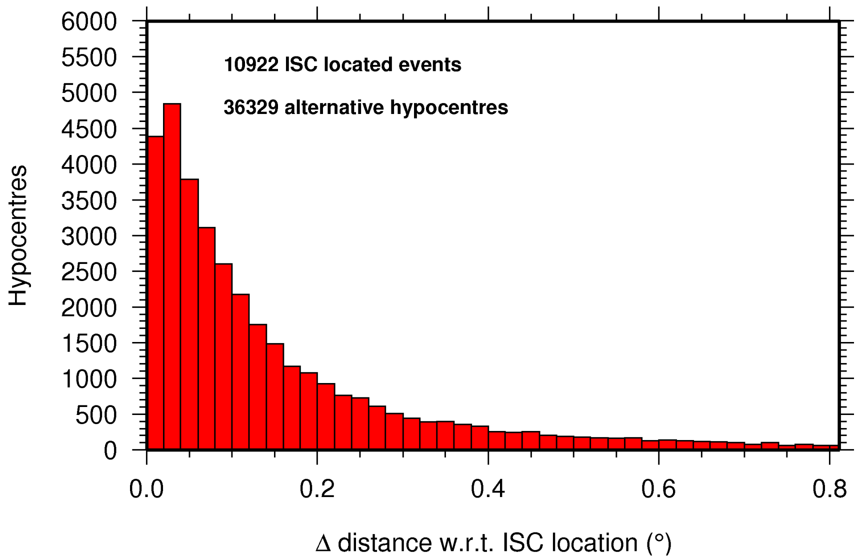

(b)

Figure 12.9: Histograms to show the distribution of back-azimuth and great-circle distance with respect to the ISC computed hypocentre. In (b), distances greater than the 95th percentile are not shown.

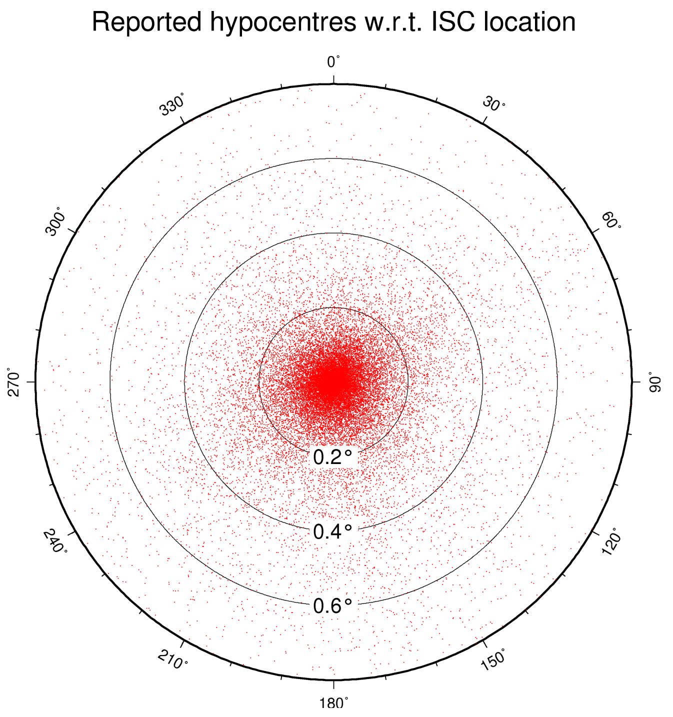

(a)

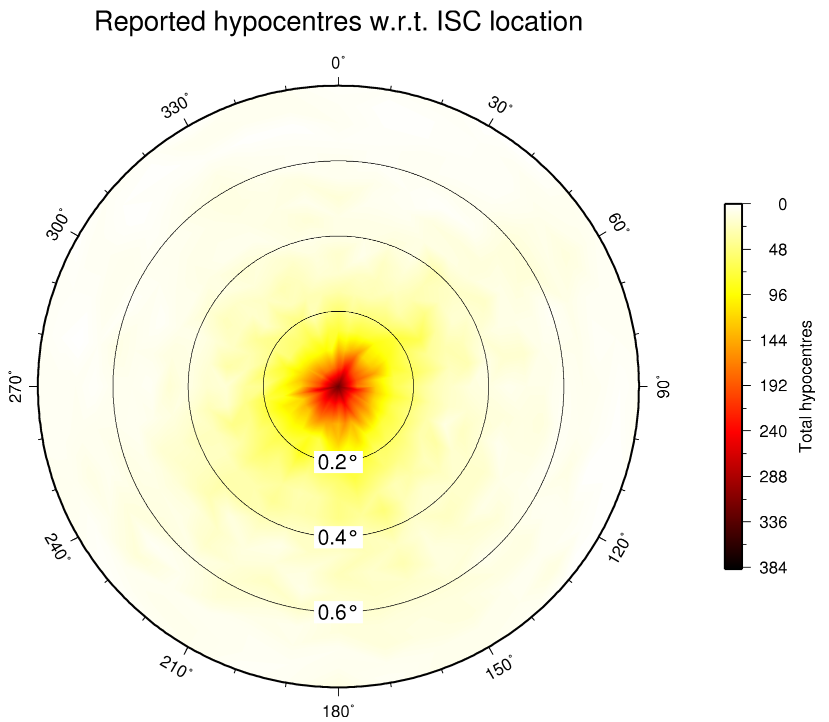

(b)

Figure 12.10: Discrepancy of hypocentres in terms of back-azimuth and great circle distance, with respect to the ISC computed hypocentre. Hypocentres with distances greater than the 95th percentile are not shown. (a) shows all hypocentres; (b) shows the total number of hypocentres contoured.

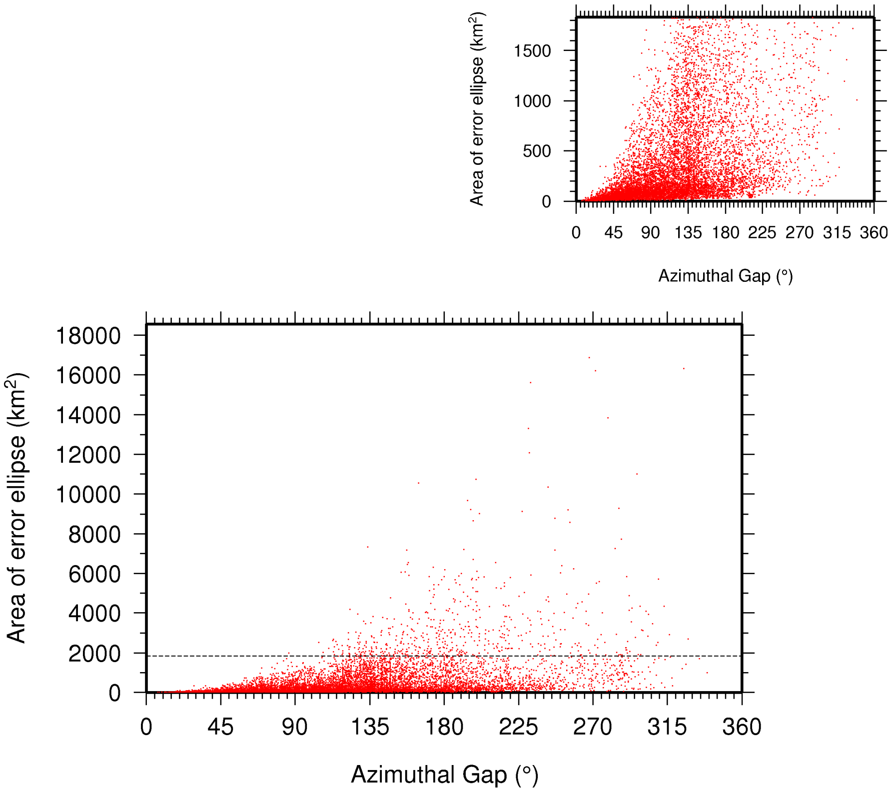

Figure 12.11: Variation of error ellipse size with azimuthal gap for ISC located events from the ISC Bulletin. The dashed line shows the 95th percentile for the area of the error ellipse. A zoom of the data below this limit is shown outset of the main figure.

12.5 Residuals and phase arrival-times

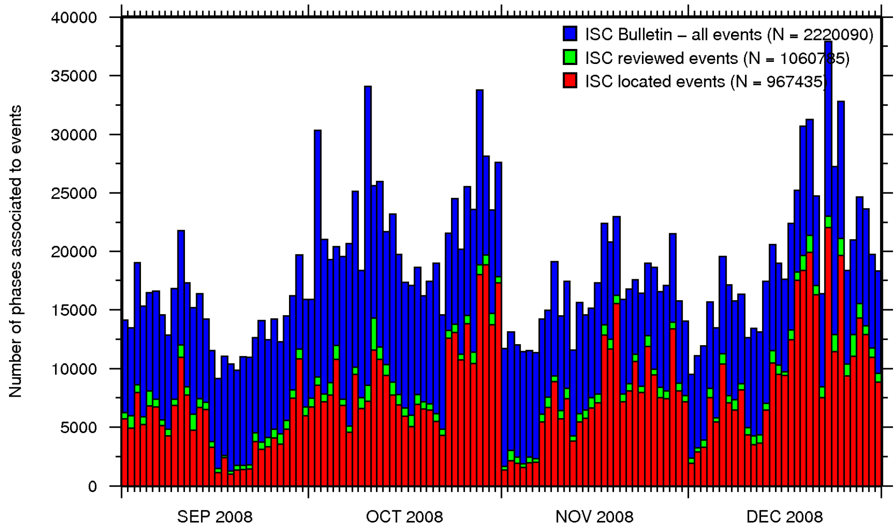

Figure 12.12: Histogram showing the number of phases that the ISC has associated to events within the bulletin for the current summary period.

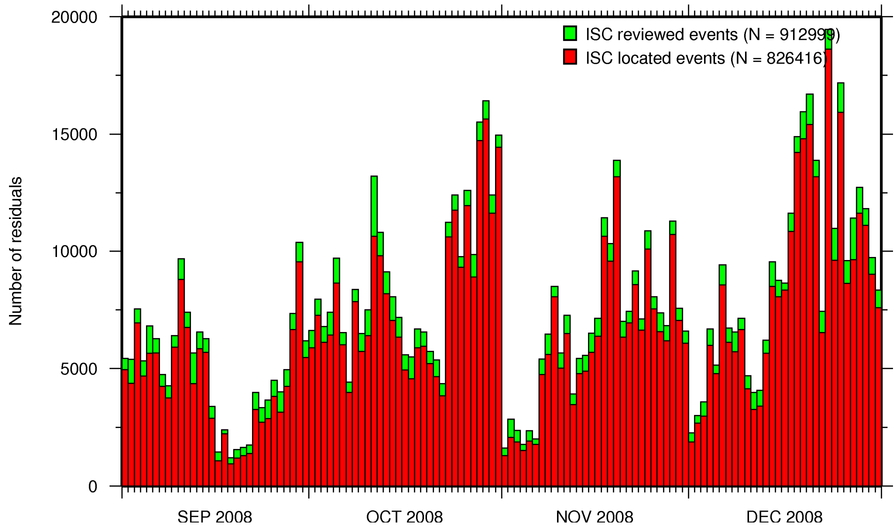

Figure 12.13: Histogram showing the number of residuals within the ISC Bulletin, for events within the current summary period. A break-down of the phases is shown in table 12.1.

12.1: Table listing the number of residuals within the ISC bulletin for each phase. The number of residuals are shown for all reviewed events and for those where there is an ISC solution.

Phase	Residuals (reviewed events)	Residuals (ISC located events)
P	318146	309042
Pb	10557	7838
PcP	6728	6612
PcS	421	421
Pdif	2502	2498
PFAKE	4095	4095
Pg	58961	52842
PKiKP	4052	4051
PKKPab	223	223
PKKPbc	1038	1038
PKKPdf	59	59
PKPab	5344	5271
PKPbc	16862	16011
PKPdf	24303	23938
Pn	261539	220671
pP	12377	12298
PP	4511	4507
pPKPab	96	96
pPKPbc	384	376
pPKPdf	977	968
PS	122	122
S	14764	14230
Sb	11106	8460
ScP	2455	2446
ScS	772	772
Sdif	43	43
Sg	51584	46641
SKKSac	272	272
SKKSdf	6	6
SKPbc	567	566
SKPdf	53	53
SKSac	163	163
SKSdf	244	244
Sn	89419	71297
sP	3927	3923
SP	61	61
SS	2645	2643
sS	1621	1619

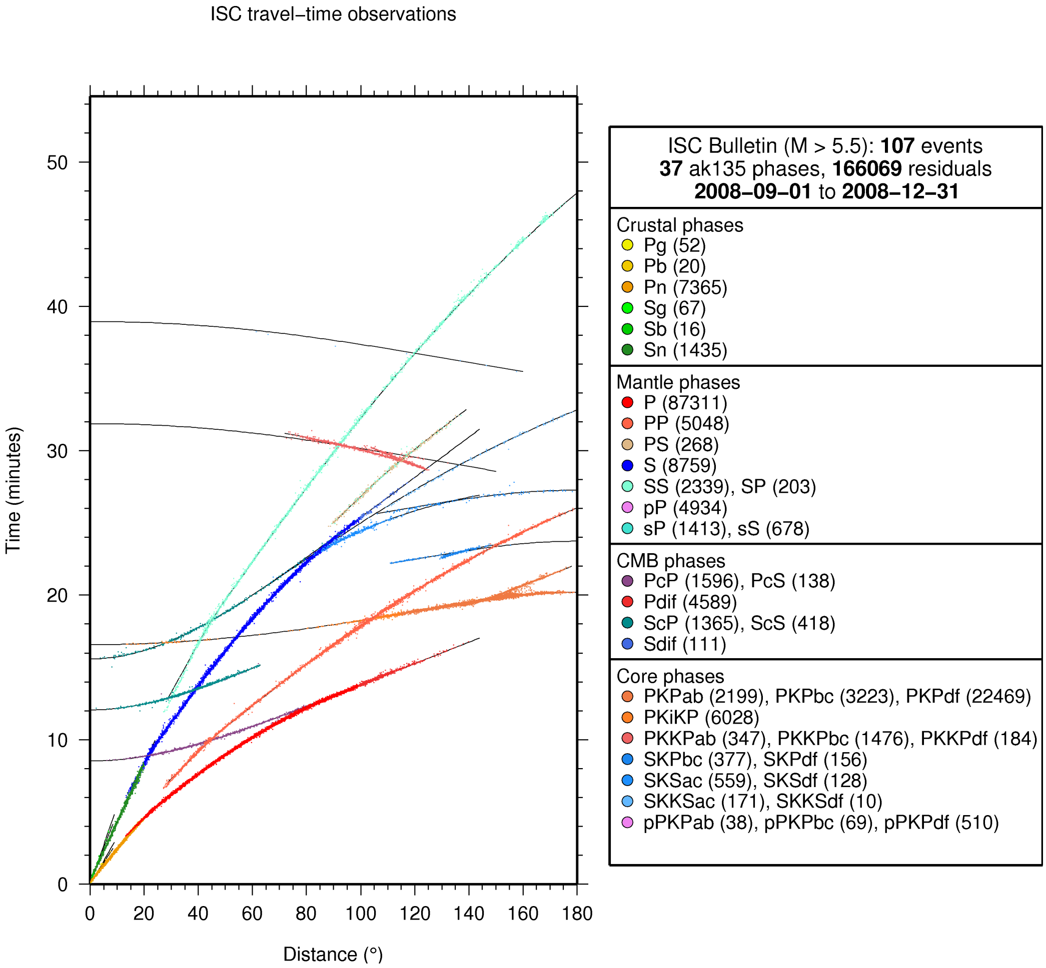

Figure 12.14: Distribution of travel-time observations derived from *ak135* residuals from the ISC bulletin for events with M > 5.5. The travel-time observations are shown relative to a 0 km source and compared with the theoretical travel-time curves (solid lines). The legend lists the number of each phase and the number of observations plotted.

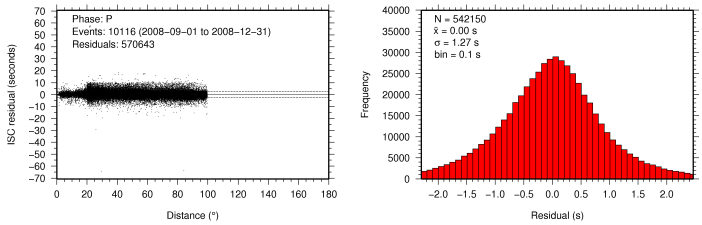

(a)

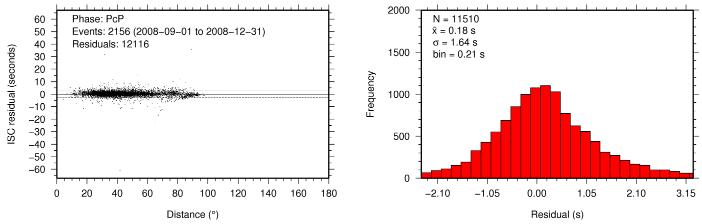

(b)

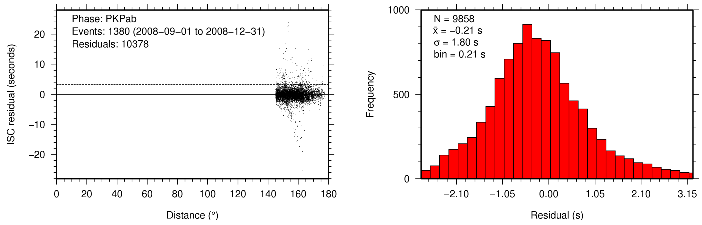

(c)

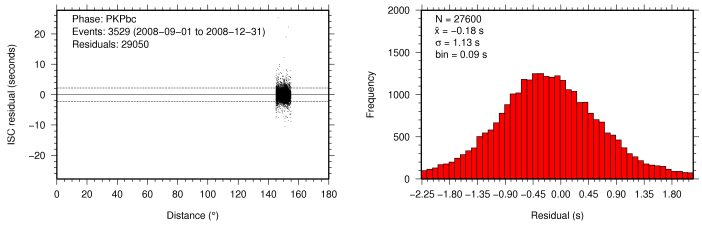

(d)

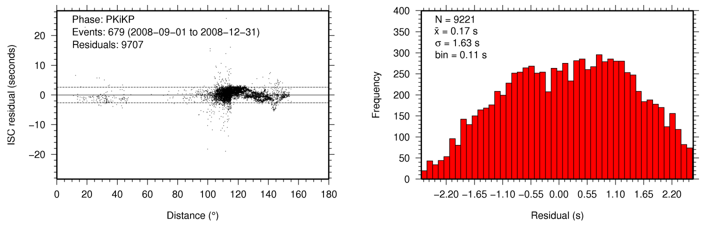

(e)

Figure 12.15: Distribution of all travel-time residuals for a number of P type *ak135* phases from the ISC bulletin. The dashed lines shows the 2.5% and 97.5% quantiles. Data outside of these lines are not plotted in the histograms.

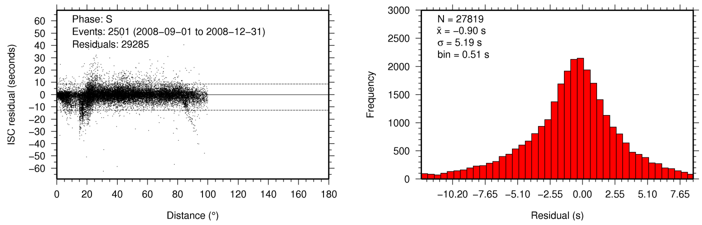

(a)

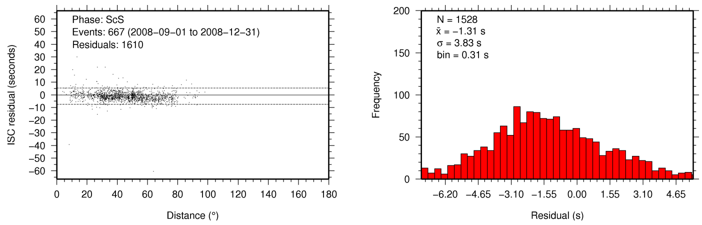

(b)

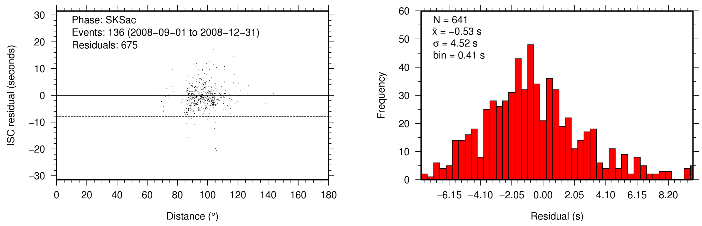

(c)

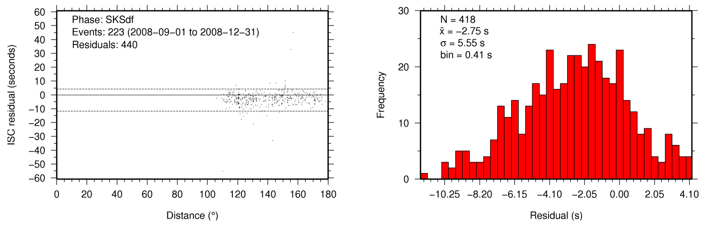

(d)

Figure 12.16: Distribution of all travel-time residuals for a number of S type *ak135* phases from the ISC bulletin. The dashed lines shows the 2.5% and 97.5% quantiles. Data outside of these lines are not plotted in the histograms.

13

ISC Magnitude data

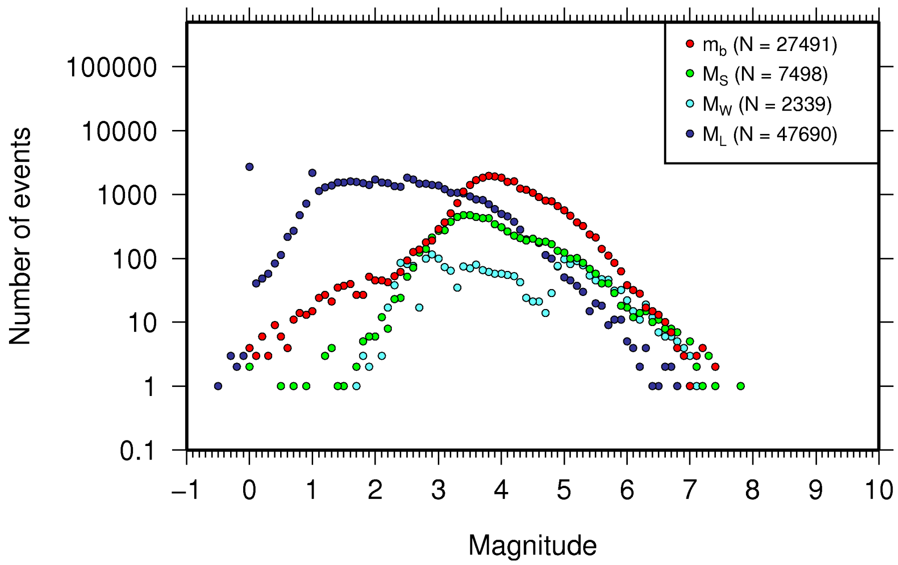

Figure 13.1: Frequency Magnitude Distribution for m_b, M_S, M_W, M_L in the ISC Bulletin.

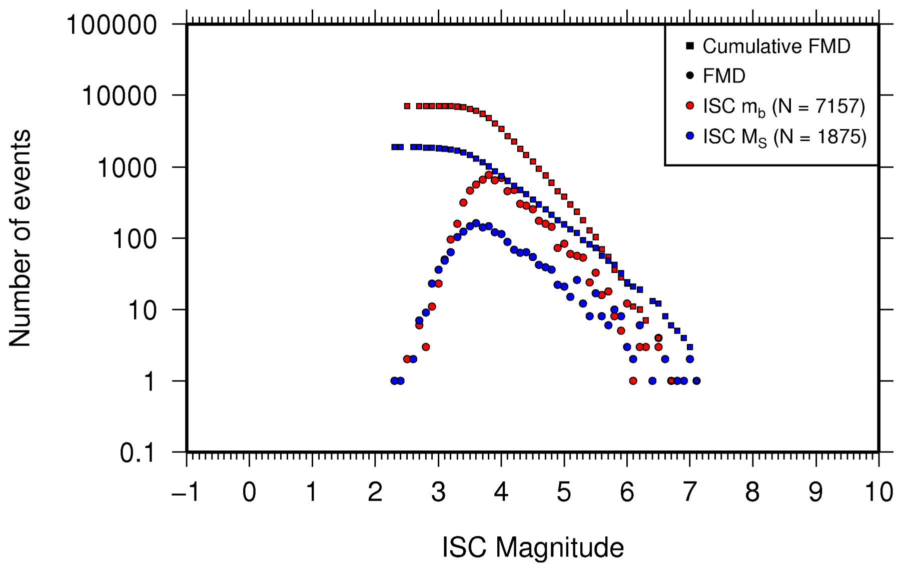

Figure 13.2: Frequency Magnitude Distribution for ISC calculated magnitudes: m_b and M_S.

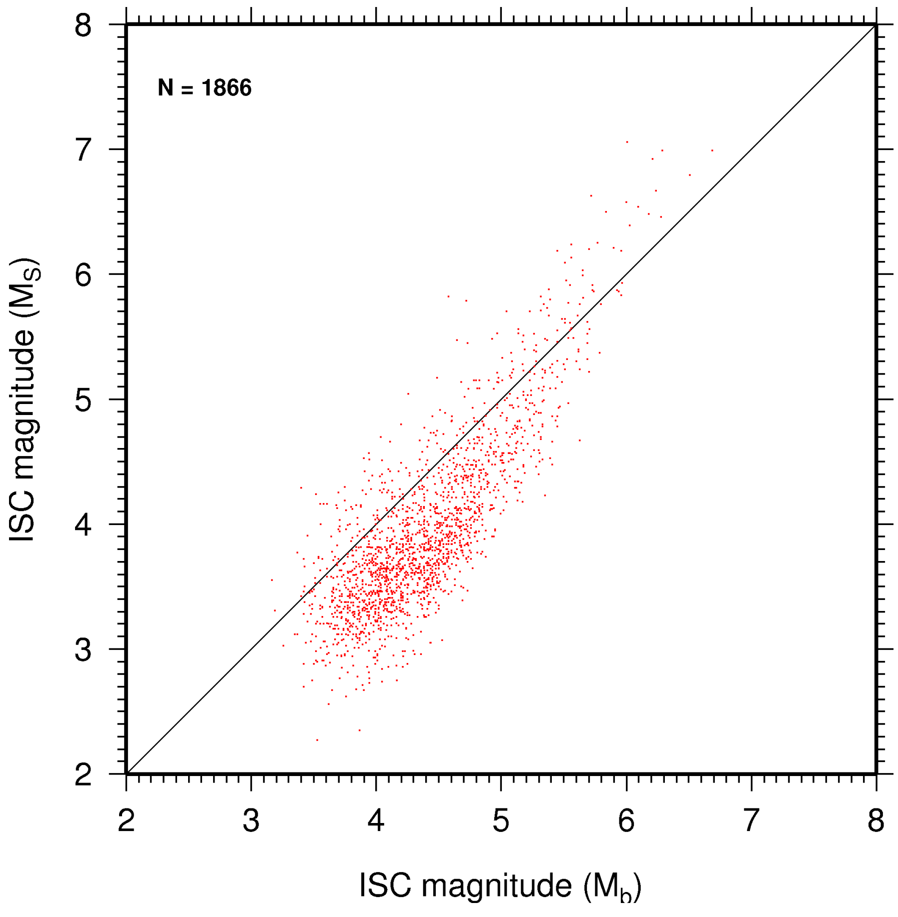

Figure 13.3: Comparison of ISC values of M_S with m_b for common event pairs.

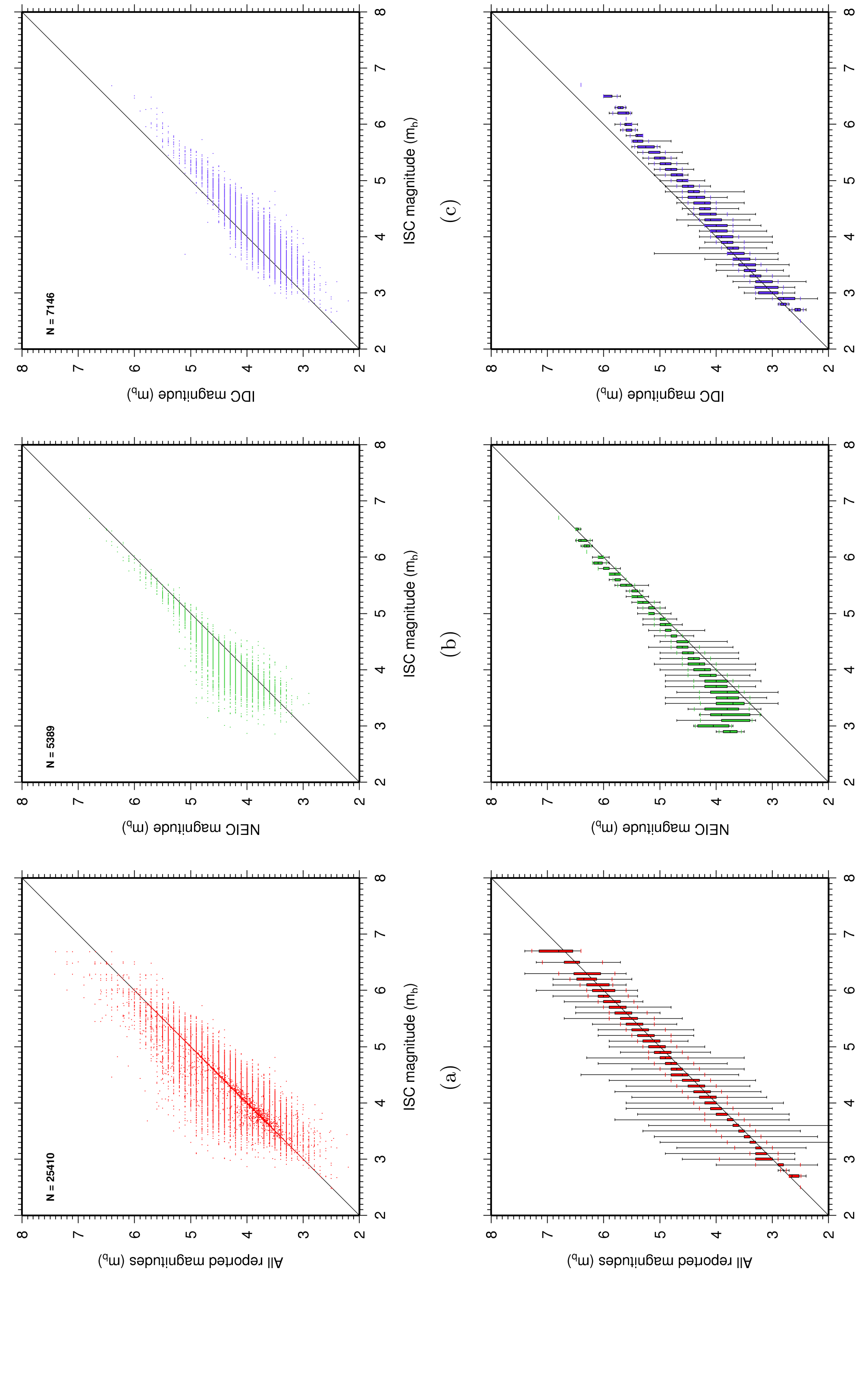

Figure 13.4: Comparison of ISC magnitude data (m_b) with additional agency magnitudes (m_b). The top row shows all individual data points, with their statistical summary shown in the box-and-whisker plots below (the 10th and 90th percentiles are shown in addition to the max and min values on the box-and-whisker plots). Left: all magnitudes reported; middle: NEIC magnitudes; right: IDC magnitudes.

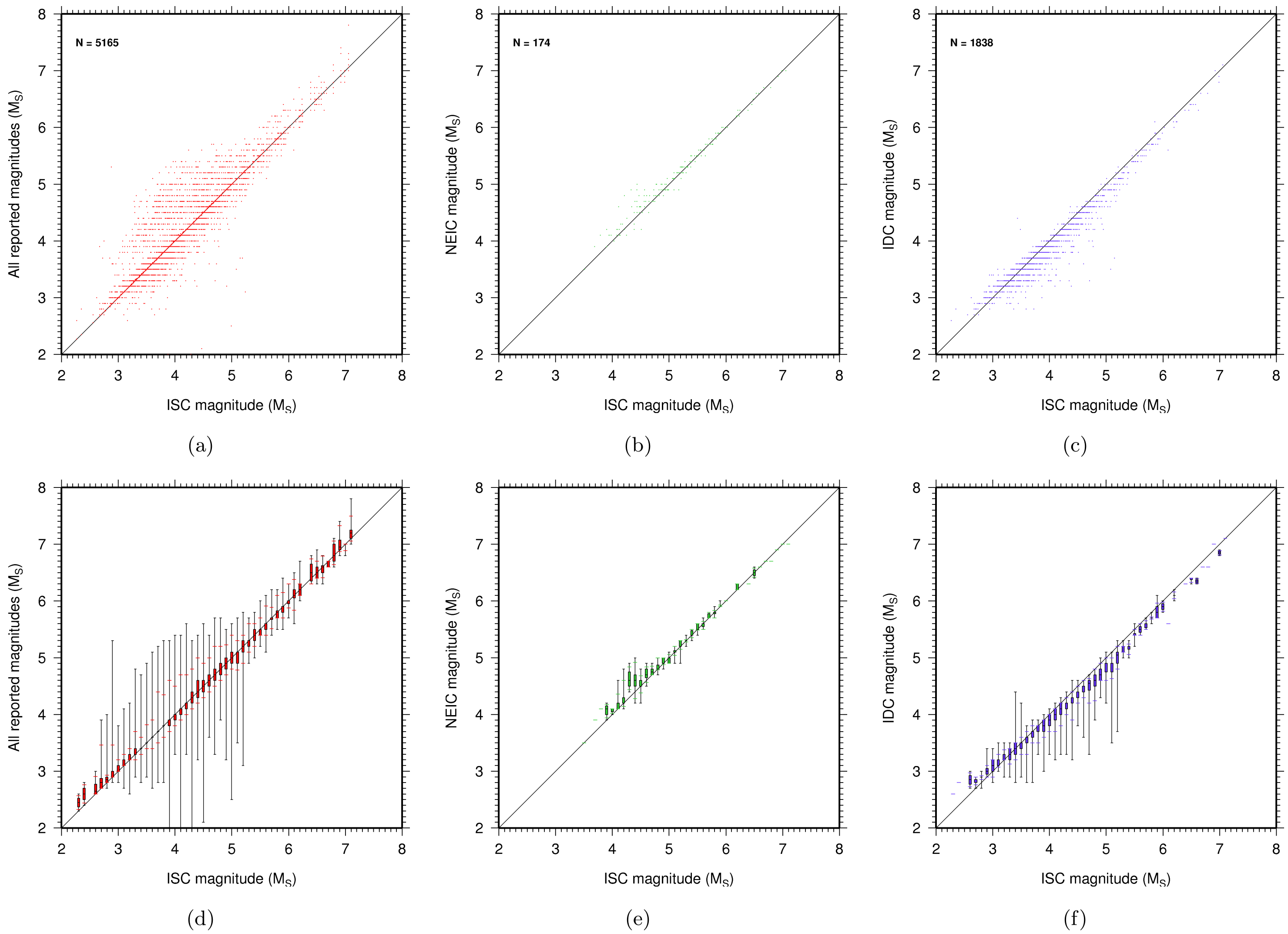

Figure 13.5: Comparison of ISC magnitude data (M_S) with additional agency magnitudes (M_S). The top row shows all individual data points, with their statistical summary shown in the box-and-whisker plots below (the 10th and 90th percentiles are shown in addition to the max and min values on the box-and-whisker plots). Left: all magnitudes reported; middle: NEIC magnitudes; right: IDC magnitudes.

13.1: Table listing each magnitude type within the ISC Bulletin for this summary period. The number of events with values for each each magnitude type is listed. The agencies reporting those magnitude types are listed, together with the total number of values reported.

Magntiude type	Events (ISC Bulletin)	Events (ISC reviewed)	Events (ISC relocated)	Agencies reporting magnitude type (number of values)
M	584	236	180	DJA (44), FDF (202), PRU (18), RSPR (20), SKO (320)
mB	1338	1338	1337	BJI (1317), DJA (84)
mb	12645	11332	7944	BGS (81), BJI (1285), CRAAG (2), CSEM (620), DHMR (1), DJA (555), DMN (5), GUC (2), IDC (10054), IGIL (7), IGQ (62), INMG (1), ISC (7157), ISCJB (6506), LDG (129), MAN (584), MDD (163), MOS (1792), NDI (12), NEIC (5505), NIC (20), NNC (1652), OTT (18), PDA (3), PRE (1), SKHL (95), SZGRF (296), THR (3), VIE (503)
mb1	10230	10230	7447	IDC (10230)
mb1mx	10230	10230	7447	IDC (10230)
mbh	7	7	7	SKHL (7)
mbLg	2589	107	62	MDD (2589)
mbtmp	10229	10229	7447	IDC (10229)
mbv	8	8	8	SKHL (8)
Mc	45	9	8	CSEM (45)
MD	14777	4142	2716	ATH (2543), BER (453), BGS (1), BUC (384), CASC (345), CERI (8), CNRM (82), CSEM (5928), DDA (3525), DHMR (7), ECX (301), GRAL (220), GUC (525), HDC (2), HLW (204), HVO (15), IGQ (5), INMG (24), ISK (2377), JSN (46), KISR (3), LDG (874), LDO (9), MEX (1066), NCEDC (59), NOU (301), PDA (256), PDG (76), PLV (13), PNSN (41), ROM (2250), RSPR (1937), SEA (17), SJA (17), SNET (12), SOF (93), SSNC (3), TRN (323), TUN (8), UCR (5)
ME	58	58	58	NEIC (58)
MG	442	294	242	AEIC (124), ARE (1), ATH (10), BUC (2), GUC (61), ISK (2), JMA (145), LIM (5), MDD (52), NIC (3), ROM (2), RSPR (3), TAP (1), THE (2), WEL (29)
ML	40046	9674	6651	AEIC (557), ALG (3), ARE (1), ARO (7), ATH (874), AUST (50), BEO (1019), BER (525), BGR (309), BGS (32), BJI (828), BNS (41), BRA (2), BUC (2), BUG (26), BUT (7), CASC (186), CLL (125), CRAAG (178), CSEM (11189), DDA (152), DHMR (158), DMN (37), ECX (331), FDF (1), GEN (373), GUC (2206), HEL (3081), HLW (198), HVO (2), HYB (1), IDC (4938), IGIL (187), INMG (614), IPEC (334), ISK (468), ISN (2), KISR (295), KMA (20), KNET (177), KRSC (308), LDG (1469), LDO (2), LEDBW (41), LIM (2), LIS (3), LJU (534), MAN (584), MDD (1), MRB (2), NAO (626), NCEDC (44), NDI (105), NEIC (86), NIC (95), NOU (286), NSSP (3), OTT (98), PAS (137), PDA (292), PDG (231), PGC (607), PLV (4), PMR (119), PPT (38), PRE (662), PRU (49), REN (23), REY (34), ROM (2319), SFS (102), SKO (317), SLC (57), SSNC (3), STR (502), SVSA (2), SZGRF (66), TAP (5190), THE (3250), THR (250), TIR (177), TUN (1), UCC (36), UPP (1173), VIE (907), WAR (154), WBNET (4043), WEL (3009), ZUR (225)
MLv	1355	956	653	DJA (1355)
MN	414	149	141	MDD (98), NEIC (25), OGSO (2), OTT (211), PGC (2), TEH (88), WES (2)
MPV	1	1	1	NERS (1)
mpv	1811	672	559	NNC (1811)
MS	4708	4674	3757	ASRS (6), BGS (29), BJI (1047), CSEM (97), IDC (3984), IGIL (7), IGQ (62), ISC (1875), ISCJB (1737), LDG (82), MAN (586), MOS (351), NEIC (180), NOU (28), NSSP (21), SKHL (24), SZGRF (118), VIE (21)
Ms1	3983	3983	3434	IDC (3983)
ms1mx	3983	3983	3434	IDC (3983)
Ms7	1051	1043	1037	BJI (1051)
msh	23	23	22	SKHL (23)
msha	4	4	4	SKHL (4)
MW	2084	1285	1147	ATH (1), BRK (16), CAR (3), CRAAG (4), CSEM (86), DJA (87), ECX (3), FUNV (735), GCMT (579), NCEDC (1), NEIC (257), NIC (67), NIED (569), OTT (8), PAS (2), PDA (1), PGC (288), ROM (1), SLM (12), UPA (2), USGS (24), WEL (1)
Mw(mB)	84	84	84	DJA (84)
Mwp	6	6	6	DJA (6)

14

Regional analysis

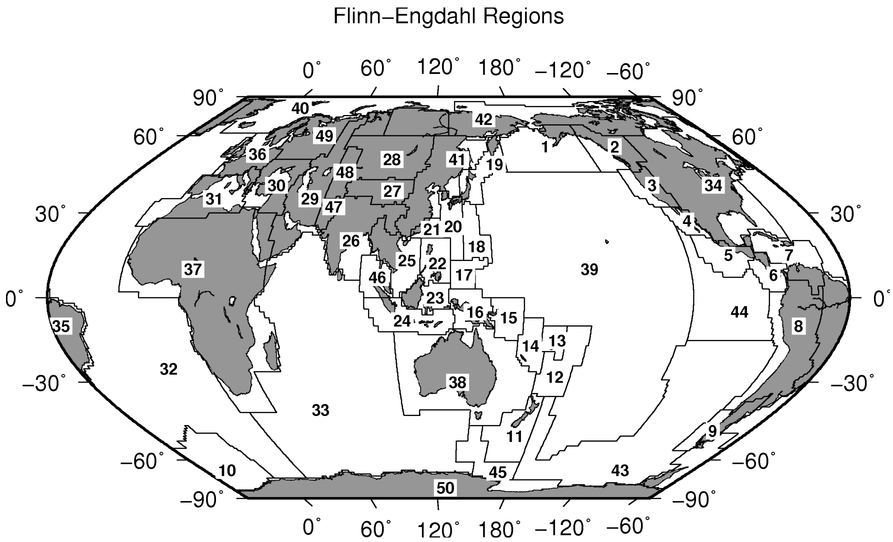

Figure 14.1: Map of all Flinn-Engdahl seismic regions.

14.1 1. Alaska-Aleutian Arc

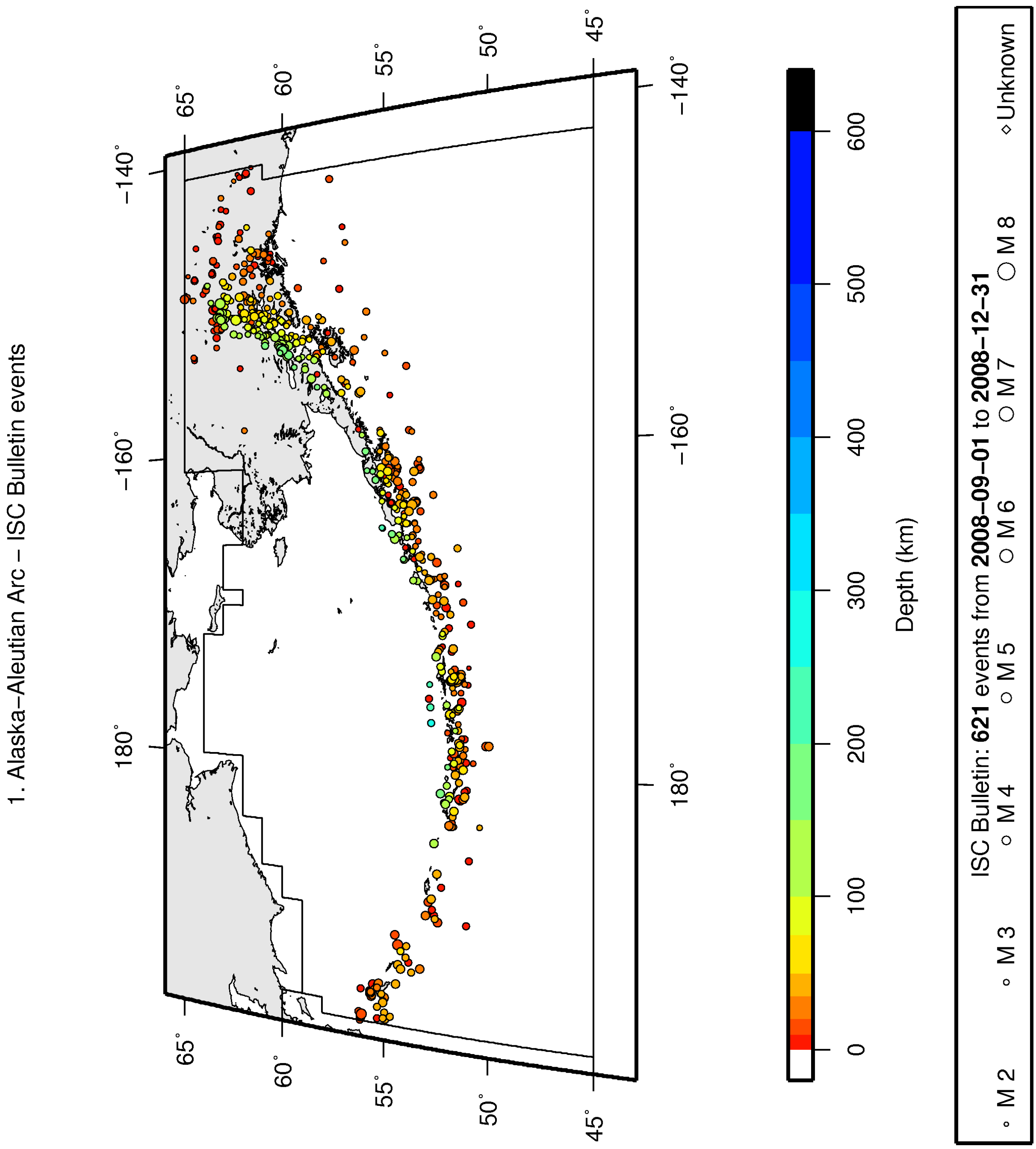

Figure 14.2: Map of seismicity for this seismic region from all events in the ISC Bulletin.

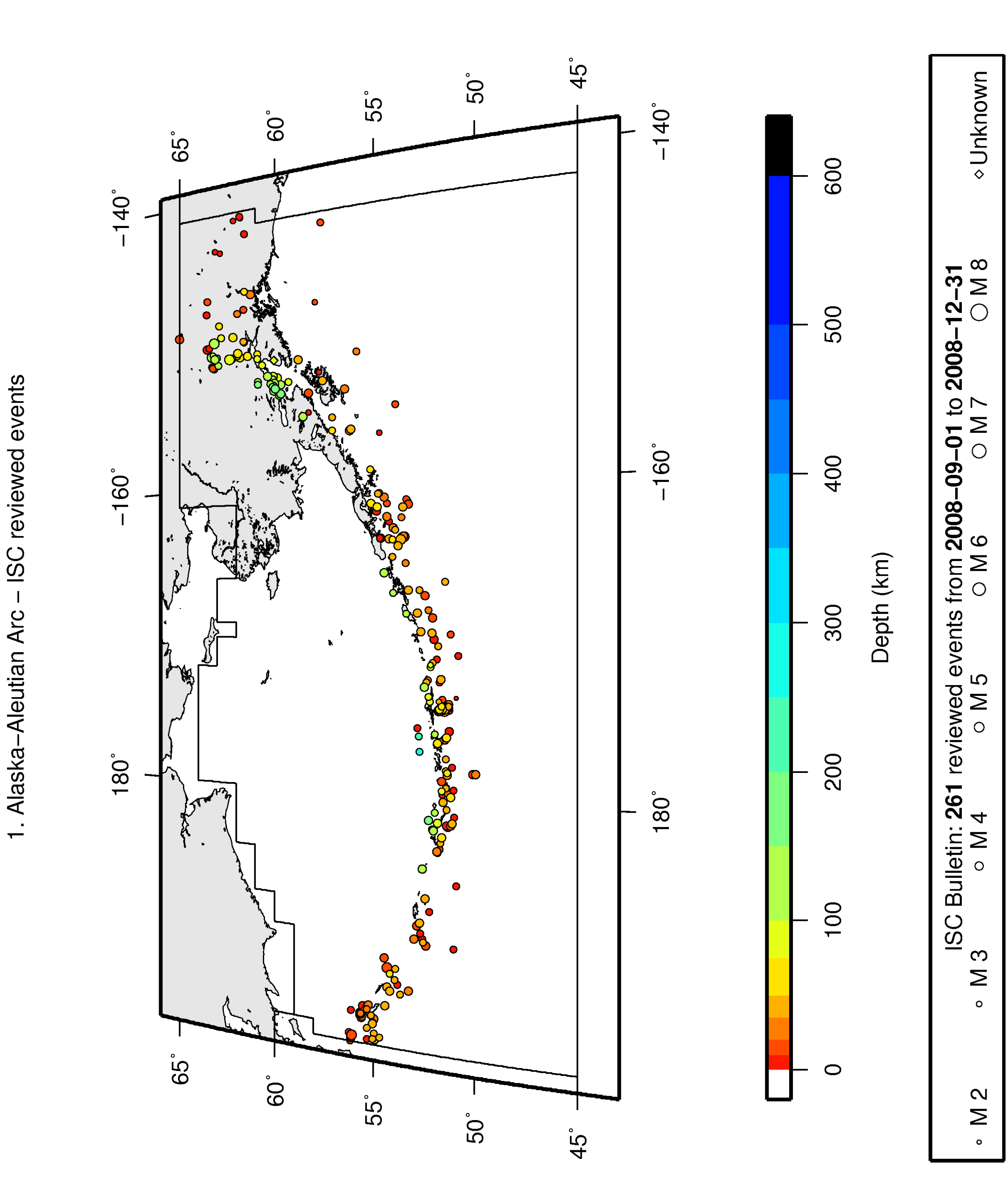

Figure 14.3: Map of seismicity for this seismic region. Shows only those events in the ISC Bulletin that have been reviewed.

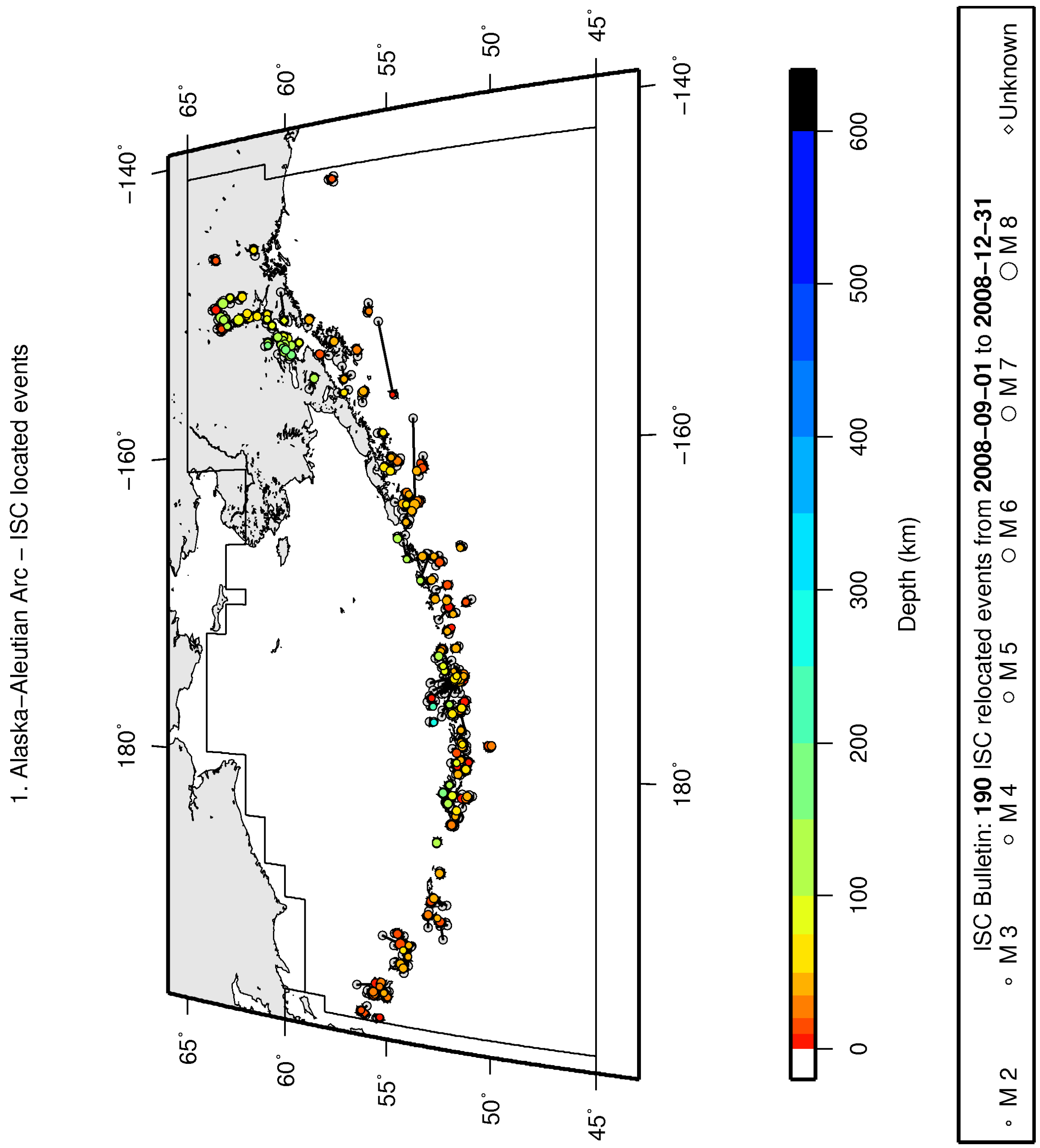

Figure 14.4: Map of seismicity for this seismic region. Shows only those events in the ISC Bulletin that have been located by the ISC. The alternative hypocentres for these events are plotted as grey circles, with vectors pointing to the ISC solution.

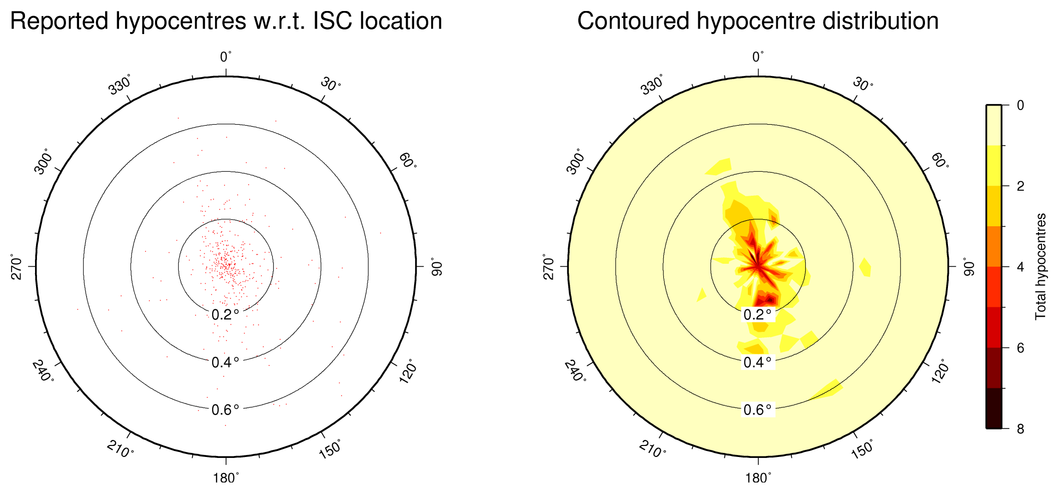

Figure 14.5: Distribution of hypocentres for events with an ISC determined hypocentre. Left - all alternative hypocentres plotted w.r.t. the ISC locations; right - contour plot of all alternative hypocentres plotted w.r.t. the ISC locations. Plots are limited to hypocentres which fall within the 95th percentile.

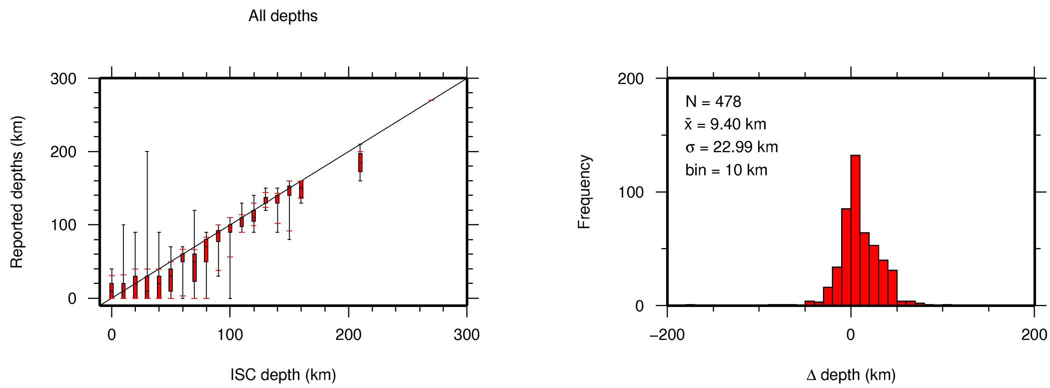

Figure 14.6: Distribution of all hypocentre depths for events with an ISC determined hypocentre. Left - box-and-whisker plot showing the maximum and minimum values as error bars, with the 10th and 90th percentiles shown as red horizontal lines. The box shows the 25th to 75th percentile, with the median displayed as a horizontal line. Depths are binned to the nearest 10 km. Right - histogram showing the distribution depth variation for the complete range of depths. Δ is the *ISC depth* $-$ *reported depth*.

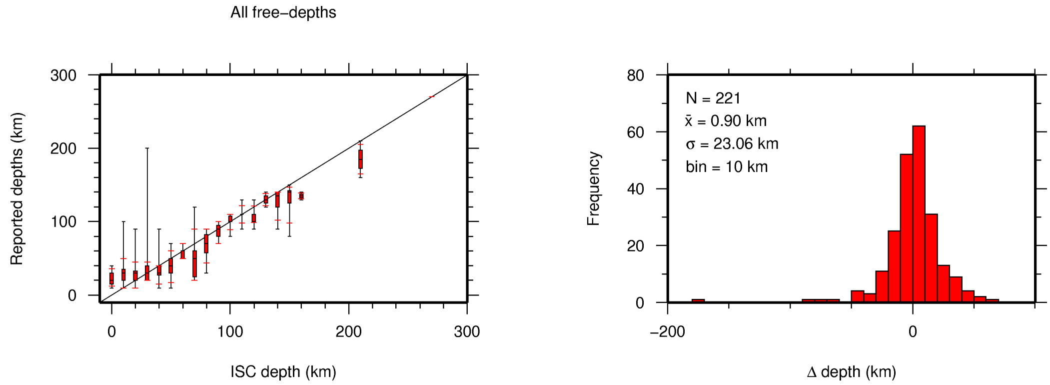

Figure 14.7: Distribution of free-depth hypocentres (reported as) for events with an ISC determined hypocentre (also free-depth). These include depth-phase solutions. Left - box-and-whisker plot showing the maximum and minimum values as error bars, with the 10th and 90th percentiles shown as red horizontal lines. The box shows the 25th to 75th percentile, with the median displayed as a horizontal line. Depths are binned to the nearest 10 km. Right - histogram showing the distribution depth variation for the complete range of depths. Δ is the *ISC depth* $-$ *reported depth*.

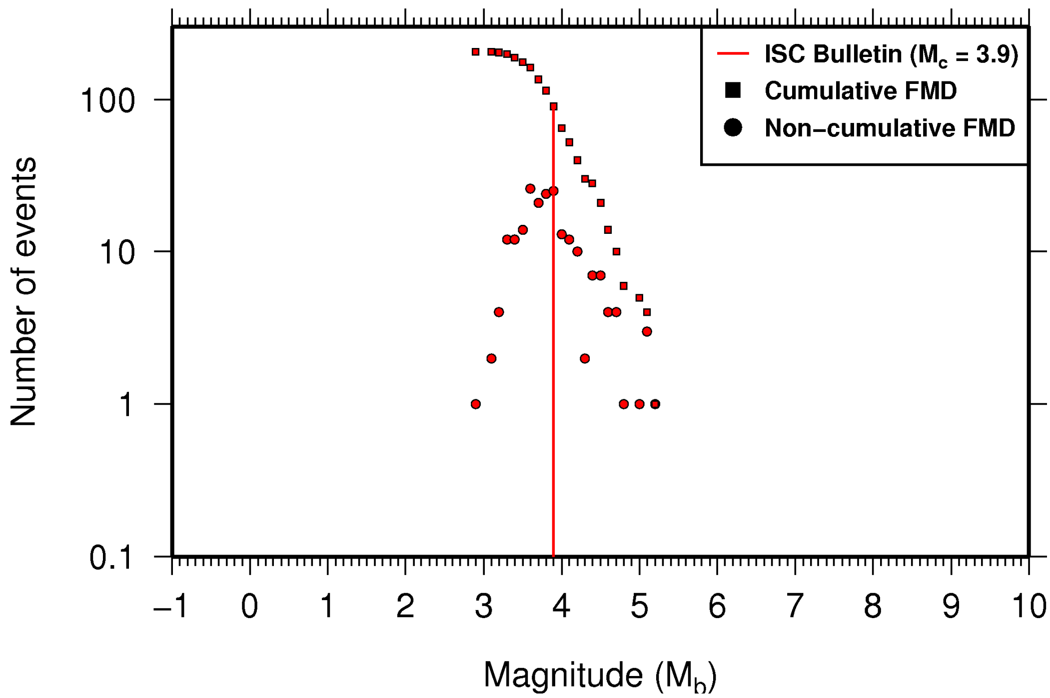

Figure 14.8: Frequency magnitude distribution (FMD) for events from the ISC Bulletin in this Flinn-Engdahl region. The magnitude of completeness (M_c) is shown. Note: only events with values of m_b are represented in the figure.

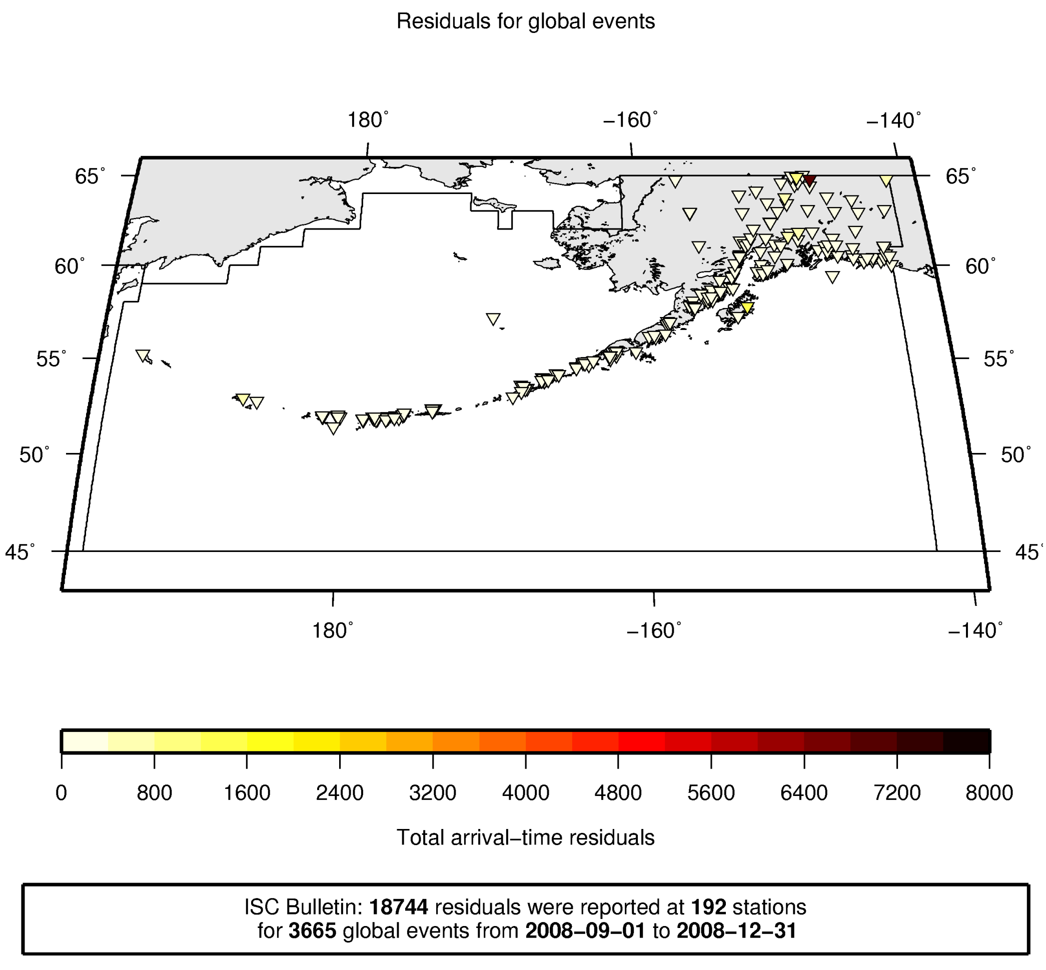

Figure 14.9: Plot of stations with *ak135* residuals in the ISC Bulletin from all events (worldwide).

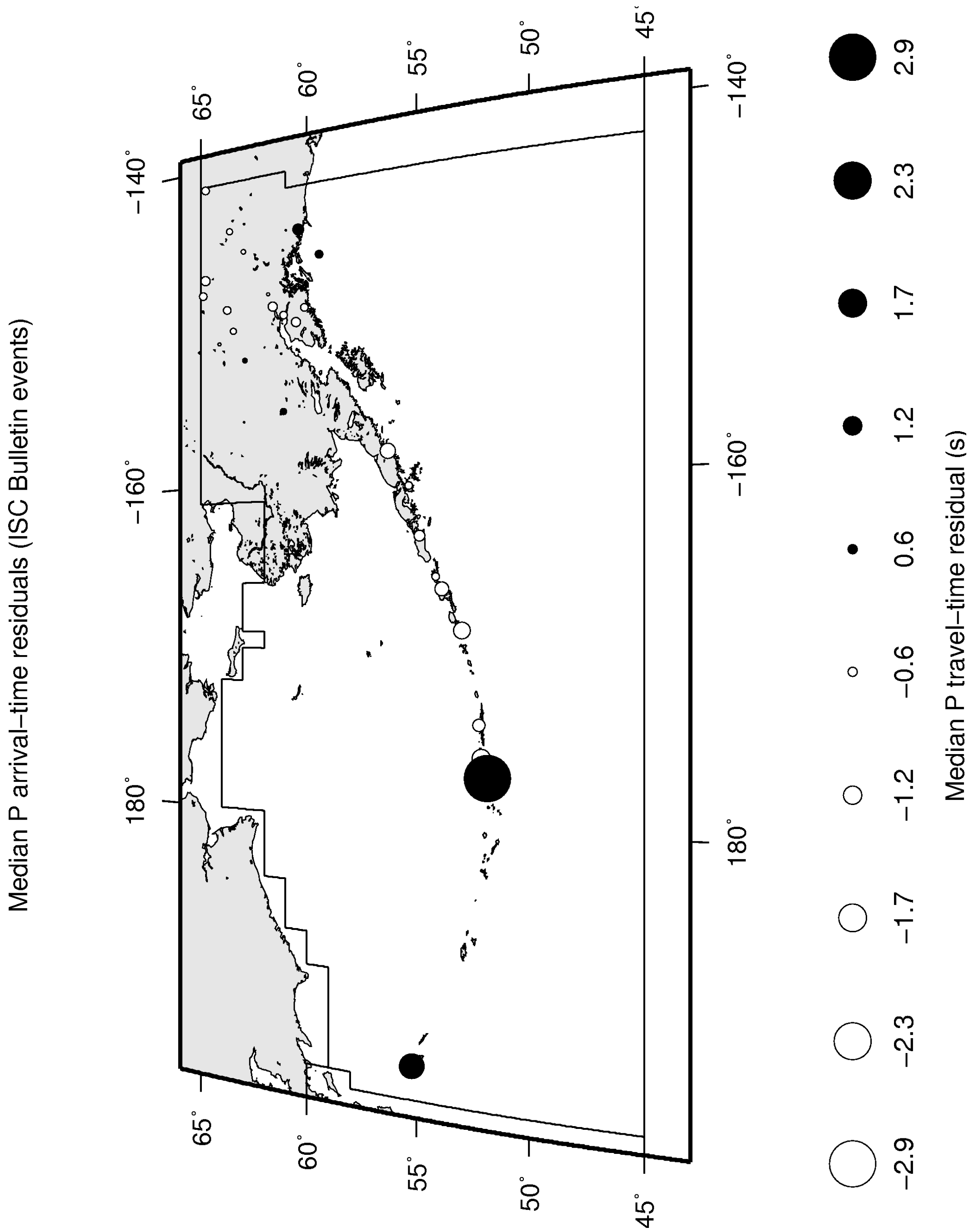

Figure 14.10: Plot of the median P-wave travel-time residual for each station.

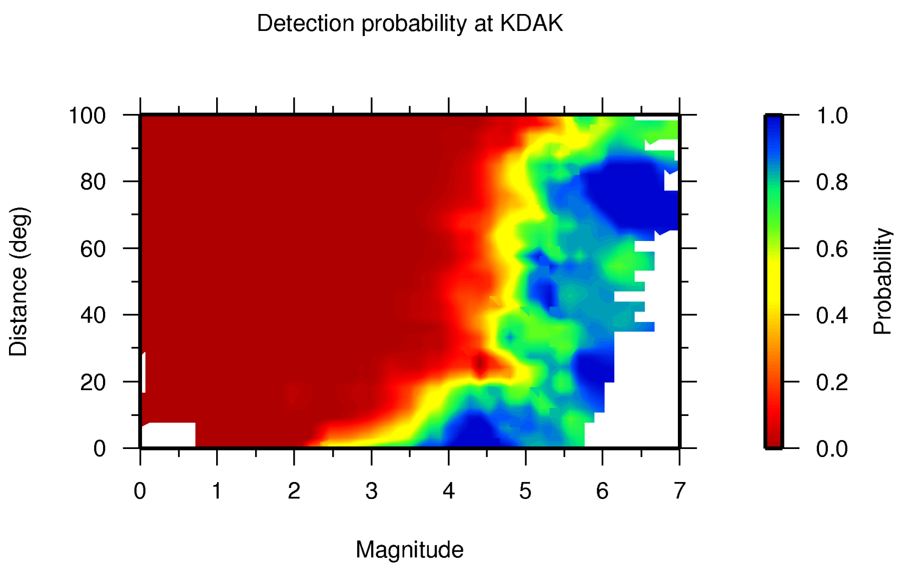

Figure 14.11: Detection probabilities for station KDAK, which has the highest number of arrivals in this region, for this summary period. Areas without sufficient data are clipped.

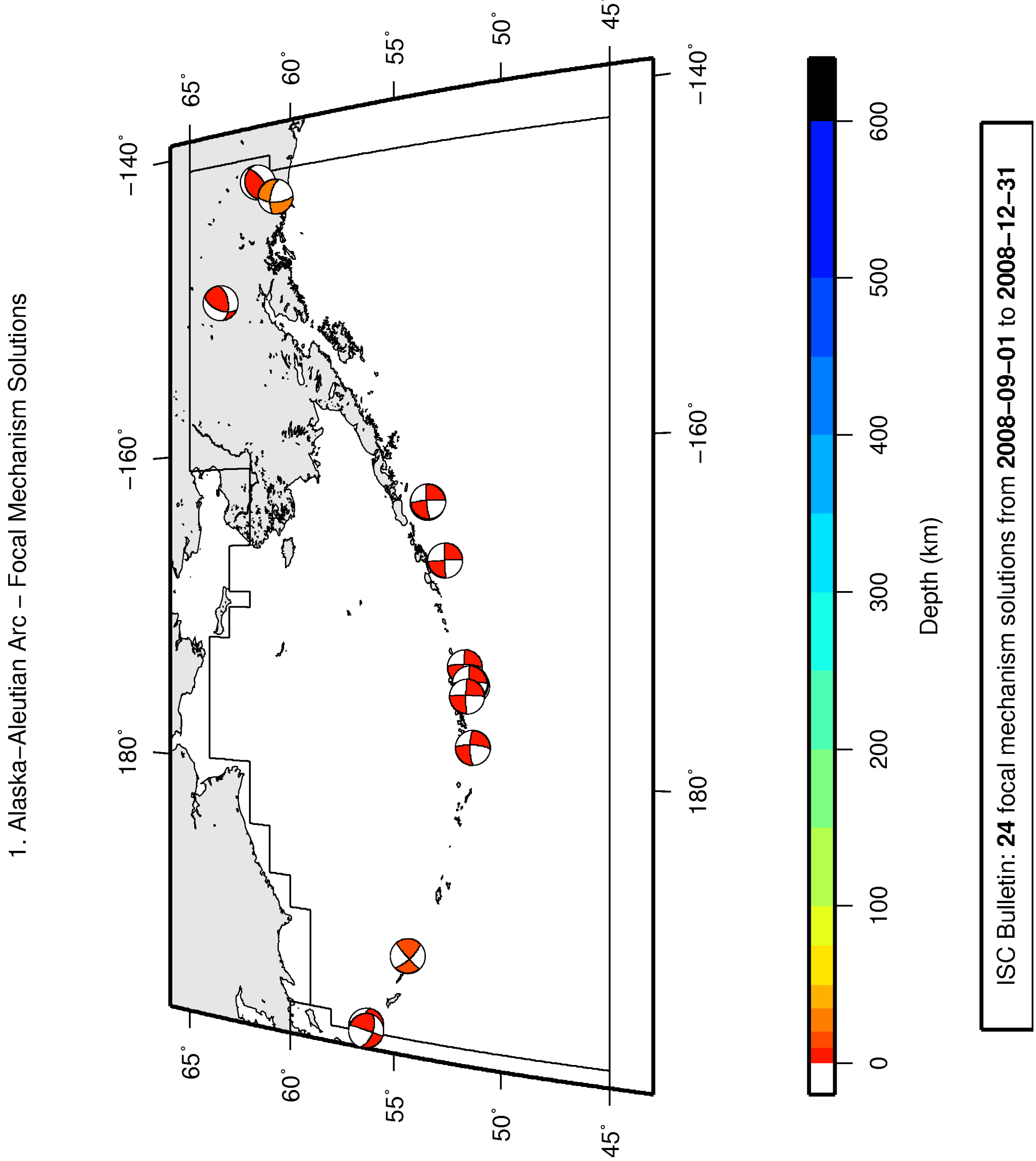

Figure 14.12: Map of focal mechanism solutions for this seismic region.

15

Leading data contributors to the ISC

BD, ED:

- Stations that recorded most events in the reviewed Bulletin.
- Stations that report largest average number of secondary phases used.
- Top 10 stations with the highest *proportion* of amplitudes.
- Agencies that delivered data on time.

References

Adams, R., A. Hughes, and D. Gregor (1982), Analysis procedures at the international data centre, *Physics of the Earth and Planetary Interiors*, *30*, 85–92.

Amante, C., and B. Eakins (2009), ETOPO1 1 arc-minute global relief model: procedures, data sources and analysis, *NOAA Technical Memorandum NESDIS NGDC-24*, NOAA.

Avery, H., J. Berrill, P. Coursey, M. D. B.L. Deam, C. Francois, J. Pettinga, and M. Yetton (2004), The Canterbury University strong-motion recording project, in *Proceedings of 13th World Conference on Earthquake Engineering*, Canadian Association for Earthquake Engineering.

Beavan, J., S. Samsonov, M. Motagh, L. Wallace, S. Ellis, and N. Palmer (2010), The M_W 7.1 Darfield (Canterbury) earthquake: geodetic observations and preliminary source model, *Bulletin of the New Zealand Society for Earthquake Engineering*, *43*, 228–235.

Bennett, T., V. Oancea, B. Barker, Y.-L. Kung, M. Bahavar, B. Kohl, J. Murphy, and I. Bondár (2010), The nuclear explosion database NEDB: a new database and web site for accessing nuclear explosion source information and waveforms, *Seismological Research Letters*, *81*, doi:10.1785/gssrl.81.1.12.

Bolt, B. (1960), the revision of earthquake epicentres, focal depths and origin time using a high-speed computer, *Geophysical Journal of the Royal Astronomical Society*, *3*, 434–440.

Bondár, I., and K. McLaughlin (2009a), Seismic location bias and uncertaintyin the presence of correlated and non-gaussian travel-time errors, *Bulletin of the Seismological Society of America*, *99*, 172–193.

Bondár, I., and K. McLaughlin (2009b), A new ground truth data set for seismic studies, *Seismological Research Letters*, *80*, 465–472.

Bondár, I., and D. Storchak (in press), Improved location procedures at the International Seismological Centre, *Geophysical Journal International*.

Bondár, I., E. Engdahl, X. Yang, H. Ghalib, A. Hofstetter, V. Kirchenko, R. Wagner, I. Gupta, G. Ekström, E. Bergman, H. Israelsson, and K. McLaughlin (2004), Collection of a reference event set for regional and teleseismic location calibration, *Bulletin of the Seismological Society of America*, *94*, 1528–1545.

Bondár, I., E. Bergman, E. Engdahl, B. Kohl, Y.-L. Kung, and K. McLaughlin (2008), A hybrid multiple event location technique to obtain ground truth event locations, *Geophysical Journal International*, *175*, doi:10.1111/j.1365,246X.2008.03,867x.

Chang, A., R. Shumway, R. Blandford, and B. Barker (1983), Two methods to improve location estimates - preliminary results, *Bulletin of the Seismological Society of America*, *73*, 281–295.

Dziewonski, A., and F. Gilbert (1976), The effect of small, aspherical perturbations on travel times and a re-examination of the correction for ellipticity, *Geophysical Journal of the Royal Astronomical Society*, *44*, 7–17.

Engdahl, E., R. van der Hilst, and R. Buland (1998), Global teleseismic earthquake relocation with improved travel times and procedures for depth determination, *Bulletin of the Seismological Society of America*, *88*, 722–743.

Flinn, E., and E. Engdahl (1965), Proposed basis for geographical and seismic regionalization, *Reviews of Geophysics*, *3*(1), 123–149.

Flinn, E., E. Engdahl, and A. Hill (1974), Seismic and geographical regionalization, *Bulletin of the Seismological Society of America*, *64*, 771–993.

Forsyth, P., D. Barrell, and R. Jongens (2008), Geology of the Christchurch area, *1:250000 geological map 16*, Institute of Geological and Nuclear Sciences, GNS Science, Lower Hutt, New Zealand.

Gledhill, K., J. Ristau, M. Reyners, B. Fry, and C. Holden (2011), The Darfield (Canterbury, New Zealand) M_W 7.1 earthquake of September 2010: a preliminary seismological report, *Seismological Research Letters*, *82*, doi:10.1785/gssrl.82.3.378.

Jeffreys, H., and K. Bullen (1940), *Seismological Tables*, British Association for the Advancement of Science.

Kennett, B. (2006), Non-linear methods for event location in a global context, *Physics of the Earth and Planetary Interiors*, *158*, 45–64.

Kennett, B., E. Engdahl, and R. Buland (1995), Constraints on seismic velocities in the Earth from traveltimes, *Geophysical Journal International*, *122*, 108–124.

Kennett, B., E. Engdahl, and R. Buland (1996), Ellipticity corrections for seismic phases, *Geophysical Journal International*, *127*, 40–48.

Murphy, J., and B. Barker (2006), Improved focal-depth determination through automated identication of the seismic depth phases pP and sP, *Bulletin of the Seismological Society of America*, *96*, 1213–1229.

Petersen, T., K. Gledhill, M. Chadwick, N. Gale, and J. Ristau (2011), The New Zealand national seismograph network, *Seismological Research Letters*, *82*, doi:10.1785/gssrl.82.1.9.

Quigley, M., R. V. Dissen, P. Villamor, B. Litchfield, D. Barrell, K. Furlong, T. Stahl, B. Duffy, E. Bilderback, D. Noble, D. Townsend, J. Begg, R. Jongens, W. Ries, J. Claridge, A. Klahn, H. Mackenzie, A. Smith, S. Hornblow, R. Nicol, S. Cox, R. Langridge, and K. Pedley (2010), Surface rupture of the Greendale fault during the M_W 7.1 Darfield (Canterbury) earthquake, New Zealand: initial findings, *Bulletin of the New Zealand Society for Earthquake Engineering*, *43*, 236–242.

Sambridge, M. (1999), Geophysical inversion with a neighbourhood algorithm, *Geophysical Journal International*, *138*, 479–494.

Sambridge, M., and B. Kennett (2001), Seismic event location: non-linear inversion using a neighbourhood algorithm, *Pure and Applied Geophysics*, *158*, 241–257.

Storchak, D., J. Schweitzer, and P. Bormann (2003), The IASPEI standard seismic phases list, *Seismological Research Letters*, *74*(6), 761–772.

Villaseñor, A., and E. Engdahl (2005), A digital hypocenter catalog for the International Seismological Summary, *Seismological Research Letters*, *76*, 554–559.

Villaseñor, A., and E. Engdahl (2007), Systematic relocation of early instrumental seismicity: Earthquakes in the International seismological summary for 1960–1963, *Bulletin of the Seismological Society of America*, *97*, 1820–1832.

Young, J., B. Presgrave, H. Aichele, D. Wiens, and E. Flinn (1996), The Flinn-Engdahl regionalisation scheme: the 1995 revision, *Physics of the Earth and Planetary Interiors*, *96*, 223–297.